Ultrafast photoinduced intra- and intermolecular charge transfer and solvation

Dissertation der Fakultät für Physik

der Ludwig-Maximilians-Universität München

vorgelegt von

Tanja Bizjak

aus Zagreb, Kroatien

München, den 2. August 2004

To my parents
and my sister

„Experiments are the only means of knowledge at our disposal.

The rest is poetry, imagination.”

Max Planck

ABSTRACT

Intra- and intermolecular charge transfer as well as internal conversion processes are studied in various molecular systems. The dynamics of these fundamental photoinduced processes are investigated by pump-probe femtosecond spectroscopy and steady-state fluorescence. Transient spectra are obtained using white light continuum as probe, while time resolved measurements are performed by probing at specific wavelengths with non dispersive detection. Noncollinearly phase matched optical parametric amplifiers (NOPAs) are used as tunable pump and probe pulse sources. This technique enables to study ultrafast phenomena with an unprecedented time resolution of 60 fs for UV-C excitation pulses at 270 nm.

Upon excitation of their structural subunits, **triphenylmethane lactones** (phenolphthalein and malachite green lactone) undergo ultrafast photoinduced **electron transfer** (ET) with the formation of a radical ion pair of their structural subunits. The phenol radical cation is formed by ET with a time constant of 50 fs and 80 fs after excitation to the S_1 state of phenolphthalein in acetonitrile and ethyl acetate, respectively. In malachite green lactone both $S_2 \rightarrow S_1$ electronic relaxation and ET are completed within 150 fs in aprotic (acetonitrile and ethyl acetate) as well as in protic environment (methanol). Subsequently, in methanol the opening of the lactone ring is detected directly by observing the appearance of the malachite green cation absorption band on a 2 - 4 ps time scale. The results demonstrate that the ET in these molecules occurs faster than the time scale of inertial solvation dynamics, while the lactone ring opening occurs on the time scale of longitudinal dielectric relaxation. It is assumed that on one side an intramolecular vibrational mode promotes the charge transfer and on the other side diffusive solvation dynamics is responsible for the breakage of the C-O bond in the lactone ring.

The controversial behavior of the excited biochromophore **indole** in water, which fluoresces on a nanosecond time scale and undergoes **photoionization** within 60 fs, is explained with an ultrafast branching occurring immediately after excitation. The excited indole population is divided by the ultrafast branching into a fraction (62%) which exhibits a $^1L_a/^1L_b$ state reversal and a fraction (38%) that undergoes photoionization generating indole radicals and solvated electrons. The electron solvation dynamics is resolved to occur with a time constant of 350 fs. From the comparisons with the photoionization dynamics in neat water and in 1-methylindole the origin of the solvated electron has been found to be the intermolecular electron transfer to the solvent and not an H-transfer to the solvent.

Internal conversion (IC), an important nonradiative process occurring in organic compounds upon the UV radiation, is explored in **o-hydroxybenzaldehyde** (OHBA), a molecule that exhibits excited state intramolecular proton transfer (ESIPT). It is shown that the IC of OHBA proceeds as a thermally activated process over an energy barrier of about 200 meV caused by an avoided crossing between the $\pi\pi^*$- and $\pi\sigma^*$-state. The IC shows pure statistical behavior depending on the total excitation photon energy although the preceding ESIPT is a balistic motion of a well-defined wavepacket. Thus, the coordinates involved in the ESIPT and in the IC are found to be orthogonal.

KURZFASSUNG

In der vorliegenden Arbeit werden an drei unterschiedlichen molekularen Systemen sowohl intra- und intermolekularer Ladungstransfer- als auch interne Konversionsprozesse untersucht. Die Dynamiken dieser fundamentalen photoinduzierten Prozesse werden mit Anrege-Abtast-Femtosekundenspektroskopie und stationärer Fluoreszenzspektroskopie untersucht. Während zeitaufgelöste Messungen durch Abtasten bei einer speziellen Wellenlänge mit nichtdispersiver Detektion durchgeführt werden, werden transiente Spektren mit Lichtimpulsen eines Weißlicht-Kontinuums ermittelt. Dabei wird erstmals eine Zeitauflösung von 60 fs bei Anregungswellenlängen im fernen UV-Bereich (270 nm) erreicht, indem nichtkollinear phasenangepaßte, optisch parametrische Verstärker als durchstimmbare Anrege- und Abtast-Impulsquellen eingesetzt werden.

Nach Anregung ihrer strukturellen Untereinheiten durchlaufen **Triphenylmethanlaktone** einen ultraschnellen **Elektrontransfer** (ET), wobei ein Radikal-Ionenpaar entsteht. Nach Anregung von Phenolphthalein in den S_1-Zustand wird das Phenol-Radikal-Kation durch einen ET mit $\tau = 50$ fs in Acetonitril und mit $\tau = 80$ fs in Ethylacetat gebildet. In Malachitgrünlakton ist die elektronische $S_2 \rightarrow S_1$ Relaxation und der ET sowohl in aprotischen als auch in protischen Lösungsmitteln innerhalb von 150 fs abgeschlossen. In Methanol wird anschließend die Öffnung des Laktonrings direkt durch das Erscheinen der Absorptionsbande des Malachitgrünkations auf einer 2 - 4 ps Zeitskala beobachtet. Die Ergebnisse zeigen, dass der ET in diesen Molekülen schneller stattfindet als die inertiale Solvatisierungsdynamik, während die Öffnung des Laktonrings auf der Zeitskala der longitudinalen dielektrischen Relaxation geschieht. Es wird angenommen, dass einerseits intramolekulare Vibrationsmoden den Ladungstransfer vermitteln und anderseits die diffusive Solvatisierungsdynamik für das Aufbrechen der C-O Bindung im Laktonring verantwortlich ist.

Das widersprüchliche Verhalten des angeregten Biochromophors **Indol** in Wasser, das auf der einen Seite auf einer Nanosekundenzeitskala fluoresziert, auf der anderen Seite eine **Photoionisation** innerhalb von 100 fs aufweist, wird mit einer ultraschnellen Verzweigung erklärt, die unmittelbar nach der Anregung stattfindet. Die angeregte Indolpopulation wird durch die ultraschnelle Verzweigung in zwei Subensembles aufgeteilt: 62% der angeregten Moleküle zeigen eine sogenannte $^1L_a/^1L_b$ Zustandsumkehr und 38% erzeugen durch eine Photoionisation ein Indol-Radikal und ein im Lösungsmittel solvatisiertes Elektron. Dessen Solvatationsdynamik wird mit $\tau = 350$ fs beschrieben. Aus den Vergleichen mit der Photoionisationsdynamik von reinem Wasser und von 1-Methylindol wird der Ursprung des solvatisierten Elektrons als intermolekularer ET zum Lösungsmittel identifiziert, anstatt eines Wasserstoff-Transfers, der in der Literatur oft angenommen wird.

Am Beispiel von **o-Hydroxybenzaldehyd** (OHBA) wird die **interne Konversion** (IK) untersucht, ein wichtiger nichtstrahlender Prozess, der in organischen Verbindungen nach UV Anregung auftritt. OHBA zeigt einen intramolekularen Protontransfer im elektronisch angeregten Zustand (ESIPT). Es wird gezeigt, dass die IK von OHBA thermisch aktiviert über eine Energiebarriere von etwa 200 meV abläuft, die durch eine vermiedene Kreuzung zwischen dem $\pi\pi^*$- und dem $\pi\sigma^*$-Zustand entsteht. Die IK zeigt abhängig von der Energie des Anregungsphotons ein rein statistisches Verhalten, obwohl der initiale ESIPT eine ballistische Bewegung eines wohldefinierten Wellenpaketes ist. Daraus ergibt sich, dass die bei ESIPT und IK beteiligten Koordinaten orthogonal zueinander sind.

Contents

Contents

1 Introduction

Life on earth is constantly under the influence of solar radiation. This has both beneficial and negative consequences. Almost all of the energy available for living beings can be traced back to solar energy converted to chemical energy by the process of photosynthesis [1]. This fundamental electron transfer process can also enable us to get access to new energy resources, such as solar cells [2]. However, light particular in the ultraviolet spectral range induces photodegradation of organic material and can be responsible for cell damage and even cell death. Photophysical and photochemical rearrangements, charge transfer and electronic relaxation processes induced by the mixing of electronic states represent the essential ingredients of the photoinduced dynamics in organic compounds. In this thesis fundamental aspects of intra- and intermolecular electron transfer as well as internal conversion are investigated by studying the response of selected model systems to UV radiation.

Investigations of emission and absorption spectra of molecules have already provided a wealth of knowledge about their electronic structure. The advent and continued development of pulsed lasers makes it possible to investigate ultrafast dynamical processes in a variety of systems, ranging from small molecules to complex biological systems. Pump-probe techniques nowadays allow to trace photophysical and photochemical processes on the time scale of molecular motion, that is mostly femtosecond timescale (1 femtosecond=10^{-15} s). This concept has lead to the birth of the research area called femtochemistry for which the 1999 Nobel Prize in chemistry was awarded to Ahmed H. Zewail [3]. A novel pump-probe spectrometer system based on noncollinearly phase matched optical parametric amplifiers (NOPAs) was developed in our laboratory [4, 5]. It provides us with tunable pump pulses in the UV and probe pulses in a broad spectral region between 230 and 1600 nm. This allows us to study ultrafast phenomena like charge transfer and electronic relaxation processes with an unprecedented time resolution of 60 fs for UV-C excitation pulses at 270 nm.

Because of its fundamental importance photoinduced charge transfer in donor-acceptor systems has been intensely studied in the last decades [6]. Intensive studies on charge transfer systems consisting of semiconductor and organic dye molecule were performed because of their usage in solar cells and have led to the fascinating evidence that intermolecular charge transfer can occur in less than 6 fs [7] or even 3 fs [8]. However studies on intramolecular charge transfer dynamics on the 10 fs time scale are very scarce and very few molecular systems have been found to be suitable model system [9-11]. A search for new donor-acceptor systems with high charge transfer rates is very important both for practical reasons and for the deeper understanding of various factors controlling this fundamental process. A very promising class of molecules are triphenylmethane lactones because of their

well defined geometry and weak ground state coupling. They are investigated here for the first time by means of femtosecond spectroscopy. The appearance of radical cations, which are the products of charge transfer in these systems, was resolved in time and served as the direct evidence for an extremely fast intramolecular electron transfer of 50 fs.

Due to the increasing amount of solar UV radiation on earth, recent scientific research focuses on the investigation of changes and dynamics in organic compounds induced by UV radiation. Photoionization is a nonradiative photoinduced process observed in the constituents of the DNA (nucleic acid bases) [12], as well as in amino acids (like tryptophan), which are the essential building blocks of human proteins [13-16]. In an aqueous environment photoionization generates solvated electrons and radicals which have a high chemical reactivity and contribute strongly to light induced degradation processes.

Despite the extensive knowledge on photoionization in neat water there are only few studies investigating the electron solvation in the vicinity of biomolecules - particularly of the tryptophan chromophore, indole [17-20]. Up to now the initial photodynamics of indole has not been resolved yet, although it is central to the generation and nature of indole radicals generated parallel with the long living solvated electrons [21-23]. In this thesis the excited state dynamics of indole is studied and the mechanism of electron solvation is described for the first time. Combining steady state and femtosecond spectroscopic observations, the controversial behavior of the excited indole, which fluoresces on a nanosecond time scale and undergoes photoionization within 100 fs, is explained with an ultrafast branching occurring immediately after excitation.

Much attention has been focused on the role of solvation relaxation processes in molecular dynamics [24-29], such as ultrafast inertial solvation dynamics [30-32] or longitudinal dielectric relaxation [33-37]. Within the scope of this thesis molecular dynamics in various solvents is investigated in order to determine their importance for intra- and intermolecular electron transfer.

Despite constant UV radiation living material manages to survive. It is assumed that evolution has selected molecular building blocks with particularly short excited-state lifetimes to minimize dangerous photoreactions in living cells [38-40]. The nonradiative process is presumably ultrafast internal conversion back to the electronic ground state [12]. In such a way the molecules quickly dissipate the photon energy before more severe chemical rearrangements can take place. Since the molecules exhibiting excited state intramolecular proton transfer (like o-hydroxybenzaldehyde) show a rather fast internal conversion from the electronically excited state to the ground state they are ideal model systems to investigate this process. In addition, these molecules are used as efficient UV protectors and their fast internal conversion plays an important role in converting high energy quanta to heat, an energy form of much lower destructive potential [41-43]. In this work internal conversion of

o-hydroxybenzaldehyde is explored using time resolved and steady state spectroscopy. The interplay of bright and dark electronic states is discussed as a possibility to circumvent the energy gap law.

The thesis is organized as follows. Chapter 2 gives some background on electronic and charge transfer processes relevant to the interpretation of the results presented later. In Chapter 3 various aspects of the experimental approach are discussed. In Chapter 4 the intramolecular electron transfer and the initial dynamics in triphenylmethane lactones in different solvents are investigated. Chapter 5 presents the study of the excited state dynamics of indole in water and a comparison to other solvents. In Chapter 6 the statistical behavior of the internal conversion in o-hydroxybenzaldehyde and the interplay of the three participating electronic states are explored. Finally, in Chapter 7 summary of the results of this thesis is given.

2 Relaxation processes after photoexcitation in solutions

Here an overview is given about the relaxation processes occurring after the photoexcitation of molecules in order to provide the necessary background for the discussion of the results presented in the following chapters.

After photoexcitation excited molecules in liquids experience various relaxation processes, which can be classified in 4 major categories: electronic relaxation, solvent relaxation, orientational relaxation and vibrational relaxation [44]. The topic of this work deals with the two former ones. Orientational relaxation is avoided in this work by using the "magic" polarization configuration of 54.7° between pump and probe laser beams as discussed in Section 3.4.3.

The electronic and solvent relaxations are explored by means of stationary spectroscopy as well as time resolved spectroscopy. Since many different processes are involved in the excited state relaxation it is not possible to get a clear picture of molecular dynamics observing and investigating only the reactants and products. Especially because some of the relaxations are extremely fast.

2.1 Characterization by stationary spectroscopy

In condensed and liquid phase, the excess vibrational energy is typically lost very fast to the surroundings and is not observable in the steady state spectroscopy. After the vibrational relaxation an electronic transition occurs and the molecule returns to the electronic ground state. A return to the ground state happens by emission of a photon or via radiationless transitions. Radiationless transitions were divided into two general classes by Kasha [45]: (1) internal conversion, where the molecule does not change its electron spin state (singlet → singlet or triplet → triplet), and (2) intersystem crossing, where the electron spin does change (singlet ↔ triplet). The emission behavior is embodied in two rules: Kasha's rule and Vavilov's law [46]. Kasha's rule states that if a molecule emits, it will always be from the lowest excited state of a given spin multiplicity. If the emission occurs from the lowest excited singlet it is named fluorescence and from the lowest excited triplet state is known as phosphorescence. Vavilov's law states that the fluorescence quantum yield is essentially independent of the excitation wavelength.

The fluorescence quantum yield (Φ_F) is defined as the ratio between the number of emitted photons and the number of absorbed photons. It can be expressed using the rates of the deactivation channels [47]:

$$\Phi_F = \frac{N_{emit}}{N_{abs}} = \frac{k_{rad}}{k_{all}} = \frac{k_{rad}}{k_{rad} + k_{IC} + k_{ISC} + k_{ET}} = \frac{1/\tau_{rad}}{1/\tau_{fl}}, \qquad (2\text{-}01)$$

where k_{rad} is the rate for the radiative return to the ground state, k_{IC} for the internal conversion, k_{ISC} for the intersystem crossing and k_{ET} for the energy transfer. τ_{fl} is the excited state lifetime usually observed from a fluorescence decay and thus also known as a fluorescence lifetime. If the spontaneous emission of radiation is the only pathway for return to the ground state, the average statistical time that the molecule spends in the excited state is called the natural radiative lifetime τ_{rad}. The radiative lifetime depends mostly on the oscillator strength of the corresponding electronic transition [48] and to some extend on the environment. Thus, the solvent can influence the radiative lifetime either by means of its effect on the transition moment or through its refractive index [47].

2.2 Characterization by femtosecond spectroscopy

To observe the evolution of chemical reactions in order to understand molecular excited state dynamics time resolved spectroscopy has to be applied. Since some of the molecular electronic relaxation or charge transfer processes are extremely fast, ultrashort laser pulses (< 100 fs) are needed to resolve these phenomena in time. For pump-probe spectroscopy two laser beams are spatially crossed in a sample, one exciting the molecules and the other detecting a spectral response of the molecules in time. This experimental method is discussed in more details in Chapter 3.

By means of the presented experimental techniques the following ultrafast phenomena are studied within this thesis: intramolecular electron transfer in triphenylmethane lactones, charge transfer to solvent generating solvated electrons from indole and internal conversion of o-hydroxybenzaldehyde.

2.3 Electron transfer (ET)

2.3.1 The classical Marcus theory

Over the past half century the theory behind one of the most common reactions in chemistry and biology, the theory of electron transfer has been investigated. Electron transfer, one of the simplest of chemical events, profoundly affects chemical reactivity by inverting normal electron densities in an electron donor-acceptor pair, thus activating previously inaccessible reaction modes. The basic principles presented below are discussed in several reviews [49-52].

The transition between the donor D and acceptor A occurs assuming the horizontal Franck-Condon principle, that is the nuclear configuration of the reactant and product is the same at the point of the transition state and the internal energy is conserved. Both the reactant (DA) and the product (D^+A^-) have a potential energy which is a function of many intra- and intermolecular nuclear coordinates resulting in a multidimensional potential surface. The coordinates undergoing significant changes during electron transfer include the separation distance of the reactants, the molecular structure of the reactants and the orientation of the solvent molecules. In transition state theory a reaction coordinate is introduced, so that the potential energy surface can be reduced to a one-dimensional profile.

Marcus showed [53] that the system is represented in Gibbs (free) energy space, the Gibbs energy profiles along the reaction coordinate can be approximated as parabolas with the same curvatures. If the change of entropy in the discussed systems (extremely fast reactions) can be approximated with zero, a change of Gibbs energy (named also free enthalpy) equals a change of enthalpy.

The parabolic free-energy surfaces as a function of the reaction coordinate are illustrated in Figure 2.1 for a variety of conditions. The parameter shown in the diagram are: λ, the reorganization energy due to changes in bond distances and angles as well as solvation, which represents the change in free energy if the reactant is deformed to the equilibrium configuration of the product without transferring the electron; ΔG, the free reaction energy, which is the difference in free energy between the equilibrium configurations of the reactant and product states (the driving force); and ΔG^*, which corresponds to the free activation energy for ET. From analytical geometry of intersecting parabolas a relationship between the two free energies follows:

$$\Delta G^* = \frac{\lambda}{4} \cdot \left(1 + \frac{\Delta G}{\lambda}\right)^2 \tag{2-02}$$

The rate constant for ET processes is dependent on the free activation energy, ΔG^* and can be expressed as:

$$k_{ET} = A \cdot e^{-\frac{\Delta G^*}{k_B T}} \tag{2-03}$$

where k_B is the Boltzman constant and T the temperature.

As shown in Figure 2.1 there are three free energy regimes after Marcus, each corresponding to another dependence of the ET rates on the free reaction energy ΔG. In the normal regime ($\Delta G < \lambda$ and $-\Delta G < \lambda$) the activation energy (ΔG^*) decreases if the free reaction energy (ΔG) is increased, leading to an increase of the ET rate. In the inverted regime ($-\Delta G > \lambda$) increasing further the free reaction energy leads to an increase of the activation energy and consequently to a decrease of the ET rate.
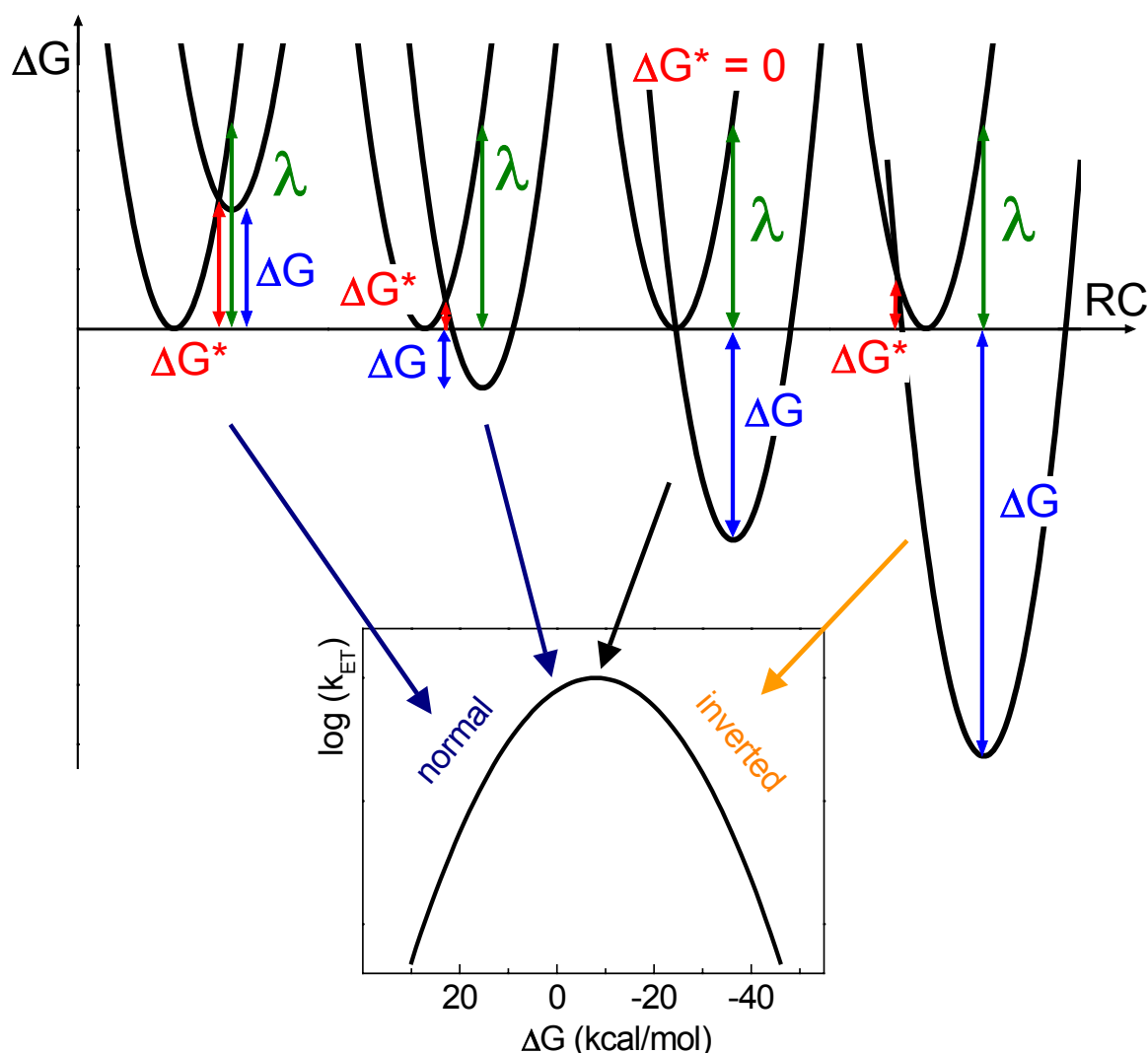
Figure 2.1 The free energy regimes after Marcus (top) and the corresponding dependence of the transfer rates on the free reaction energy (bottom). In the normal regime the ET rate increases with decreasing the free activation energy until the value ΔG* = 0 (ΔG = -λ). Further on, in the inverted region, an increase of the free activation energy causes a decrease of the ET rate. RC is the reaction coordinate.

The maximum of the ET rate which corresponds to the fastest ET processes appears for a small negative values of ΔG as presented in the bell-shaped curve in Figure 2.1.

The first step in determining the feasibility of an electron-transfer pathway for a bimolecular ET reaction should involve an evaluation of the free reaction energy changes (*ΔG*) using the Weller equation [54]:

$$\Delta G = -E_{00} + E(D^+/D^0) - E(A^0/A^-) - E_{IP}, \qquad (2\text{-}04)$$

where E_{00} is the energy difference between the S_0 and S_1 states, $E(D^+/D^0)$ the oxidation

potential of the electron donor, $E(A^0/A^-)$ the reduction potential of the electron acceptor and E_{IP} the ion pair stabilisation energy estimated from:

$$E_{IP} = \frac{1}{4 \cdot \pi \cdot \varepsilon_0} \frac{e^2}{\varepsilon_S \cdot d_{IP}} , \qquad (2\text{-}05)$$

where e is the electron charge, ε_S the dielectric constant of the solvent and d_{IP} the distance between the donor and the acceptor moiety. The estimation of the free reaction energy given in (2-04) can be illustrated by means of the energy gap.

2.3.2 Special features for solvated electron reactions

Since its spectral identification in 1962 [55] the solvated electron in water has been attracting much interest in wide fields in chemistry, physics and biology because of its fundamental importance [56]. In addition to the features considered above, which the generation of solvated electrons and ordinary electron transfers have in common, those of the solvated electron possess several novel aspects [57, 58].

(1) The electronic wave function of a solvated electron, spread over several solvent molecules, should be very sensitive to orientation fluctuations of these molecules, unlike that of an ordinary reactant.

(2) Since the solvated electron is generated there is a change in number of particles.

(3) Unlike many of the conventional ETs, many reactions involving solvated electrons are diffusion controlled.

2.4 Internal conversion (IC)

Internal conversion is a relaxation of the excited state via nonradiative transition to the original electronic ground state. It is not possible to detect the rates of IC directly. Since it is a competitive process to the fluorescence, the IC rate can be determined indirectly by observing the fluorescence quantum yield.

The rate of internal conversion, a radiationless transition between isoenergetic levels of different electronic states of the same multiplicity, may be of the same order of magnitude or even faster than vibrational relaxation. It depends on the energy separation between the zero vibrational levels of the electronic states involved. From experimental results reported it has been concluded that for aromatic hydrocarbons the radiationless transition $S_1 \rightarrow S_0$ is negligible if the energy difference $\Delta E(S_1 - S_0)$ between S_1 and S_0 states is larger than 60 kcal/mol. For molecules with low-lying singlet states, however it becomes increasingly more important and it can account for more than 90% of the S_1 state deactivation. These observations can be summarized and the rate of internal conversion can be described by simple exponential relationship:

$$k_{IC} = 10^{13} \cdot e^{-\alpha \cdot \Delta E(S_1 - S_0)}, \qquad\qquad (2\text{-}06)$$

which shows the dependence of the rate constant k_{IC} on the energy gap $\Delta E(S_1 - S_0)$ and which is referred to as the energy-gap law [46, 47]. A proportionality constant α is a characteristic of particularly molecular system, approximately equal to 4.85 eV^{-1} for benzenoid aromatics.

2.5 Influence of the solvation on the electronic relaxation dynamics

The term solvation refers to the surrounding of each dissolved molecule or ion by a shell of more or less tightly bound solvent molecules [59]. This solvent shell is the result of intermolecular forces between solute and solvent. For aqueous solutions the term hydration is often used. The solvation energy is considered as the change in Gibbs energy when an ion or molecule is transferred from vacuum (or the gas phase) into a solvent. The Gibbs energy of solvation is a measure of the solvation ability of a particular solvent and is a superposition of four components of different nature [59]: (1) the cavitation energy linked with the hole which the dissolved molecule or ion produces in the solvent; (2) the orientation energy corresponding to the phenomenon of partial orientation of the polar solvent molecules caused by the presence of the solvated molecule or ion; (3) the isotropic interaction energy corresponding to unspecific intermolecular long range forces (electrostatic, polarization and dispersion energy); and (4) the anisotropic interaction energy resulting from the specific formation of hydrogen bonds or donor-acceptor electron pair bonds at well localized points in the dissolved molecules.

Thus, the solvent can influence a chemical reaction in a number of ways.

2.5.1 Static solvent influence

The solvent can act in a static sense to change the energies of the reactants and products (the potential surface on which the reaction occurs) compared to the energies in the gas phase.

The difference between the ionization potential of an impurity atom or molecule in a condensed or liquid phase (I_{liq}) and in the gas phase (I_{gas}) may be expressed by the following equation [60, 61]:

$$I_{liq} = I_{gas} + P_+ + V_0, \qquad\qquad (2\text{-}07)$$

where P_+ is the adiabatic electronic polarization energy of the medium by the positive ion and V_0 is the minimum energy of a "quasi-free" electron in the liquid relative to an electron in vacuum (the conduction band edge energy of the solvent). Considering the solvent as a dielectric continuum, P_+ can be estimated from Born's equation [62]:

$$P_+ = -\frac{e^2}{2r_+} \cdot \left(1 - \frac{1}{\varepsilon_\infty}\right),$$ (2-08)

where e is the elementary charge, r_+ the effective ion radius and ε_∞ the optical dielectric constant of the solvent.

2.5.2 Dynamic solvent influence

The solvent can also act in a more dynamic way by exchanging energy and momentum with the reacting species and by responding to the change of their charge distribution. Static solvent effects have major influence on the free activation energy, ΔG^* [24]. Dynamical solvent effects appear in the frequency factor A (see 2-03) and are usually discussed in terms of friction, which can be either of collisional or dielectric origin. Collisional friction is important for reactions involving large-amplitude motion, such as isomerization and dissociation reactions. In these cases the solvent most often disables reaction by blocking the way of the desired reactive motion.

Another type of dynamical solvent effect involves the "dielectric" friction that arises in polar solvents. The coupling between solvent and reacting system in this case is electrostatic in origin. For electron and other charge-transfer reactions, such polar interactions can be quite strong, and it has long been recognized that the static aspects of this interaction can significantly affect reaction rates. Such dramatic changes mainly involve modification of the free activation energy ΔG^* by polar solvation [24].

Solvatochromism is an example for the influence of polar solvents to excited state dynamics appearing as an additional shift in fluorescence spectra of dissolved molecules [59]. The dipole moment of the solute causes the reorganization of polar solvent molecules in order to stabilize the system in the potential energy minimum. Thus a lowering of electronic states occurs. A positive or negative solvatochromism can appear depending on whether the excited state or the ground state is more strongly stabilized. Since the excited state is frequently more polar than the ground state, positive solvatochromism is commonly observed for $\pi \rightarrow \pi^*$ transitions [47]. Such a solute-solvent interaction can be easily identified since it increases with increasing solvent polarity.

Many theoretical studies tried to explain these dynamical aspects of solvation, providing a relation between the macroscopic dielectric relaxation and microscopic solvation dynamics [25, 31, 32, 37, 63]. Simple continuum models consider the solute as a point charge or point dipole in a spherical cavity. Such a model predicts an exponential response of the solvents:

$$S(t) = e^{-\frac{t}{\tau_L}}.$$ (2-09)

The solvent time scale is characterized by the longitudinal relaxation time τ_L:

$$\tau_L = \frac{\varepsilon_\infty}{\varepsilon_0} \cdot \tau_D \ ,$$

(2-10)

where ε_0 is the static (zero frequency) dielectric constant, ε_∞ is the optical (high-frequency) dielectric constant, and τ_D is the macroscopic dielectric (Debye) relaxation time. The terms of "transverse relaxation time" and "longitudinal relaxation time" are discussed and clarified in Ref. [34]. As a general rule, the transverse relaxation time represents single molecule dynamics and is not influenced by dipolar interactions while the longitudinal relaxation time includes the effects of dipolar interactions. The results of conventional dielectric relaxation measurements, which probe the response of a dielectric medium to an applied electric field in the long wavelength limit (microwaves), can be used to predict solvation dynamics on the scale of molecular distances.

The development of ultrashort laser pulses enabled time resolved fluorescence and absorption measurements that probe directly solvent polarization dynamics over molecular length scales [29, 30, 36]. For instance, the time resolved fluorescence spectrum of a chromophore whose permanent dipole moment undergoes a significant change upon optical excitation is influenced by the response of the nearby solvent molecules to this change in charge density. As the solvent molecules reorganize due to the equilibrium with the new charge distribution, the fluorescence spectrum shifts, what shows the progress of the solvation energy relaxation. This can be described with the solvation time correlation function:

$$S_{obs}(t) = \frac{\nu(t) - \nu(\infty)}{\nu(0) - \nu(\infty)} \ ,$$

(2-11)

where ν's refer to the frequencies of some characteristic point in the spectrum (e.g. its maximum or mean fluorescence frequency) at times t, zero and infinity. The observed spectral response, $S_{obs}(t)$ shows a more complicated behavior as predicted with the solvation response function, $S(t)$ (2-09) [26, 35]. The experimental studies performed by Rosenthal et al. [30] reported for the first time a biphasic nature for the solvent response. The initial fast part of the solvent response is assigned to small amplitude inertial rotational motions of solvent molecules in the first solvation shell. The slow component arises from diffusive restructuring of the first solvent shell. This effect is also known as polarization diffusion, where the solvent relaxation occurs by translational motions of the solvent dipoles along a polarization coordinate. Debye dielectric relaxation was treated as a diffusive type of mechanism, thus some authors assume that the diffusive solvation time corresponds to the longitudinal dielectric relaxation time [36]. Recently multi-exponential models were also applied to fit experimental data for various solvents [27].

Also some nonpolar solvents show solvation dynamics qualitatively similar to polar solvents [28], but they can not be simply modeled using the solvents dielectric response as empirical input.

3 Experimental methods

3.1 Experimental setups for ultrafast absorption spectroscopy

The photoinduced dynamics in lactones and indoles are investigated by femtosecond pump-probe spectroscopy. Two different setups are used depending on the light source applied for probing. Transient spectra are obtained using white light continuum as probe, while time resolved measurements are performed with a resolution of 60 fs by probing at specific wavelengths with non dispersive detection. A NOPA (described below) used as a tunable pump and probe laser source is pumped by a commercially available Ti:sapphire chirped pulse amplifier system (CPA 2001, Clark MXR), which provides 150 fs horizontally polarized pulses with ~1 mJ output energy at 775 nm and 1 kHz repetition rate. A fraction of 0.6 mJ of the output energy is sufficient to pump both setups.

3.1.1 Noncollinearly phase matched optical parametric amplifier

Noncollinearly phase matched optical parametric amplifier (NOPA) [4, 5] is used in the experiment as a tunable pump and probe laser source. It delivers pulses, which are compressible with a prism compressor to well below 30 fs and are tunable in a broad spectral region between 450 and 1600 nm. Figure 3.1 shows schematically a two-stage NOPA, which consists of (1) a stage for the generation of white light continuum in a sapphire disc by focusing a small fraction of the NIR CPA pulses. Two subsequent stages for parametric amplification of the seed white light in BBO crystals (3) are pumped by the frequency doubled (2) CPA output. The output amplifier of the first stage is used as the seed light of a second amplification stage.
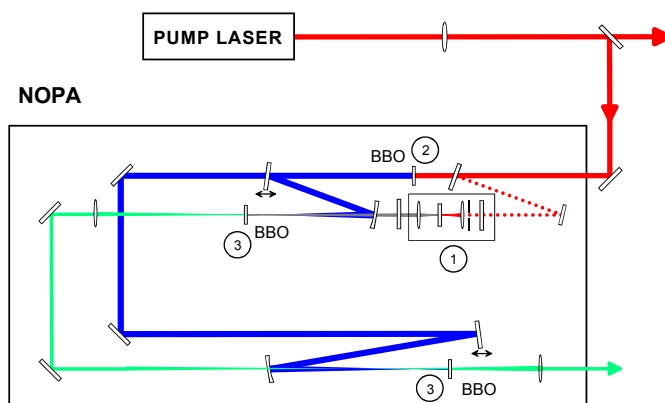

Figure 3.1 Scheme of a two-stage NOPA. Small fraction of the CPA output is used to generate a white light continuum (1). The rest of 0.25mJ CPA output is frequency doubled (2) and used as pump for two subsequent stages of parametric amplification process in BBO crystals (3).

NOPA as the probe pulse

For the two-color experiments the probe light is generated by a single-stage NOPA tuned to a wavelength of 475 ± 5 nm and compressed to ~30 fs with a fused silica prism sequence (see Figure 3.2). The spectra are measured with a fiber optic spectrometer (Ocean Optics S 2000), and a NOPA PAL intensity autocorrelator [64] is used to characterize the temporal profiles of the pulses. Values of pulse lengths are calculated assuming $sech^2$ distribution of the pulse shape [65]. Figure 3.2(a) exhibits the autocorrelation of a pulse at 478 nm that is Fourier limited according to its spectral width. A pulse at 470 nm shown in Figure 3.2(b) is not Fourier limited.
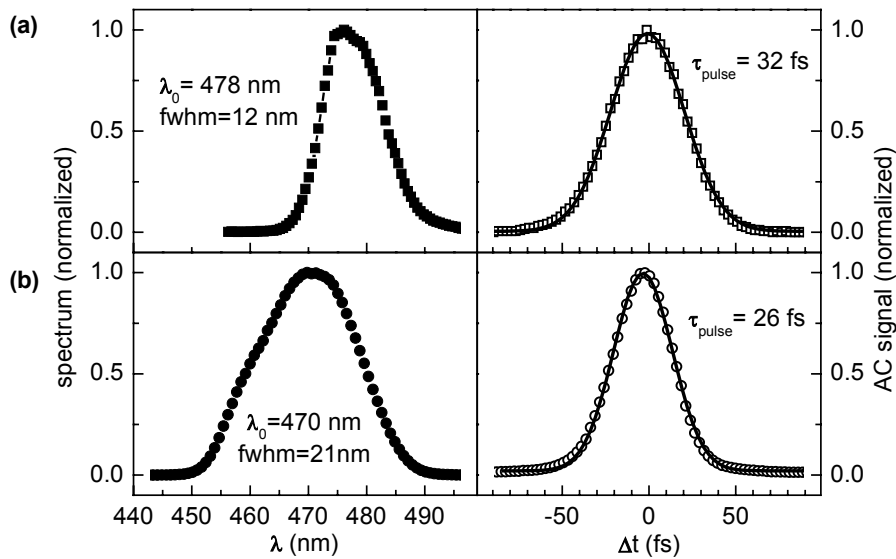
Figure 3.2 Spectra of probe pulses (full symbols) at (a) 478 nm (squares) and at (b) 470 nm (circles) and corresponding autocorrelation traces (open symbols). Values of pulse lengths are calculated assuming $sech^2$ distribution of the pulse shape.

3.1.2 UV light generation and compression

The UV excitation pulses in both setups are generated from a two-stage NOPA that delivers pulses at 540 nm with an energy of 7-8 μJ [4, 5]. Compression of the pulses in the visible spectral region to a minimum duration is performed with a fused silica double-pass prism pair. The apex angle of the prism is cut such that the angle of incidence is the Brewster angle at the central wavelength. Thus, the Fresnel reflection losses for p-polarized light are minimized and the system shows 89 % of energy transmission efficiency. The compressed visible pulses are focused by a 200 mm lens into a 110-μm thick type I BBO crystal cut at 45°. Second harmonic generation (SHG) lead to pump pulses at 270 nm with an energy of ~1-2 μJ (the highest achieved doubling efficiency was 25 %) [65]. In the first experiments the compressor in the visible spectral region is used only to compress the pulses to

a minimum duration at the SHG crystal. An additional compressor in the UV part of the beam path is used to compensate for the dispersion that the UV pulses accumulate between the SHG crystal and the sample. Since the SHG signal is vertically polarized, a special UV prism compressor was designed to keep the plane of the compressor parallel to the optical table without the need for rotating the polarization of the UV light. Fused silica prisms with an apex angle of 45 are chosen. This results in an angle of incidence of about 35° for the UV pulses. For this moderate angle of incidence a broadband anti-reflection coating for s-polarized light is available (BBAR240-420/35s; LASER COMPONENTS GmbH), which reduces the loss per surface to 2 % in the 230-460 nm region. A dielectric mirror is used as an end mirror. This UV compressor transmits 88 % of the incoming UV light.

Another way to compress the UV pulses is to use only one set of prisms in the visible beam and no additional UV compressor. It is shown (see Figure 3.3) that a better time resolution can be obtained by using the compressor only in visible. In this way the pulses are negatively chirped (overcompressed) in the visible and they are not the shortest when they arrive to the BBO crystal, resulting in a reduced SHG efficiency. On the other hand, the pulses can be stronger focused into the BBO crystal and no significant energy loss of the UV pulses is observed. The advantage of such a compression scheme is that additional second order chirp introduced by the UV prisms can be avoided, which can not be compressed as efficiently as the linear chirp. A further valuable practical aspect is that only one compressor is implemented in the setup, thus the everyday laboratory usage of this arrangement is easier.
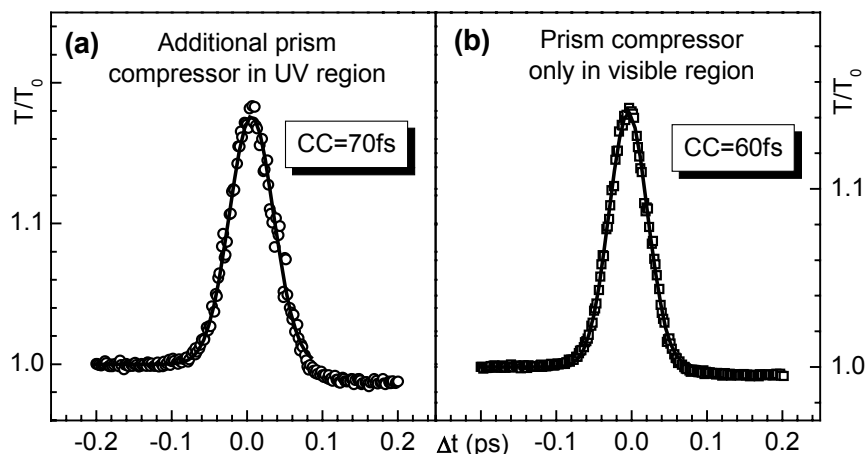

Figure 3.3 Cross-correlation signal achieved with two different ways of compression. (a) Additional prism compressor in UV region is used; (b) Prism compressor is applied only in visible region. Measured CC signals as the amplification of the probe pulse by the pump pulse (circles and squares) and the corresponding fits (solid lines).

Figure 3.4 shows two typical cross-correlation (CC) traces together with the corresponding spectra of UV pump pulses measured under the same conditions as the auto-correlation signals shown in Figure 3.2. The shown traces of CC signals are measured as the amplification of the probe pulse by the pump pulse. The width of the UV spectrum is limited by the thickness of the BBO crystal (0.11 mm) due to the phase matching [65-67]. In order to obtain an adequate amount of pump energy it is necessary to use a crystal of such a thickness. The values for the pulse length of the UV pump pulses are calculated from the width of the cross-correlation signals and the AC signal of the probe. The calculations are performed assuming sech^2 pulse shape. The value of the measured CC signal is important because it gives the time resolution of the experiment. The lengths of the individual pulses are less important and are given here only as comparative values.
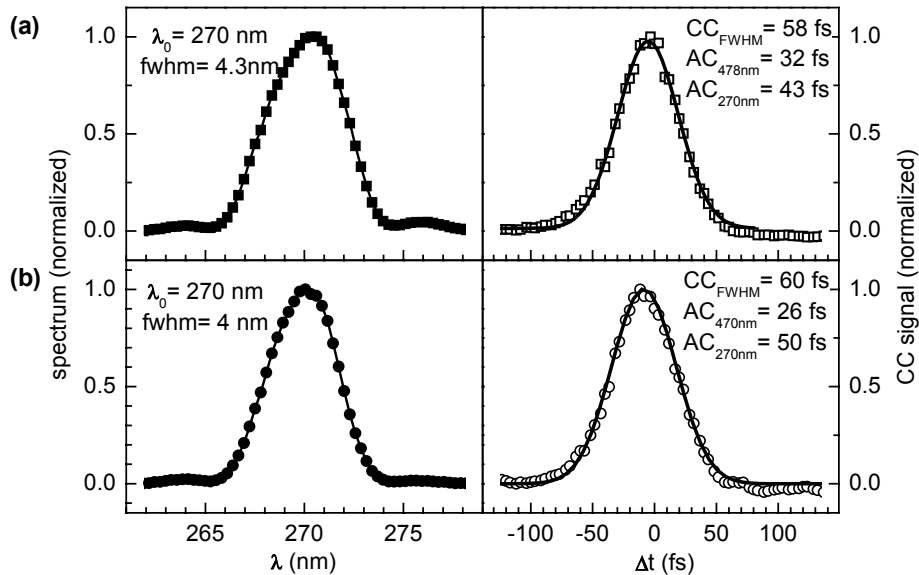
Figure 3.4 Two typical spectra of the pump pulses (full symbols) and the corresponding cross-correlations (open symbols) obtained with a probe pulses at (a) 478 nm (squares) and (b) 470 nm (circles). CC signal shows amplification of the probe pulse by the pump pulse. The calculations are performed assuming sech^2 pulse shape.

3.1.3 Two-color spectroscopy

Two-color experimental setup is shown in Figure 3.5. A commercially available Ti:sapphire chirped pulse amplifier system (CPA 2001, Clark MXR), which provides 150 fs horizontally polarized pulses with ~1 mJ energy at 775 nm and 1 kHz repetition rate is used as pump laser. The energy fraction of 0.5 mJ is applied for pumping two NOPAs to generate tunable ultrashort pump and probe pulses. A short description of the NOPAs as well as the generation of the UV excitation pulses is given above (see Section 3.1.1 and 3.1.2). Pulses generated with NOPA are compressed in a double-pass prism pair. A motorized translation stage (M-505.6PD, Physik Instrumente) is used to vary the time delay between the pump

and probe pulse up to 1 ns. The solution is pumped through a sapphire nozzle with a slit width of 120 μm to generate a free flowing liquid jet of the solution. The excited volume in the thin sample jet is thereby exchanged after each laser pulse. The excitation induced transmission change of the sample is monitored by measuring the probe energy with a photodiode (integrating photodiode module PDI-400-UV, Becker & Hickl GmbH, Berlin) after the sample with and without excitation. This is achieved with chopper (HMS Light beam chopper 221) in the pump beam that blocks every second pump pulse. Another photodiode detects a reference beam of the probe in order to normalize for the fluctuations in laser intensity. Rationing of the probe and reference signals with and without the excitation gives the final detected transmission change (T/T_0) which allows optical density change (ΔOD) as small as 10^{-3} to be readily detected.

$$\frac{T}{T_0} = \frac{S_{probe}^{excited} / S_{reference}^{excited}}{S_{probe}^{non-excited} / S_{reference}^{non-excited}} = 10^{-\Delta OD} \tag{3-01}$$
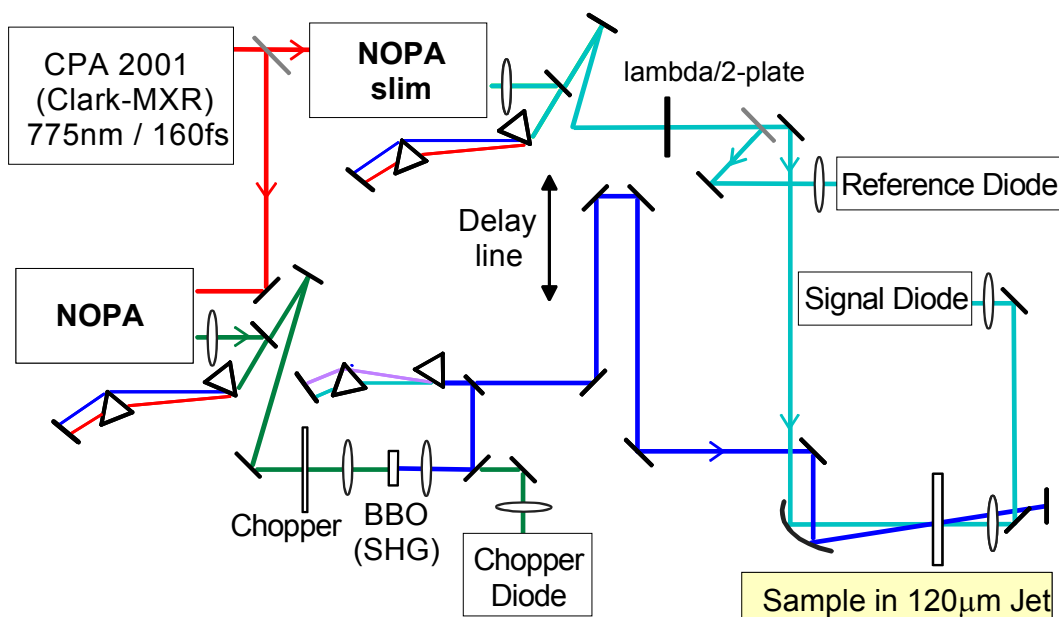
Figure 3.5 Experimental setup for two-color experiments. A commercially available CPA delivers the fundamental pulses. UV pump pulses are obtained by frequency doubling the NOPA output. A chopper wheel is used to cut every second pump pulse in order to compare signal with and without excitation. The tunable visible probe pulses are obtained from a one stage NOPA (slim). The time delay between the pump and probe pulses is obtained by moving a motorized translation stage.

3.1.4 White light continuum probing

Figure 3.6 presents experimental setup for probing with a white light continuum, which is applied to obtain transient spectra. Major parts of the experimental setup remain the same as in the two-color setup, described above (see Section 3.1.3).
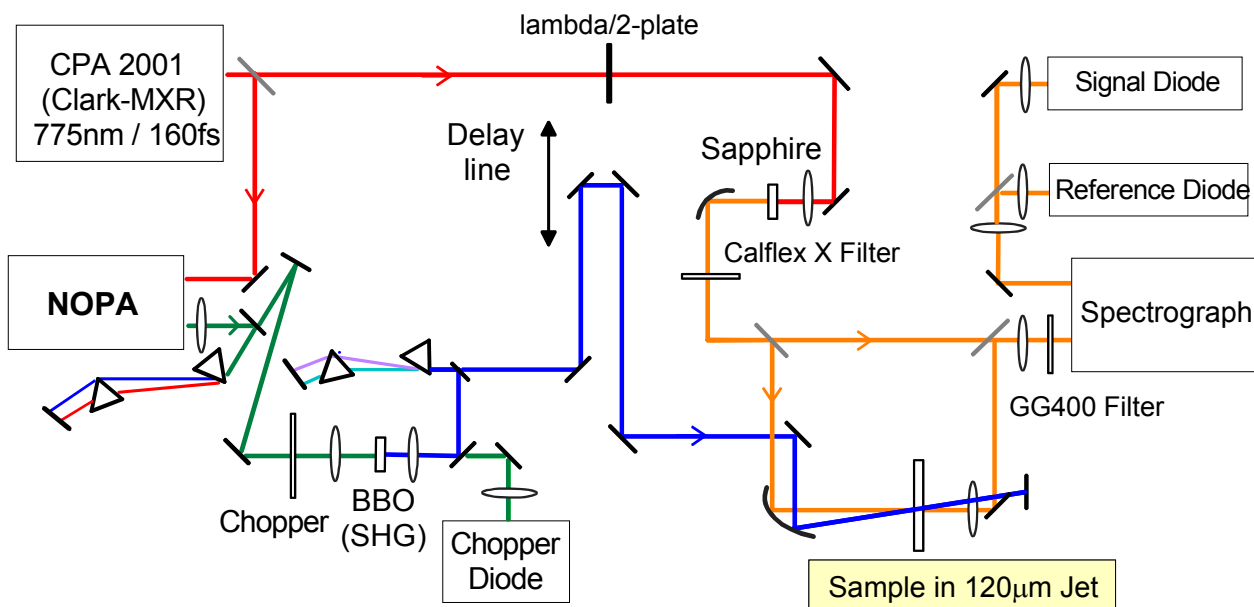
Figure 3.6 Experimental setup for probing with a white light continuum. A commercially available CPA delivers the fundamental pulses. UV pump pulses are obtained by frequency doubling the NOPA output. A chopper wheel is used to cut every second pump pulse in order to compare signal with and without pump. The white light continuum is generated in a Sapphire plate. The time delay between the pump and probe pulses is adjusted by moving a motorized translation stage.

A small fraction of several microjoules from the CPA pulses is focused by a 50 mm lens into a 2-mm thick sapphire disc in order to generate a white light continuum. The spectrum used as probe for the measurements on lactones is in the region 435-730 nm and for the measurements on indole is between 450 nm and 740 nm. As it is shown in Figure 3.7, the appropriate region of the white light continuum is determined from (a) the quantity of generated photons (signal on the detector >100 mV), (b) from the noise and (c) from the amount of light passing through a 60-μm pinhole, which is used to check the quality and beam size of the probe pulses. Radius of the probe beam at focus is about 35 μm, what is at least half the size of the radius of the pump beam. It should be noted that the foci of the different spectral components which contribute to the probe pulses are spatially shifted one to another, so the overlap with the pump pulses is made with a focus of the wavelength at the middle of the spectral region.

A white light continuum generated in CaF_2 provides significantly more seed photons especially for shorter wavelengths ($\lambda < 500$ nm) than the white light continuum generated in sapphire used in this setup [68]. Despite this knowledge, the instability of CaF_2 material upon the pump laser used in our system disables the use of such a white light continuum as probing device. The pump pulses of 150 fs have to be focused stronger, so that they destroy a CaF_2 crystal. For measurements performed in this work it is actually not critical to obtain the shorter wavelengths than already obtained when probing with a white light continuum.

The white light probe together with a reference beam is dispersed after the sample with an imaging grating monochromator (focal length 20 cm; 600 lines/mm; AMKO). The slits of the monochromator are adjusted to 1 mm, which corresponds to a spectral resolution of 8 nm. The energy of the spectral component passing through the monochromator is measured with the photodiode, mentioned above (see Section 3.1.3). Another photodiode detects a reference beam of the probe in order to normalize for the fluctuations in laser intensity.
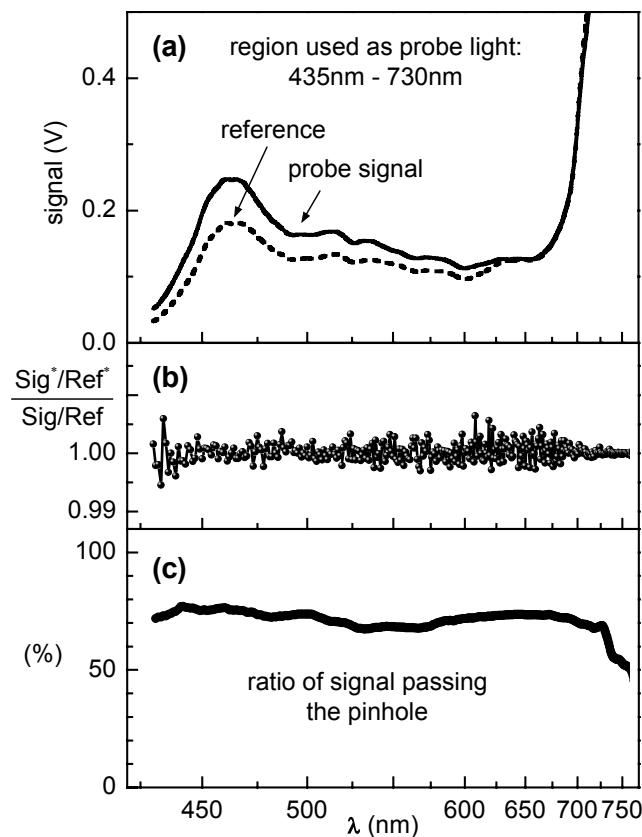
Figure 3.7(a) Spectrum of the white light continuum measured with the probe (solid line) and reference (dashed line) photodiode; (b) Noise determined from the Signal/Reference ratio with and without excitation; (c) Amount of signal passing through a 60-μm pinhole. The region of white light continuum used for probing is in this case from 435 to 735 nm.

A Calflex X filter is used to avoid saturation of the signal in the region near the fundamental wavelength. Its spectral characteristic is shown in Figure 3.8.
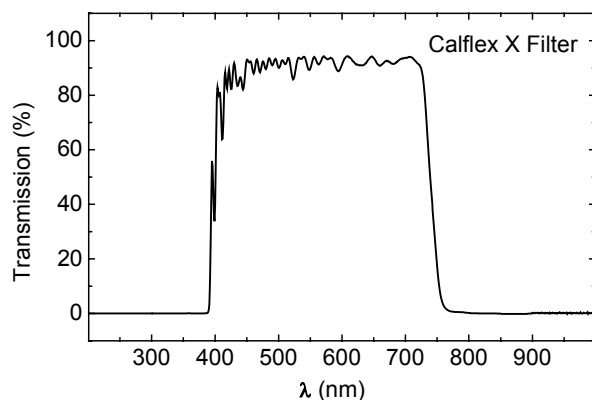
Figure 3.8 Transmission spectrum of the Calflex X filter, which is used to minimize strong signal in the region of the fundamental wavelength.

Data can be obtained in the following two ways with this setup: either spectrally resolved measurements corresponding to a fixed time delay between pump and probe or time resolved measurements at a fixed probe wavelength. The signal appears earlier at shorter wavelengths than at longer wavelengths, which is a consequence of the temporal distribution of the different spectral components of the pulse, i.e. its chirp [67].
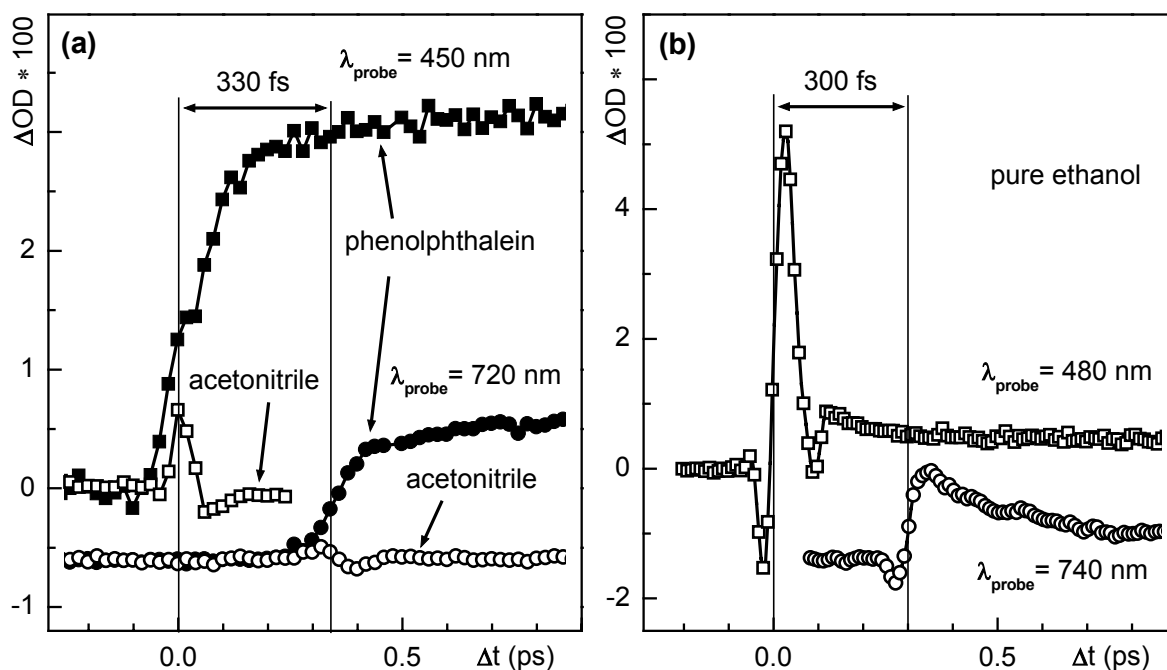
Figure 3.9 The chirp of the white light continuum determined from the delay between the signals: (a) probed at 450 nm (squares) and 720 nm (circles), for the measurements on lactones (phenolphthalein in acetonitrile); (b) probed at 480 nm (squares) and 740 nm (circles), for the measurements on indole (signal of neat ethanol).

The chirp of the white light continuum used in the experiments on lactones (see Figure 3.9(a)) leads to a delay of 330 fs between the spectral components at 450 nm and at 720 nm. This delay of 330 fs is corrected for the time resolved measurements shown in the following chapters but not in the transient spectra. The correction in the latter case is not necessary, because the spectra are measured at least 1 ps after the excitation. The same procedure is applied to the measurements on indole, where the delay between the spectral components at 480 nm and at 740 nm is 300 fs (see Figure 3.9(b)).

3.2 Time resolution of the experiment

3.2.1 NOPA-NOPA experiment

In order to determine the time resolution of the experiment, difference frequency mixing between pump (270 nm) and probe wavelength (470-480 nm) is performed at the place of the sample using a 50-μm thick type I BBO crystal cut at 45° [65]. The thickness of the used BBO crystal is chosen to satisfy the requirements set by the effective interaction length [66].

Instead of the real cross-correlation (CC) signal, amplification of probe pulse by the UV pump pulse, that occurs simultaneously with the CC signal, is detected. It is experimentally verified that both signals are giving the same values for the pulse length.

The experimentally observed influence of the window of a standard 1 mm sample cell on the width of the cross-correlations is shown in Figure 3.10. The observed result is in agreement with the calculation of the group velocity dispersion [67]. The 1.25 mm window of the fused silica sample cell causes additional dispersion of the UV pulse of several femtoseconds, while the free flowing jet of solvent (120 μm) causes less than 1 fs lengthening of the UV pulse.
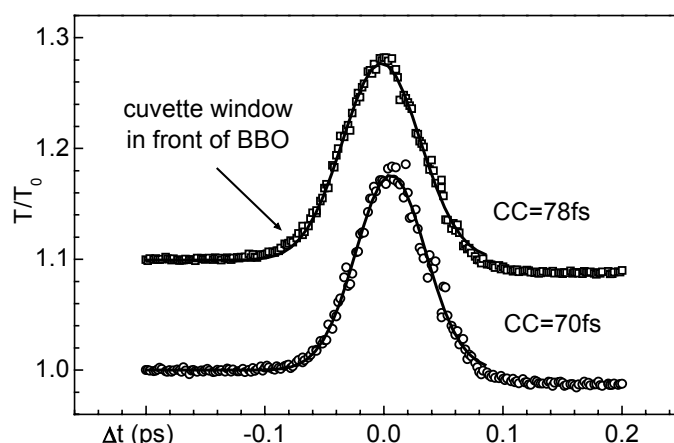

Figure 3.10 CC signal performed in BBO crystal with (squares) and without (circles) cuvette window. UV pulses are compressed with two prism compressors (one in the visible and one in the UV).

Comparison between the typical CC signal measured before and after the measurements performed on the molecules (see Figure 3.11) confirms very stable conditions during the measurements (approximately 5-10 hours).
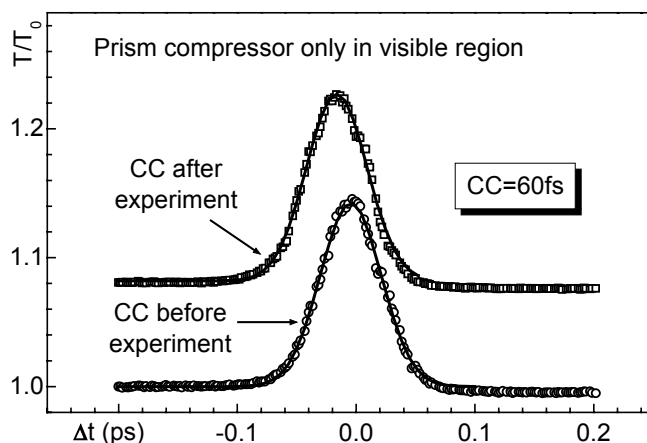
Figure 3.11 Typical CC signal of pump and probe pulses measured before (circles) and after (squares) the experimental run. The UV pulses are compressed with one prism compressor in the visible.

The achieved time resolution of sub-60 fs is close to the limit set by the group velocity mismatch [66, 67]. Due to their different group velocities, pump and probe pulses arrive at the end of the sample (120 μm jet) with a difference of 47 fs, which hinders better time resolution.

3.2.2 NOPA-white light continuum experiment

In experiments where the white light continuum is used as probe the time resolution is determined from the coherent artifact that can be observed in some solvents. As discussed below (Sect. 3.4.2) application of extreme high pump power density ($>10^{14}$ W/m^2) due to the very short laser pulses (shorter than 100 fs) and spectrally broad probe pulses (white light continuum) causes significant artifacts originating from the solvents. These signals terminate rapidly following the excitation, thus their duration is comparable with the temporal width of the pump-probe cross-correlation function. It is verified by using the NOPA-NOPA setup that this zero artifact vanishes after a time that is related to the pump-probe cross-correlation measured with a BBO crystal (see Figure 3.12), and therefore can be used for determining the time resolution of the experiment.
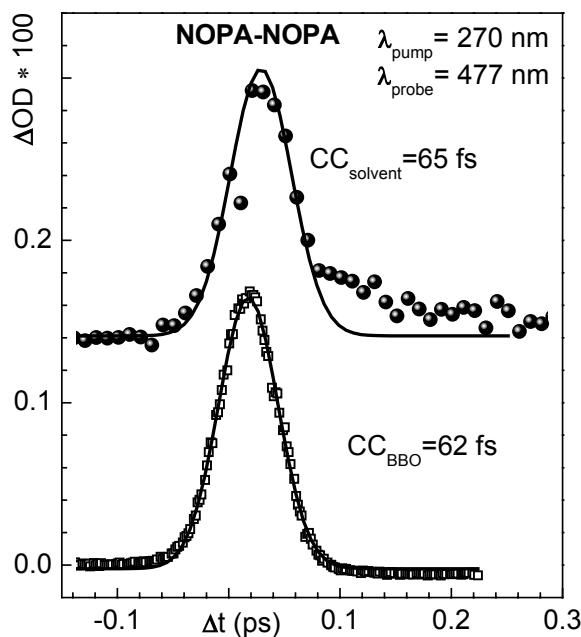
Figure 3.12 Coherent artifact around time zero measured in solvent ethyl acetate corresponds to the CC signal determined with a BBO crystal.

Figure 3.13 presents typical coherent artifact signals in solvents, that are used to determine the time resolution in measurements with a white light continuum as the probe. They are taken at two different wavelengths of the probe and are relatively shifted in time due to the temporal chirp of the spectral components of the white light. It can be noted that the coherent artifact in the blue part of the probe wavelength shows greater effect of the coherent artifact. The temporal width shows also a dependence on the probe wavelengths, resulting from the group velocity mismatch, that causes a temporal broadening of the CC signal as the probe wavelength is more far away from the pump wavelength. Such a behavior (see Figure 3.13) is in agreement with previously reported results [69].
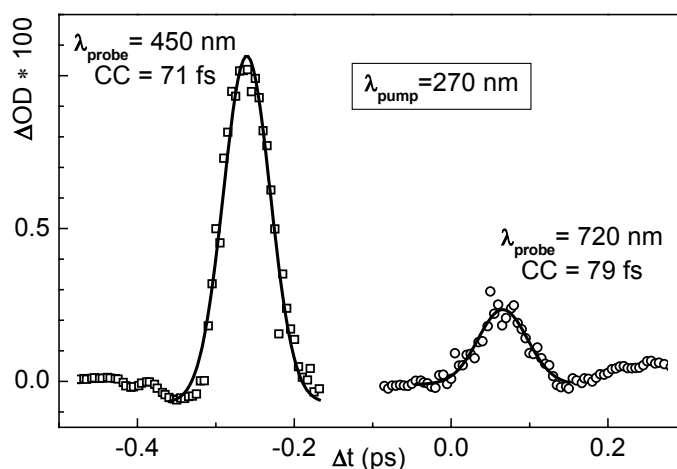
Figure 3.13 Coherent artifact in solvent ethyl acetate excited at 270 nm and probed at 450 nm and 720 nm.

3.3 Samples

3.3.1 Preparation of samples

The highest purity indole (99.7 %) and 1-methylindole (99.7%) obtained from Merck and OHBA (99.7 %) from Sigma Aldrich are used as received. Malachite green lactone (MGL) has been synthesized as described by Fischer [70] and is repeatedly recrystallized from *n*-propanol. Phenolphthalein (PP), available from Polish Chemical Reagents (POCh) and Phthalide (Pd) available from Merck are purified according to standard methods [71]. The solvents are of spectroscopic quality (Merck): acetonitrile, ethyl acetate, n-hexane and cyclohexane of UVASOL quality; ethanol and methanol of VLSI Selectipur quality and water of LIChrosolv quality. Both UV/VIS absorption and fluorescence spectra confirm the purity of the starting materials.

All investigated samples are prepared as solutions. The concentration of MGL (1.1 ± 0.2 mM), PP (10 ± 2 mM) and Pd (25 ± 4 mM) in the laser experiments yielded approximately 30 % transmission in a 0.12 mm thick jet. The concentration of indole solutions in the laser experiments is varied from 4.3 mM to 14.4 mM, which corresponds to a transmission between 50 % to 5 %. The high concentration is used in order to minimize the contribution of the solvent signal. In the case of 1-methylindole the concentration is very low (transmission of 78-92 %) because of its low solubility in water.

The steady state fluorescence and the fluorescence excitation spectra of indole and OHBA solutions are measured in a 1 cm thick cuvette. The concentration of indole sample equaled 6 μM corresponding to 41 % transmission, while the concentration of OHBA 0.1 mM corresponding to 50 % transmission.

Absorption spectra of the investigated molecules did not change during the laser measurements which proves the photo stability of all compounds under the experimental conditions used in this work.

All laser experiments presented in this work are performed at room-temperature.

3.3.2 Free-flowing jet of the liquid sample

Pump and probe beams are crossed in a free-flowing jet of the liquid sample under investigation. The use of the jet is crucial to avoid unwanted signals resulting from artifacts. The coherent artifacts discussed below (see Sect. 3.4.2) are likely to be generated not only in the solvents but also in fused silica windows of the commonly used sample cells (cuvettes). Also fused silica is a significant nonlinear absorber at the high intensities produced by femtosecond laser pulses. This nonlinear absorption can broaden and attenuate the pump pulse in the window before the sample, deteriorating the time resolution (as already shown in Figure 3.10) and prohibiting the accurate measurements of the signal dependence on the

pump pulse energy. The jet also solves problems caused by the deposition of photoproducts on the inner walls of a flow cell where the flow velocity vanishes. As shown in Figure 3.14 the observed deposition influences the intensity of the signal on longer time scales (lower part of Figure 3.14), while on the short time scale (upper part of Figure 3.14) not only the intensity but also a shape of the signal is influenced.
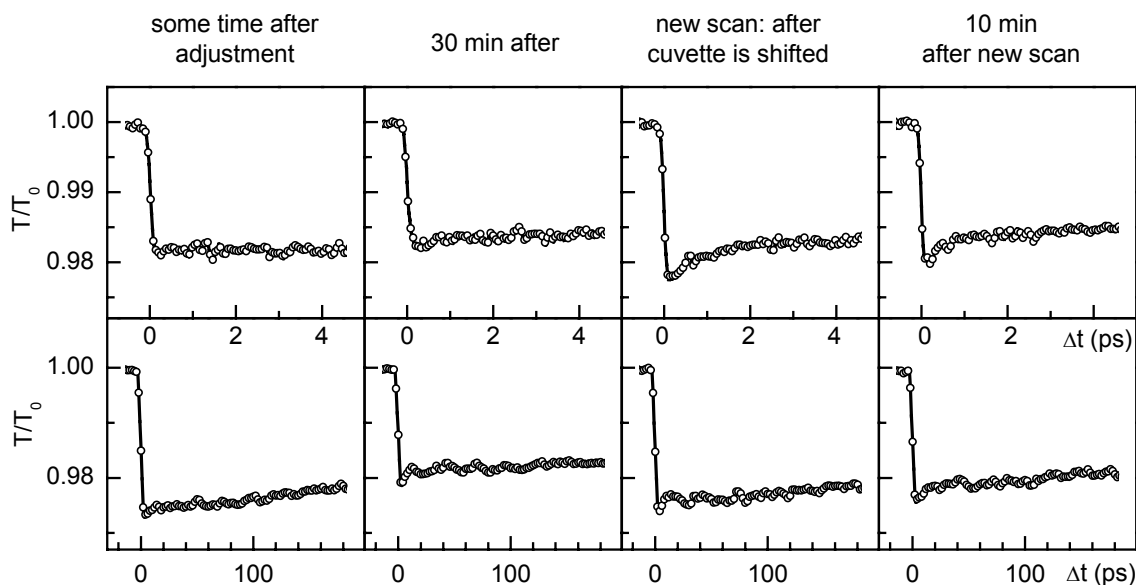
Figure 3.14 Example of the deposition of the photoproducts in the solution of malachite green lactone in cyclohexane on the window of the 120 μm thin flow cell, which causes changes of the signal intensity and shape in time. The short time scale is presented in the upper part of the figure and long time scale data in the lower part.

Careful attention to the nozzle design of the jet apparatus is important for producing a laminar flow, particularly when low-viscosity solvents such as water, acetonitrile, ethyl acetate or alcohols are used. We obtained satisfactory jets from a nozzle commonly used in dye lasers. The thickness of the jet is determined to be approximately as thick as the nozzle of 120 μm. A thin jet is required to minimize the group velocity mismatch between spectrally separated pump and probe pulses and to achieve the best time resolution. On the other hand, extremely thin jets require higher solute concentrations to obtain a measurable optical density for the pump light, which can lead to complexation problems for some solute/solvent systems [72, 73]. Therefore it is important to verify the absorption spectra of investigated systems before and after the measurements.

A gear pump (Micropump, 200 ml/min, AxFlow GmbH) is applied to pump the liquid sample through the jet-system, assuring that the excited volume is exchanged after each laser pulse.

Although it is critical for experiments presented in this work to use such a jet, one should be aware of its disadvantages. The laminar flow exhibit instabilities when bubbles are pumped through the nozzle. They contribute to the signal noise.

It is also important to take care what kind of solvent is used because some of them evaporate fast, what changes the concentration of the sample during the measurements and causes re-crystallization of the dissolved sample. This is a major problem by using n-hexane as solvent, and minor by methanol, ethanol and ethyl acetate. In order to avoid spreading of gases due to evaporation from the jet in a laboratory a home designed ventilation system is used to remove them.

3.4 Experimental considerations

3.4.1 Pump pulse energy dependence

Some measurements differ one from another due to the different obtained experimental conditions (excitation energy, concentration of sample, beam radius) at a particular day. In order to compare one to another it is important to know if and how the energy variation influences a signal.
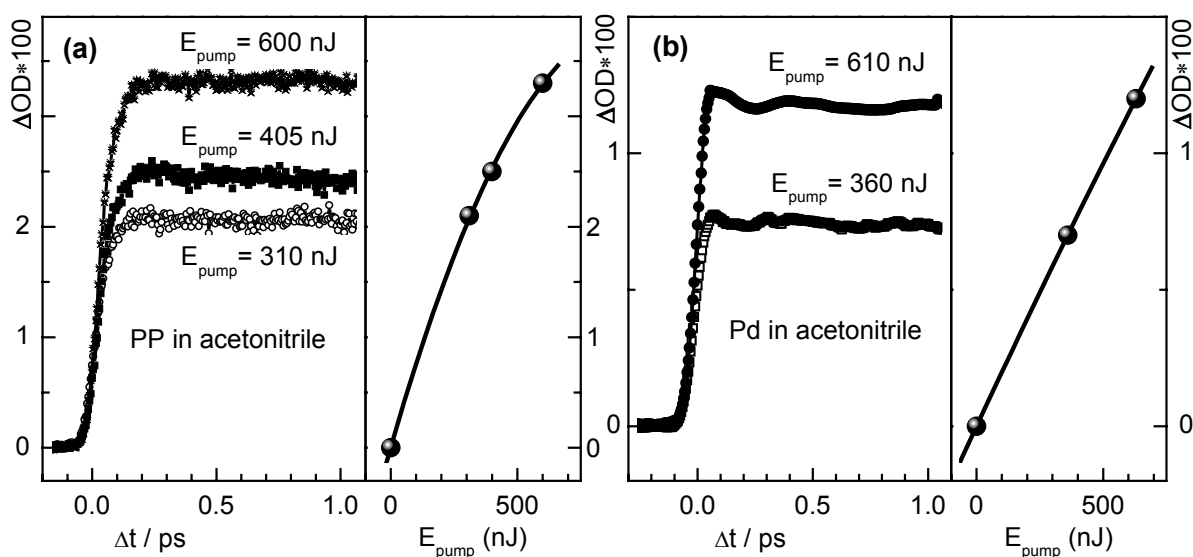
Figure 3.15 Influence of the pump pulse energy on the optical density change. Phenolphthalein (PP) dissolved in acetonitrile shows a small saturation effect (a), while phthalide (Pd) dissolved in acetonitrile shows a linear behavior (b).

As it is shown in Figure 3.15 variations of the pump (UV pulses) energy do not influence the shape of the signal. The signal from phthalide dissolved in acetonitrile (see Figure 3.15(b)) stays in the linear region of energies, and phenolphthalein (see Figure 3.15(a))

shows slight saturation with higher energies, due to its higher molar extinction coefficient at the excitation wavelength (see Figure 4.3). Throughout this work, all traces depicted together in one figure are scaled due to different pump energies assuming a linear correlation between signal and pump energy.

3.4.2 Contribution of the solvent to the signal

The investigated molecules are dissolved in different solvents, which behave differently due to theirs individual properties and show a significant dependence on the experimental conditions (pump energy, time resolution, pump and probe wavelengths). In some measurements their contributions can be ignored, however, in some cases they should be subtracted from the signal. The observed solvent effects can be divided in two major groups: coherent (zero) artifacts that vanish within the temporal overlap of the pump and probe pulse (CC signal) and signals which remain longer due to solvated electrons generated in the neat solvents.

Coherent artifacts

For low intensity radiation ($<10^{10}$ W/m^2) many simple molecular liquids and optical solids are transparent in the visible and near-UV spectral range. However, when high-power ultrashort laser pulses are applied (in our experiments: $>10^{14}$ W/m^2), these media can absorb efficiently through a multiphoton absorption mechanism [69] leading to the two-photon absorption (TPA) and stimulated Raman amplification (SRA). Furthermore, the application of a spectrally very broad probe pulse (like white light continuum) provides suitable conditions for efficient cross-phase modulation (XPM) [69, 74]. Each of the signals is produced by the simultaneous action of two photons: one from the pump and the other from the probe. Therefore their duration is directly related to the temporal response function. XPM leads to spectral modifications within the probe upon pump-induced temporal changes of the refractive index. Simultaneous absorption of a pump photon and a probe photon gives rise to TPA. The interchange of photons between pump and probe through a material's vibrational energy level gives rise to SRA.

These coherent artifacts are observed in all used solvents: acetonitrile, ethyl acetate, methanol, water, ethanol and cyclohexane, although with different strength. This difference is shown in Figure 3.16, where all six solvents used in experiments with the white light continuum as probe are presented together with the signal due to the investigated molecule in the corresponding solvent. Traces in Figure 3.16 are shown without correction for the solvent contribution, in order to make the solvent contribution more apparent. The probe wavelengths for shown solvent effects are as short as possible because the coherent artifact is getting smaller with increasing probe wavelengths as already presented in Figure 3.13.

Figure 3.16(a) corresponds to the conditions applied in the measurements of lactones and Figure 3.16(b) to those of indole. Major differences between these conditions are the different kind of the white light continuum, and a higher order of pump power density in the case of indole ($\sim 10^{15}$W/m^2). Signals are scaled to the pump energy within same experiment (lactone or indole-experiment). Due to the higher pump power density, solvent signals in indole-experiments contribute stronger to the signal. It can be also noticed that the coherent artifacts show significant structure in indole-experiments, which is related to the XPM and can be explained with the different kind of white light continuum.
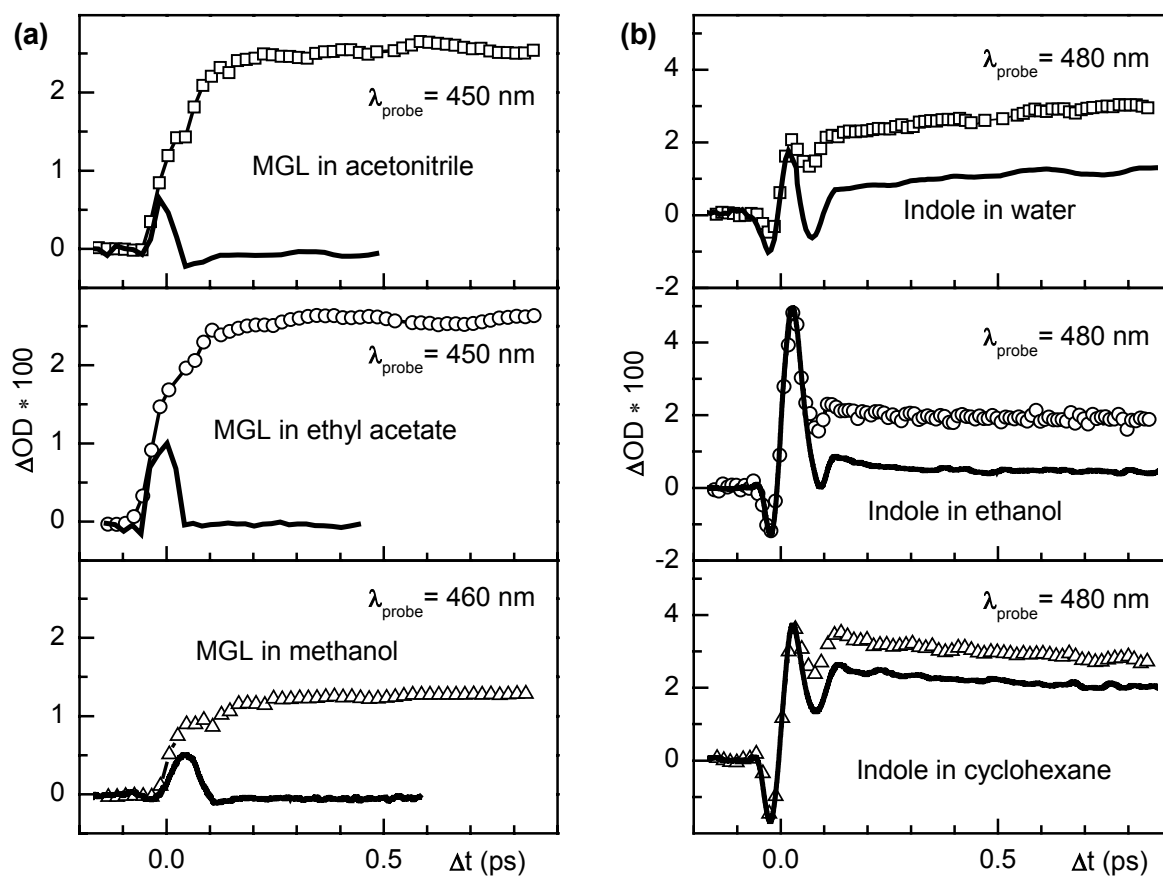
Figure 3.16 Contribution of the coherent artifact in the experiments with white light continuum as probe. (a) Signals from malachite green lactone dissolved in acetonitrile (squares), ethyl acetate (circles) and methanol (triangles). (b) Signals from indole dissolved in water (squares), ethanol (circles) and cyclohexane (triangles). Signals from the neat solvents are presented as solid lines.

The signal can be corrected for the solvent contributions (see Appendix B), but the reliability of the method in the region close after excitation is critically, especially in the case of indole (see Figure 3.17). A coherent artifact remains in the traces after subtraction of the solvent contribution.
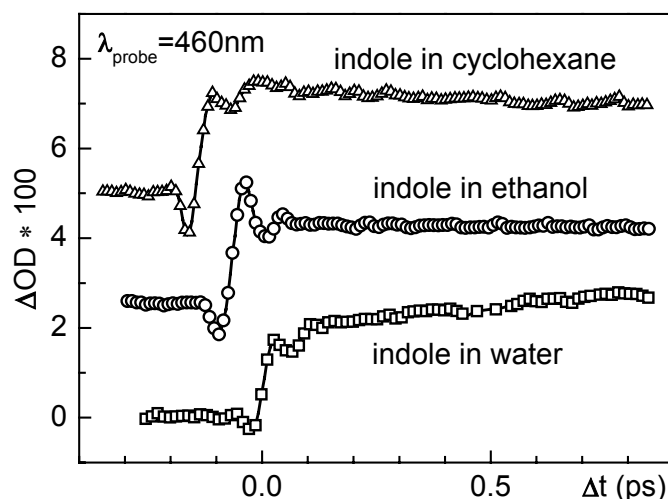
Figure 3.17 Traces of indole solutions in water (squares), in ethanol (circles) and in cyclohexane (triangles) shown in Figure 3.16(b) after subtraction of the solvent contribution. The consequence of coherent artifact is still observable.
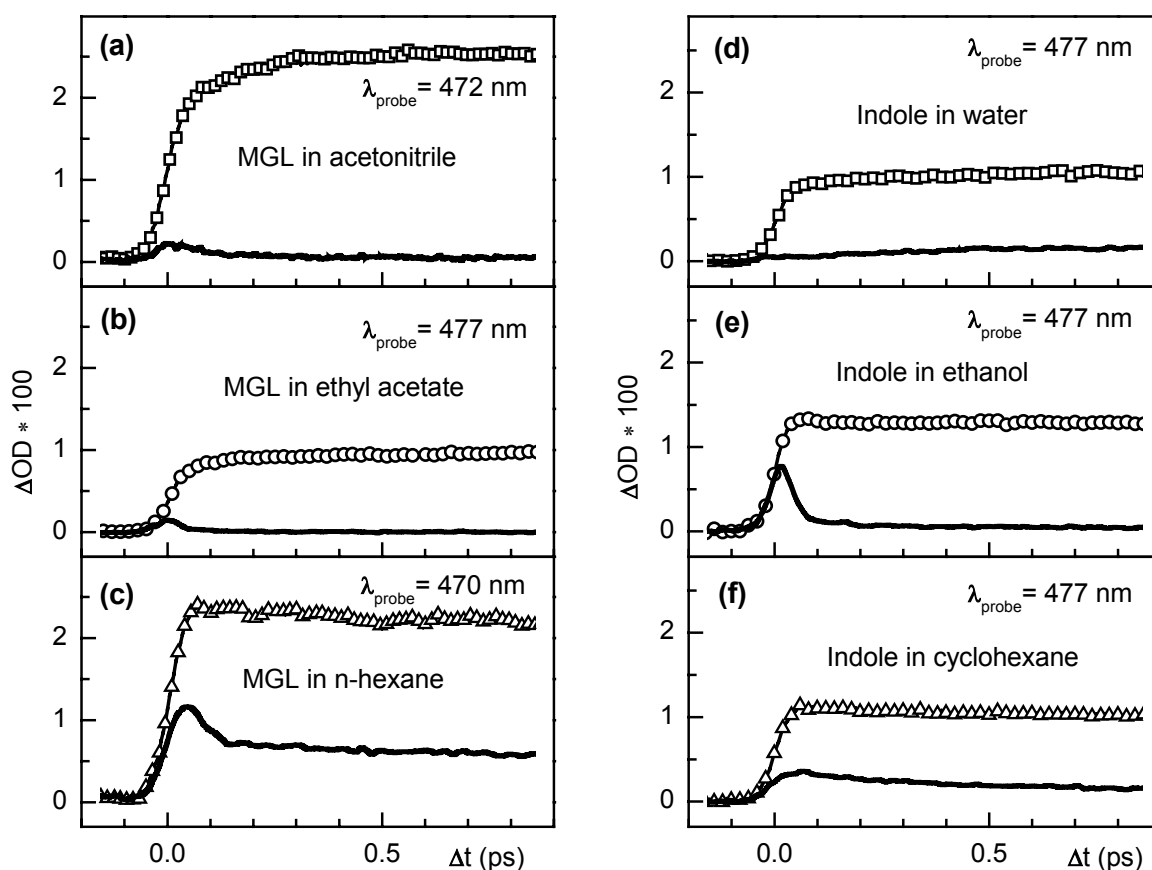
Figure 3.18 Zero artifacts in neat (a) acetonitrile, (b) ethyl acetate, (c) n-hexane compared to a signal of MGL solutions (symbols), as well as in neat (d) water, (e) ethanol and (f) cyclohexane compared to signal traces of indole solutions (symbols). The solvent signal (solid lines) observed in two-color experiments is smaller compared to the case when the white light continuum is used as probe (see Figure 3.16).

To observe the ultrafast processes it is necessary to apply a two-color setup. It is shown in Figure 3.18 that the effect observed there is small enough to be ignored for lactones dissolved in acetonitrile (a) and ethyl acetate (b) and indole dissolved in water (d). In the cases of lactones dissolved in cyclohexane (c) or n-hexane and indole dissolved in ethanol (e) or n-hexane (f) the signal has to be corrected. The subtraction in this case is possible because the shape of the coherent artifact is not as structured as with the white light continuum probe. The traces are scaled to the pump energy and the shown solvent effects are directly comparable to each other.

The contribution from acetonitrile and ethyl acetate is small enough that it has not to be subtracted from the signal for both investigated lactones, malachite green lactone (MGL) and phenolphthalein (PP) in the two-color experiment, but it is corrected for their chromophore Phthalide (Pd), as presented in Figure 3.19.
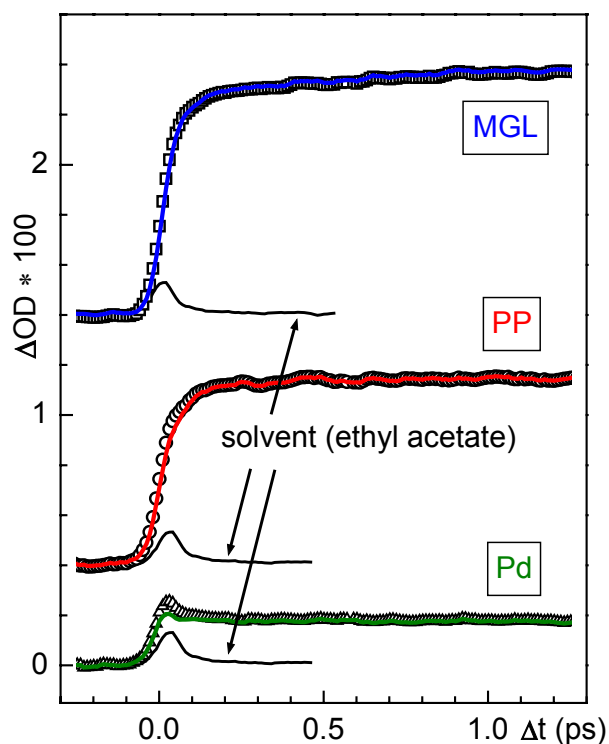
Figure 3.19 Subtraction of the solvent effect in ethyl acetate in the two-color experiment. The black symbol-curves present the data before subtraction of the solvent signal (black lines) and the color lines (MGL-blue, PP-red; Pd-green) present the signals after the subtraction.

Long time contributions

Application of the high pump power density ($>10^{15}$W/m^2) in the region of very short wavelengths (270 nm) enables photoionization of neat solvents due to the two-photon absorption process. This causes a significant signal in a broad spectral region, which corresponds to the broad absorption spectrum of solvated electrons as a product of photoionization [55, 75-84]. The solvents used for indole solutions, water, ethanol and cyclohexane show significant contributions to the signal. These contributions are subtracted in the way presented in Appendix B. The result of the subtraction procedure is illustrated in Figure 3.20. Traces with two different concentrations of indole dissolved in water as well as of neat water are shown in Figure 3.20(a). The low concentrated solution shows a behavior more similar to that of neat water. After appropriate subtraction both indole solutions show the same behavior (see Figure 3.20(b)), similar to the behavior of the high concentrated solution, where the contribution of solvent is smaller because most of the pump energy is absorbed by indole molecules. It demonstrates that the solvent contributions are completely removed.
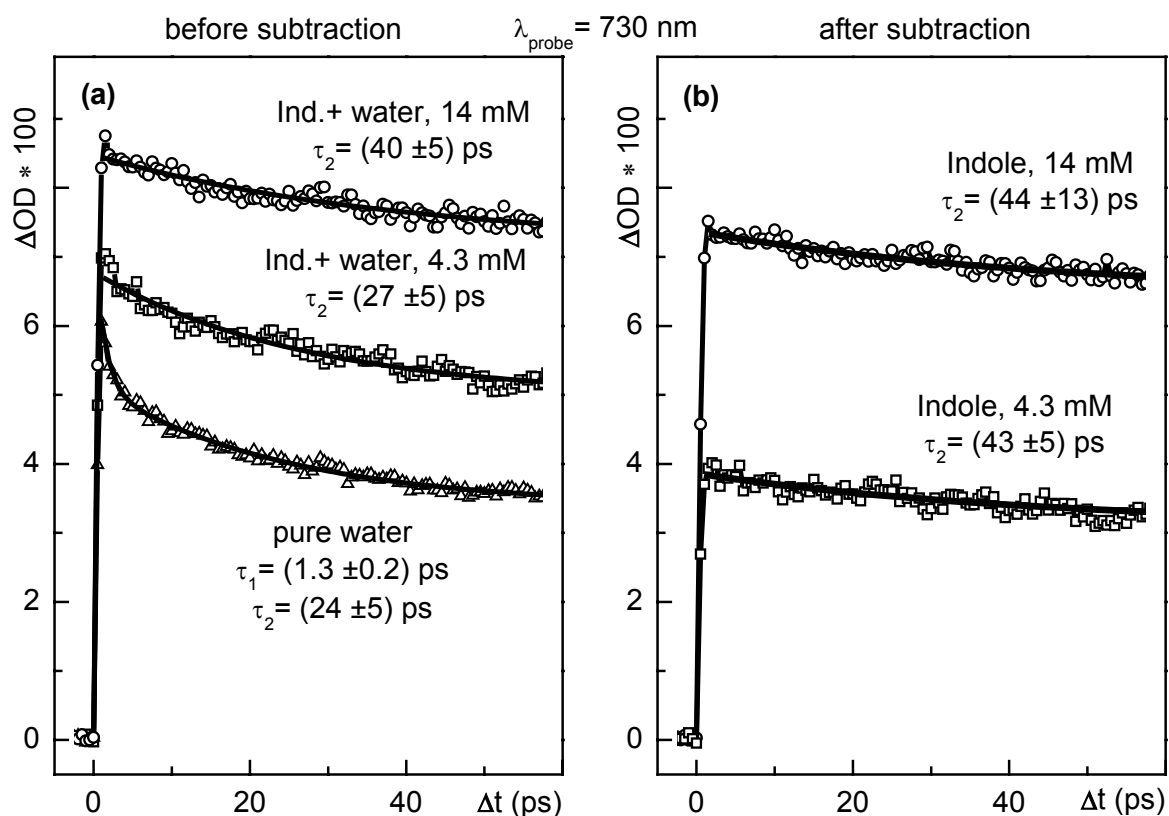
Figure 3.20(a) Measured traces of neat water (triangles), indole solution with lower (squares) and higher concentration (circles) and corresponding fits (solid lines). (b) Signal of both, lower (squares) and higher (circles) concentrated solution shows the same behavior after subtraction of the solvent contribution

Long time contributions of the solvent obscure not only the time resolved traces, but also the transient spectra, so the same procedure of subtraction is applied. By comparing the contribution of water and ethanol in the two different setups (see Figure 3.21) it can be seen that the observed signals of both the indole solution and the neat solvent are stronger when a white light continuum is used as probe. The reason for this is an order of magnitude higher pump power density, due to the smaller spot of the pump beam at the focus and shorter pump pulse duration.
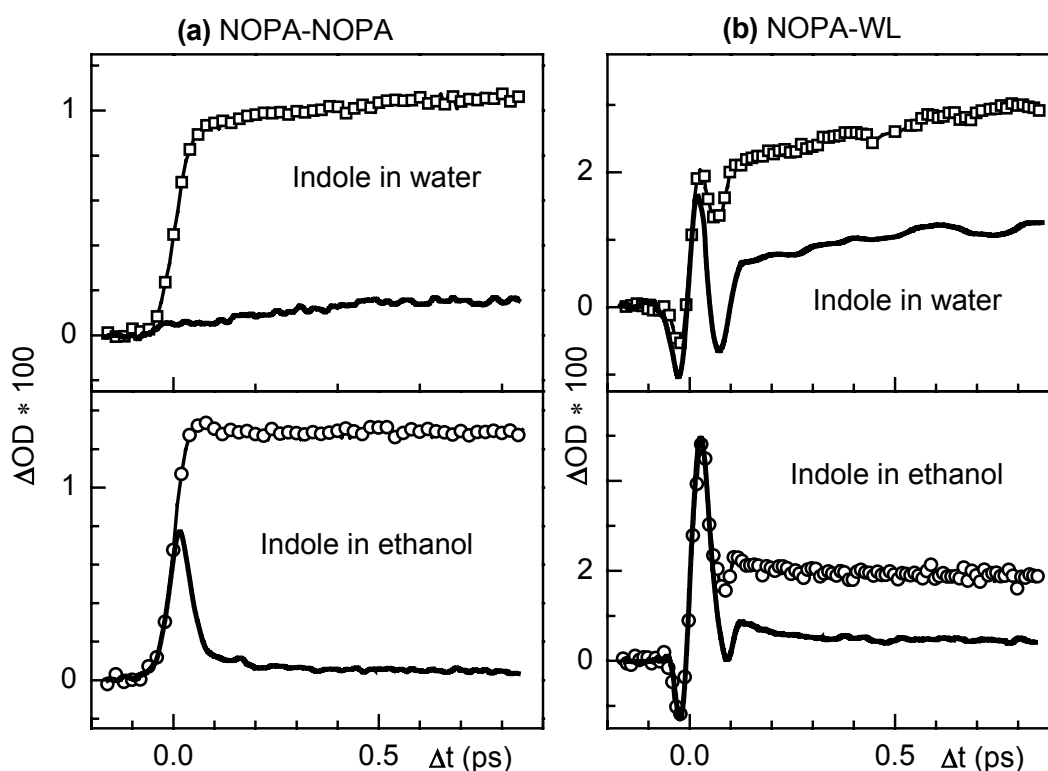
Figure 3.21 Comparison of the solvent contribution (solid lines) to the signal of Indole dissolved in water (squares) and ethanol (circles) under two different experimental conditions: (a) probing with one color and (b) with a white light continuum.

This is verified for neat water measured with similar pump energies but different pump pulse durations and different sizes of the pump beam in the focus, leading to a different pump power densities. Traces in Figure 3.22 are normalized for the maximum of the coherent artifact and show the increase of the long time solvent contribution with shortening of the pulses. This contribution comes from the solvated electrons generated in neat solvents.
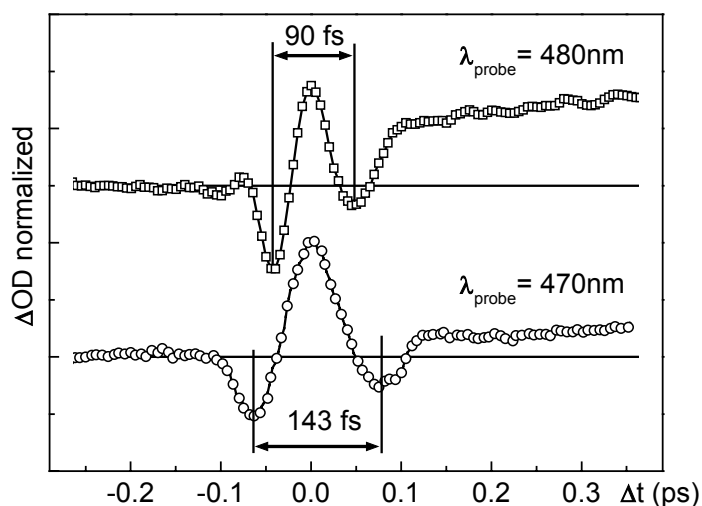
Figure 3.22 Signal in neat water probed in the blue spectral region. Signal measured with a better time resolution (squares) show greater contribution to the signal due to the photoinduced solvated electrons observed in the time after coherent artifact.

Acetonitrile, ethyl acetate and methanol used as solvents in lactone solutions show no contribution to the signal on long time scale. Therefore their contributions to the transient spectra measured at least 1 ps after excitation can be ignored as shown in Figure 3.23.
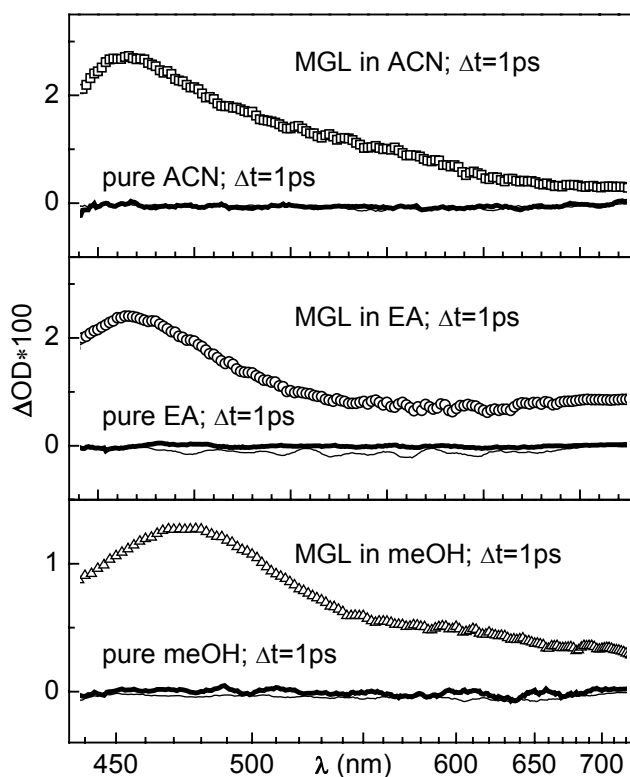
Figure 3.23 Transient spectra of (a) acetonitrile, (b) ethyl acetate and (c) methanol used as solvents (thick line) for solutions of lactones (symbols) show no contribution to the signal when probed 1 ps after excitation. Thin lines denote the signal before excitation.

All traces discussed in this work are presented after subtraction of the solvent contribution if needed.

3.4.3 Orientational relaxation

The orientational relaxation of excited molecules can show additional dynamics dependent of the polarization of the pump and probe pulses [85, 86]. In this experiment the polarization between the pump and probe pulses is set with a half-wave plate in the probe beam to the parallel, perpendicular and the "magic angle" configuration. No significant changes are observed in the measured traces. Figure 3.24 shows that the shape of the signal of malachite green lactone dissolved in acetonitrile remains the same when the polarization is changed, only the intensity differs a little. The other investigated molecules show the same behavior. Nevertheless, the polarization between pump and probe is set to the magic angle in all measurements presented in this work. This "magic" configuration of 54.7° between two beams eliminates the possibility that the orientational relaxation of investigated molecules has an influence on the signal [87].
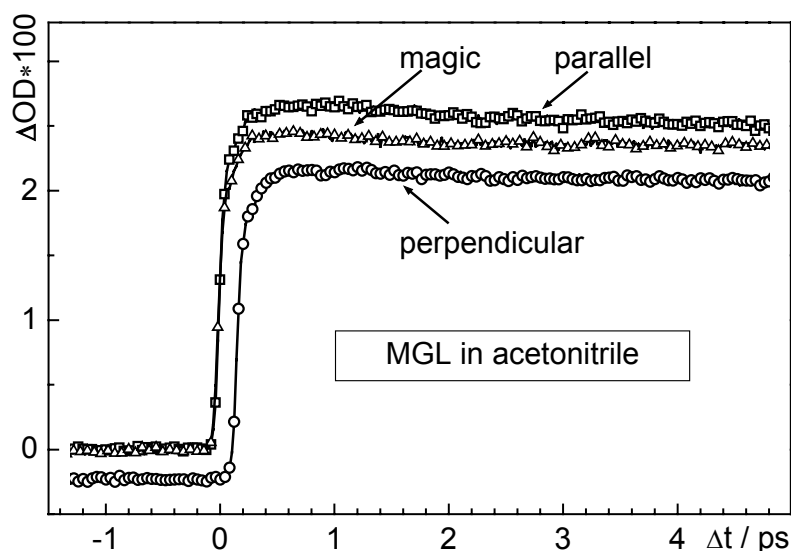
Figure 3.24 Polarization dependence of the transient absorption of malachite green lactone in acetonitrile. Polarization of the pump and probe light is set to the parallel (squares), perpendicular (circles) and magic angle configuration (triangles). It shows a small influence on the intensity, however, no influence on the shape of the signal. Trace corresponding perpendicular angle configuration is shifted along x and y axes for better visibility.

3.5 Steady state measurements

Absorption spectra are recorded with a UV-VIS double monochromator with a resolution of 0.1 - 1 nm (Lambda 19, Perkin Elmer) and a diode array spectrograph (Specord S 100, Analytikjena).

The steady state fluorescence spectra of lactones are measured with a spectrofluorometer (FS900, Edinburgh Analytical Instruments). The fluorescence spectra are recorded as a function of wavelength and subsequently multiplied by factor λ^2 in order to convert counts per wavelength into counts per wavenumber.

The steady state fluorescence and fluorescence excitation spectra of indole and OHBA are measured by using a fluorescence double spectrometer (Fluorolog-2, Spex). The variation of excitation intensity radiation with wavelength is corrected by a quantum counter with the dye rhodamine B, which works reliably in the spectral region between 200 - 600 nm. The dispersion of the spectrometer is 1.8 nm/mm, which corresponds to the spectral resolution in the experiments of 3-5 nm. The absolute values of fluorescence quantum yields are obtained by comparison to dyes with known fluorescence yields.

4 Electron transfer and solvation in triphenylmethane lactones

4.1 Introduction

4.1.1 Charge transfer systems

Photoinduced charge transfer (CT) in donor-acceptor (D-A) systems is a fundamental photophysical process, very intensely studied for several last decades [6]. Effective transformation of the energy of absorbed photon into the energy of emerging charge transfer D^+-A^- state requires the CT process to be as fast as possible. With 6-fs electron transfer reported for strongly coupled dye/semiconductor colloidal systems [7] and even sub-3-fs charge transfer time for bi-isonicotinic acid bound to rutile TiO_2 surface, the research on heterogeneous CT have reached recently a very low femtosecond limit [8]. On the other hand, the studies on *intramolecular* CT dynamics on 100 fs time scale are very scarce. In early work diffusive solvation dynamics was shown to be a rate limiting factor for a number of barrierless electron transfer (ET) reactions in condensed phase and the rate constants were correlated with longitudinal dielectric relaxation time of the solvent (τ_L) [33] or with viscosity of solvents [88]. Further experimental studies have demonstrated that the rate of both intramolecular [89] and intermolecular [90] barrierless ET reactions can far exceed τ_L (reaching $k_{ET} = 10^{13}$ s^{-1}), indicating that other factors, e.g. ultrafast inertial solvation dynamics [30] or couplings of intramolecular vibrational modes [25, 91], play critical roles in ET processes. In such a system, where the acceptor molecule is dissolved in electron-donating solvent as shown for nile blue dissolved in N,N-dimethylaniline (DMA) [92, 93], oxazine 1 in DMA [94-96] or perylenes dissolved in DMA [97] there is always uncertainty because of multiple donor sites if an observed rate constant should be identical to the ET constant or not. This uncertainty could be avoid if a single-molecule D-A systems are observed. The work on *intramolecular* CT dynamics occurring on a time scale of inertial solvation is still at the outset and very few molecular systems have been found suitable for such studies. Recently, nile blue linked to 3-ferrocenophane group was shown to undergo ET within 90 fs [9] and both ultrafast inertial solvation dynamics and intramolecular vibrational modes were found to promote ET process in a ruthenium mixed valence compound in H_2O within $80-100$ fs [10]. Somewhat longer CT (200 fs) was observed in porphyrin-imide dyads [98, 99] and in dimers of perylenediimide chlorophyll analogues (170 fs) [100]. Very recently Kovalenko *et al.* proposed that intrinsic ET process in cyano-

bianthryl proceeds within 10 fs [11]. D-A systems with so high ET rates are very important for deeper understanding of various factors controlling CT processes that occur on the time scale comparable to that of vibrational relaxation, inertial solvation or electronic dephasing.

4.1.2 Introduction to the investigated systems

Charge transfer (CT) is a fundamental process in chemistry and has been investigated in a very broad range of molecular systems [6, 101]. However, in the case of ultrafast CT occurring on a time scale comparable to that of vibrational relaxation, inertial solvation or quantum dephasing only a limited number of experimental studies have been performed so far [9-11, 96, 97, 99, 100].
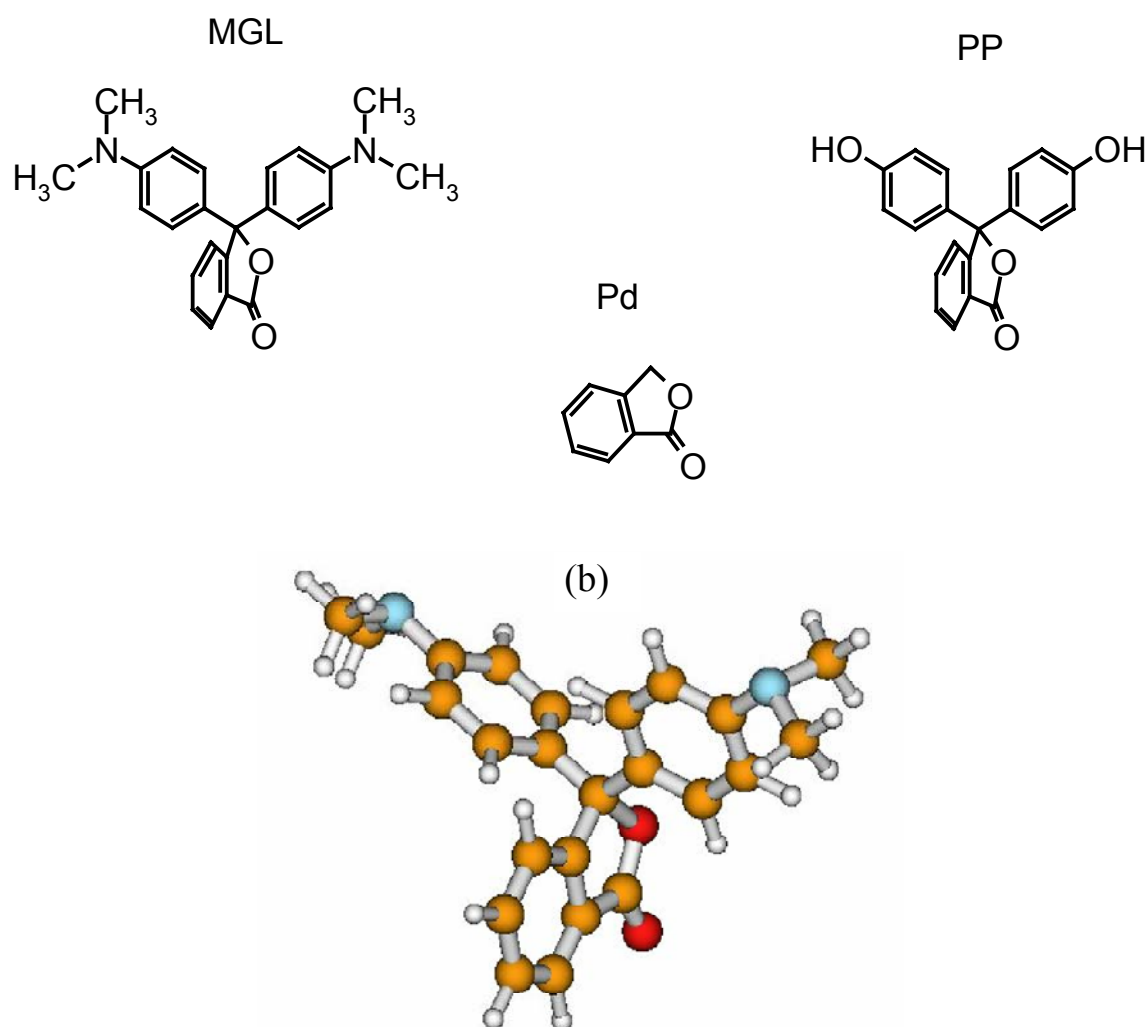

Figure 4.1 Structural formulae of the molecules investigated in this study: malachite green lactone (MGL), phenolphthalein (PP) and phthalide (Pd). In MGL and PP the Pd moiety is perpendicularly oriented to the rest of the molecule, as well as the planes of the two identical chromophores with respect to each other. (b) 3D structure of MGL

A very promising class of molecules to investigate the underlying mechanisms of ultrafast CT processes are the lactone forms of triarylmethane dyes (LTAMs) [102]. They exhibit a well-defined geometry due to a central tetrahedral carbon atom that links the donor (D) groups to the acceptor (A) moiety. Two of them, malachite green lactone (MGL) and phenolphthalein (PP), whose chemical structures are presented in Figure 4.1, have been investigated in this work together with their common electron acceptor moiety phthalide (Pd), which is used as a reference molecule. Both MGL and PP are relatively simple molecular systems with D and A units built around a tetrahedral carbon atom. Such an arrangement of D and A results in a weak electronic coupling between them in the ground state and the absorption transitions in LTAMs in lower energy regions are localized on their structural subunits [103].

Despite such a decoupling of structural subunits, the excitation of MGL (localized on one of the dimethylaniline (DMA) groups) does not lead to any "local" fluorescence from the DMA chromophore. Instead, MGL displays a broad, strongly solvatochromic fluorescence band (see Figure 4.3(a)) which has been ascribed to a highly polar CT state [103]. Structurally related leuco forms of malachite green exhibit also an absorption spectrum being a sum of their structural subunits [104, 105]. Since malachite green leuconitrile (MGCN) displays only fluorescence from primarily excited DMA moiety [106], the absence of "local" fluorescence from DMA moiety in MGL indicates a rapid deactivation channel of the locally excited chromophore, which has been ascribed to an ultrafast electron transfer from excited DMA group to phthalide moiety. This assignment together with the estimated charge transfer (CT) rate of $(0.13 \text{ ps})^{-1}$ has been based on the analysis of steady state fluorescence spectra of MGL and the photophysics of structurally related compounds [103].

PP is another LTAM with low energy absorption transitions localized on its structural subunits. PP also displays fluorescence from a highly polar excited state populated upon electron transfer (ET) from one of the phenol rings to the Pd moiety [107]. Lack of "local" fluorescence from the primarily excited structural subunit strongly indicates an ultrafast CT process also in the PP molecule.

The solvents used to study the dependence of the CT kinetics on solvent polarity are shown in Figure 4.2. Their static dielectric constants as a measure of polarity, longitudinal dielectric relaxation and diffusive solvation times are presented in Table 4.1.

(a) n-hexane   (b) ethyl acetate   (c) acetonitrile   (d) methanol
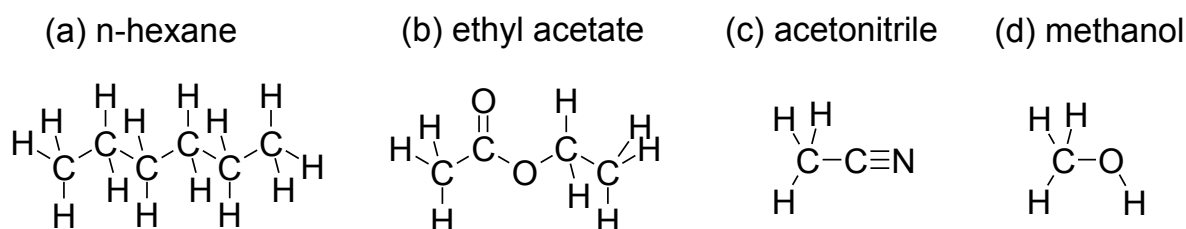
Figure 4.2 Structural formulae of solvents used in the kinetic study on lactones: (a) n-hexane, (b) ethyl acetate, (c) acetonitrile and (d) methanol.

Table 4.1
Static dielec. const. and relax. times of solvents used in the experiments on lactones

solvent	static diel. constant	longitudinal relax. time (ps)	diffusive solv. time (ps)
hexane	1.88^a	$--^e$	$--^e$
ethyl acetate	6^b	1.7^f	$2.3 - 2.7^g$
acetonitrile	$36 - 39^c$	0.2^h	$0.4 - 0.9^i$
methanol	$31 - 34^d$	$2.9 - 3.1^j$	$3.2 - 3.3^k$

^{a} **at 291°K from [59, 108];** ^{b} **at 298 K from [109]: 6.02, [110]: 6.11;** ^{c} **at 298 K from [109]: 35.94, [24]: 37.3, [110]: 38.8;** ^{d} **from [110]: 31.2, at 298 K from [111]: 32.63, [109]: 32.66, [24]: 33.7;** ^{e} **Time constant is not known;** ^{f} **taken from [36];** ^{g} **taken from [36]: 2.3-2.7 ps, [26]: 2.6 ps;** ^{h} **taken from [24, 35];** ^{i} **taken from [36]: 0.4-0.9 ps, [35]: 0.4 ps, [26]: 0.5 ps, [27]: 0.63 ps;** ^{j} **taken from [35]: 2.9 ps, [112]: 3.1 ps;** ^{k} **taken from [27]: 3.2 ps, [35]: 3.3 ps.**

The solvent can influence a chemical reaction in a dynamic way by exchanging energy and momentum with reacting species and by responding to the change of their charge distribution. More about the role of solvent relaxation in determining the rates of charge transfer reactions is discussed in Section 2.5.

In this chapter the dynamics of charge transfer in MGL and PP in aprotic media is presented. It has been directly measured with femtosecond pump-probe spectroscopy by monitoring the build-up of cation radicals of the electron-donating moieties formed in the CT process. Very short build-up times (below 0.05 ps for PP in acetonitrile) show that the CT process occurs on the time scale of inertial solvation dynamics and indicate an important role of a high-frequency intramolecular vibrational mode. In addition, the behavior of MGL

dissolved in protic media (methanol) is investigated, where an opening of the lactone ring appears.

4.2 Steady state spectroscopy of LTAMs in solvents of different polarity

Figure 4.3 shows steady state absorption and fluorescence spectra of PP, MGL and Pd dissolved in solvents of different polarity. The absorption spectra do not show any traces of absorption in the visible, indicating that only colorless lactone forms and no colored ionic forms (e.g. MG cation: MG^+ [113] or PP dianion: PP^{2-} [114]) are present in the solution.

The first absorption band of MGL around 310 nm strongly overlaps with the red edge of the much stronger second absorption band (see Figure 4.3(a)), which is excited at 270 nm, the pump wavelength in the time resolved experiments. Both bands show weak dependence on solvent polarity. Small red shift of absorption bands with increasing solvent polarity is compared to the similar spectra of the structurally related lactone form of tetramethylrhodamine. It differs from MGL only by presence of an oxygen bridge, which links two DMA moieties into a rigid bis(dimethylamino)-xanthene system. Its absorption spectrum shows an additional long-wave band, which is ascribed to a CT transition from the bis(dimethylamino)-xanthene unit to the phthalide unit based on the significant red shift of the band with increasing solvent polarity [102]. Because of the absence of such an effect in absorption spectra of MGL, no CT absorption transition between the DMA rings and the phthalide moiety could be identified [103]. Owing to orthogonal orientation of structural subunits, the absorption spectrum of MGL in the low energy region ($\lambda > 250$ nm) is a superposition of contributions from the two DMA groups and the Pd moiety. At 270 nm the contribution from Pd moiety to MGL absorption is less than 5% (from comparison of molar extinction coefficients in Figure 4.3(a) and (c)), which means that predominantly the DMA groups are optically excited and subsequently the charge is transferred from the excited donor to the ground state acceptor. Due to the same orthogonal orientation of structural subunits, the first absorption band of PP (see Figure 4.3(b)) can also be considered as a sum of absorption transitions localized on the phenol groups and on Pd moiety. There is no band in the absorption spectrum which exhibits any dependence on solvent polarity, so again no direct CT transition could be identified [107]. Comparable molar extinction coefficients of phenol [115] and phthalide in the 250 - 290 nm region result in similar probabilities for each of these PP structural subunits to be excited at 270 nm, so that not only local excitation of phenol group, but also that of Pd moiety must be considered.
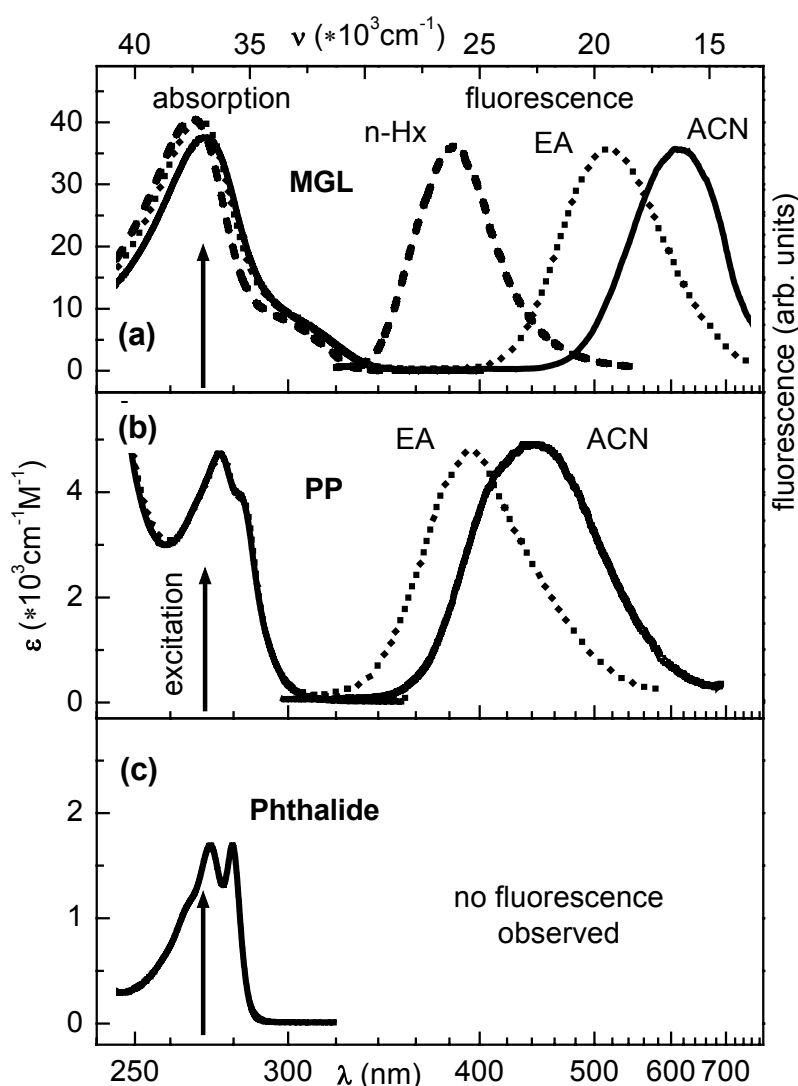
Figure 4.3 Steady state absorption and fluorescence spectra of (a) MGL, (b) PP and (c) Pd in acetonitrile (solid line), ethyl acetate (dotted line) and n-hexane (dashed line). The shift of the fluorescence spectrum increases in line with solvent polarity. Small shift of the absorption spectra is observed only for MGL. For phthalide no fluorescence has been found. The excitation wavelength is indicated in the spectra.

Both MGL and PP show a remarkable effect of solvent polarity on fluorescence spectra (see Figure 4.3). Unusual large Stokes shift, strong solvatochromic effect and large half-width of the fluorescence band point to the conclusion that the fluorescence in both molecules is displayed from a highly polar charge transfer (CT) state. The dipole moments of the emitting state determined from solvatochromic plots of fluorescence maxima are 25.0 D and 21.0 D for MGL and PP, respectively, and correspond to ET distances of 0.52 nm and 0.44 nm, suggesting full electron transfer from the DMA group to the Pd moiety in MGL and from the phenol group to Pd moiety in PP [103, 107]. The ground state dipole moment of MGL, estimated from molecular mechanics calculations, is equal to 5.5 D [103]. The

absence of any fluorescence from the locally excited chromophore in both investigated LTAMs indicates very fast conversion of the primarily excited Franck-Condon (FC) state to the CT state due to intramolecular ET. As already reported [116], Pd shows no fluorescence at all, while the fluorescence of phenol and DMA should occur in the wavelength region between $280-320\,\text{nm}$ and $310-420\,\text{nm}$ respectively [115], where no fluorescence is observed.

It has to be noted that the fluorescence spectrum of PP in aprotic solvents is presented here for the first time. Till now PP has been generally perceived as a non-luminescent molecule and except for two studies reporting very weak fluorescence from PP ionic forms in protic environments [117, 118], no luminescence studies on PP in aprotic media could have been found in literature.

4.3 Transient absorption spectra show radical cation signature

4.3.1 Phthalide
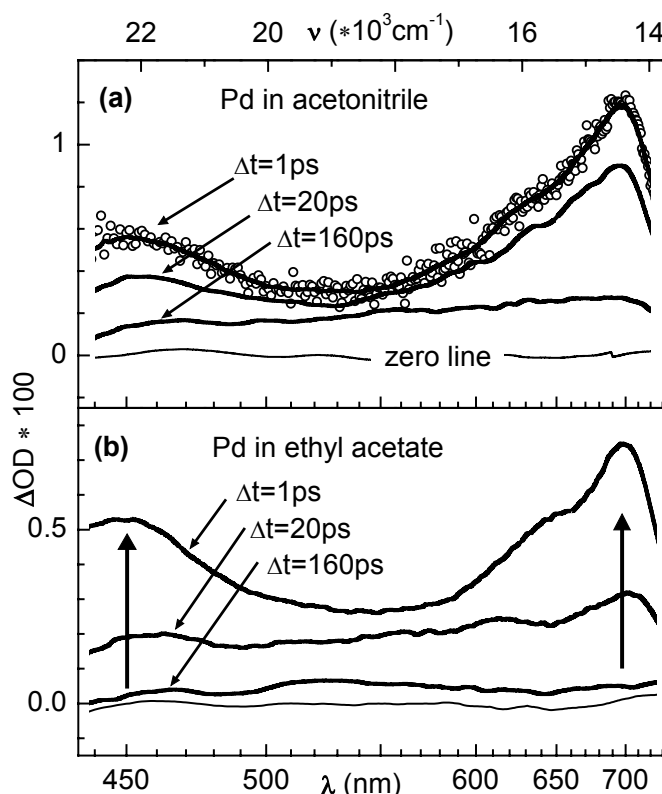
Figure 4.4 Transient spectra of Pd in (a) acetonitrile and (b) ethyl acetate recorded 1 ps, 20 ps and 160 ps after excitation show two broad bands due to the ESA, which decay simultaneously. Open circles are the data measured at a delay of 1 ps before averaging of 10 adjacent data points. The thin lines show the signal recorded before the excitation. Thick arrows indicate the probe wavelengths used in measurements shown in Fig. 4.5.

Transient absorption spectra are measured between 435 nm and 730 nm, where none of the studied molecules shows any ground state absorption. Transient spectra of Pd in acetonitrile and in ethyl acetate (see Figure 4.4(a) and (b), respectively) recorded 1 ps after excitation exhibit a strong transient absorption band at 695 nm and a weaker one at 455 nm. These two broad bands are ascribed to the excited state $S_n \leftarrow S_1$ absorption (ESA) of the excited chromophore Pd.

Both bands decay simultaneously with two exponential decay times, one on a 50 ps and one on a nanosecond time scale. However, in acetonitrile they decay slower ($\tau_1 = 87$ ps; $\tau_2 > 1$ ns) as in ethyl acetate ($\tau_1 = 12$ ps; $\tau_2 = 0.33$ ns). This is verified by probing at two fixed wavelengths corresponding to the two maxima of the ESA (see Figure 4.5). As observed in steady state experiment (see Section 4.2) Pd shows no fluorescence, so the observed decays of ESA bands can be attributed to the ISC transition from S_1 state to T_1 triplet state, as previously reported [116].
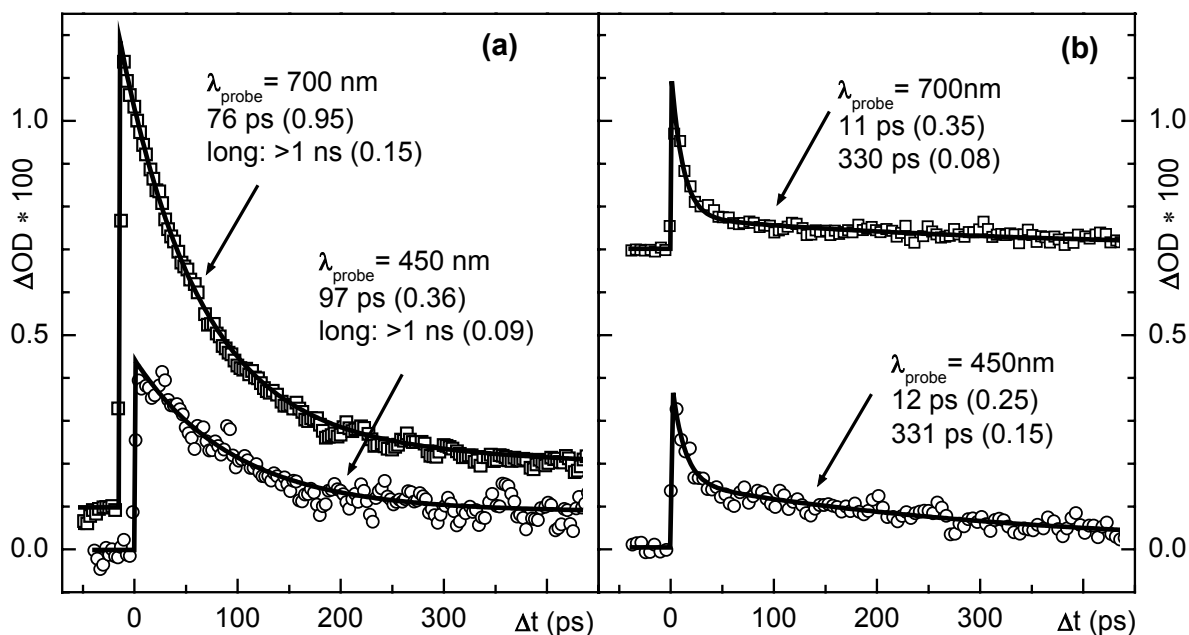
Figure 4.5 Time resolved measurements with the white light continuum probe. Pd in (a) acetonitrile and (b) ethyl acetate is probed at 450 nm (circles) and at 700 nm (squares). Both maxima decay simultaneously with a two-exponential decay: the two decay times are shorter in ethyl acetate. Traces recorded at 700 nm are shifted along x and y axes in (a) and along y axis in (b) for better visibility.

4.3.2 Phenolphthalein

Transient absorption spectra of PP in acetonitrile shown in Figure 4.6(a) consist mainly of a broad band with a maximum at 440 nm which decays exponentially with a decay time of 0.8 ns. The band can be ascribed neither to $S_n \leftarrow S_1$ absorption of phenol, which has maximum of ESA at 600 nm [119]), nor to $S_n \leftarrow S_1$ absorption of the Pd moiety, which has its stronger ESA maximum at 695 nm, as shown in Figure 4.4. The 440 nm band matches very well to the absorption band of the phenol radical cation [120], shown in Figure 4.6(c).
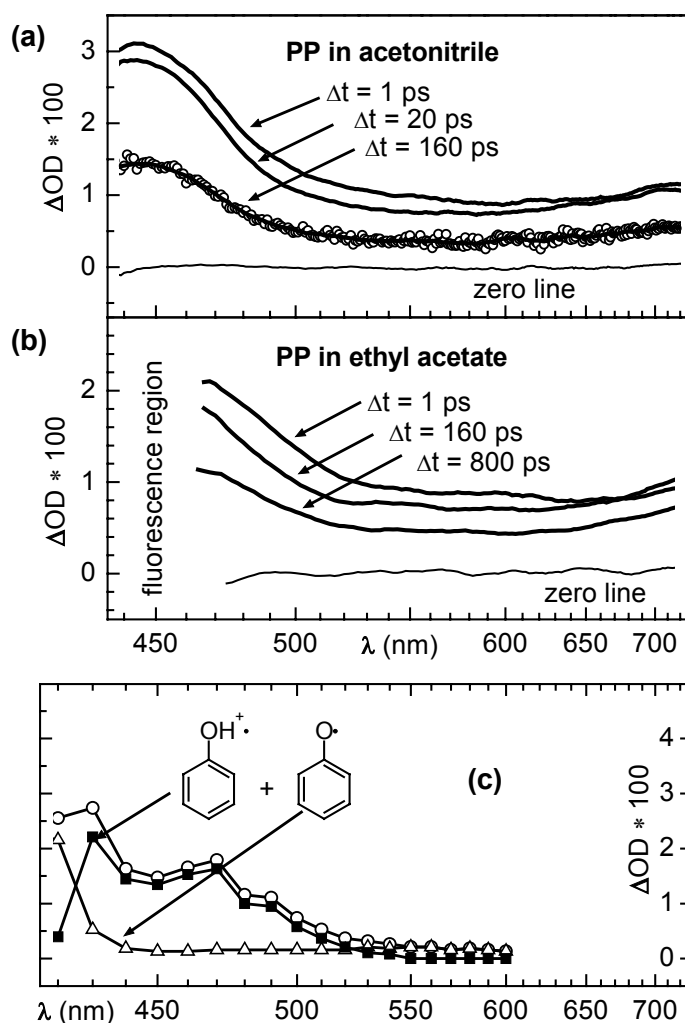
Figure 4.6 Transient absorption spectra measured at a delay of (a) 1 ps, 20 ps and 160 ps after optical excitation of PP in acetonitrile and (b) at 1 ps, 160 ps and 800 ps after excitation of PP in ethyl acetate. The region where spontaneous fluorescence obscures the transient absorption spectrum is noted. Open circles represent the data recorded at a delay of 160 ps before averaging of 10 adjacent data points. The zero (thin solid) line shows the signal before the excitation. (c) Absorption spectra of phenol radicals and radical cations together (circles) and phenol radicals (triangles) taken from Ref. [120]. The absorption spectrum of phenol radical cations is the difference of both spectra (squares).

The appearance of the 440 nm-band in the transient absorption spectrum measured 1 ps after optical excitation proves that the photoinduced CT in PP is completed in less than 1 ps. No spectroscopic data on phthalide radical anion (Pd·$^-$) has been found, but the absence of other bands in the observed transient spectrum of PP in the wavelength region of 500 – 700 nm indicates that its contribution to the transient absorption spectra must be weak.

As indicated in Figure 4.6(b), in the region of wavelengths shorter than 470 nm PP in ethyl acetate displays strong spontaneous fluorescence compared with the probe white light and inhibits measurements in this wavelength region. However, the same kind of behavior can be observed as for PP in acetonitrile. A strong band with the maximum in the wavelength region above 470 nm appears within 1 ps after excitation but decays slower as in the case of PP in acetonitrile. Phenol radical cation is again responsible for the appearance of this absorption band, indicating a photoinduced CT process.

4.3.3 Malachite green lactone

Figure 4.7(b) shows transient absorption spectra of MGL in acetonitrile. The trace recorded 1 ps after excitation to the S_2 state shows a strong band at 465 nm that extends far to the red and decays exponentially with a decay time of 0.45 ns (see next Section 4.4), which corresponds to the fluorescence decay time known from literature [103]. The shape of the spectrum coincides with the spectrum obtained in ns measurements [103]. Although the absorption transitions are localized on MGL structural subunits, the dominant transient absorption band at 465 nm cannot be assigned neither to $S_n \leftarrow S_1$ absorption of DMA which has its maximum at 600 – 620 nm [121], or to $S_n \leftarrow S_1$ absorption of Pd (shown in Figure 4.4(a)). The band agrees well with the absorption band of the DMA radical cation [122] shown in Figure 4.7(a), which again indicates completion of photoinduced CT in MGL within less than 1 ps.

Figure 4.7(c) shows that the 465 nm band of MGL in ethyl acetate changes its shape (becomes narrower) within the first few picoseconds after excitation while its maximum slightly increases. These changes reflect the temporal evolution (either red shift or narrowing of spectrum) of the fluorescence spectrum of MGL in ethyl acetate (see Figure 4.3(a)) during diffusive solvation of the emerging CT state (diffusive solvation times reported for acetonitrile and ethyl acetate are given in Table 4.1). At early delay times it leads to a reduced absorption signal at probe wavelengths below 490 nm and some picoseconds later to a dent of the absorption between 500 nm and 580 nm. The effect of temporal fluorescence changes on the transient absorption spectrum of MGL in acetonitrile is reduced due to the more red shifted fluorescence.
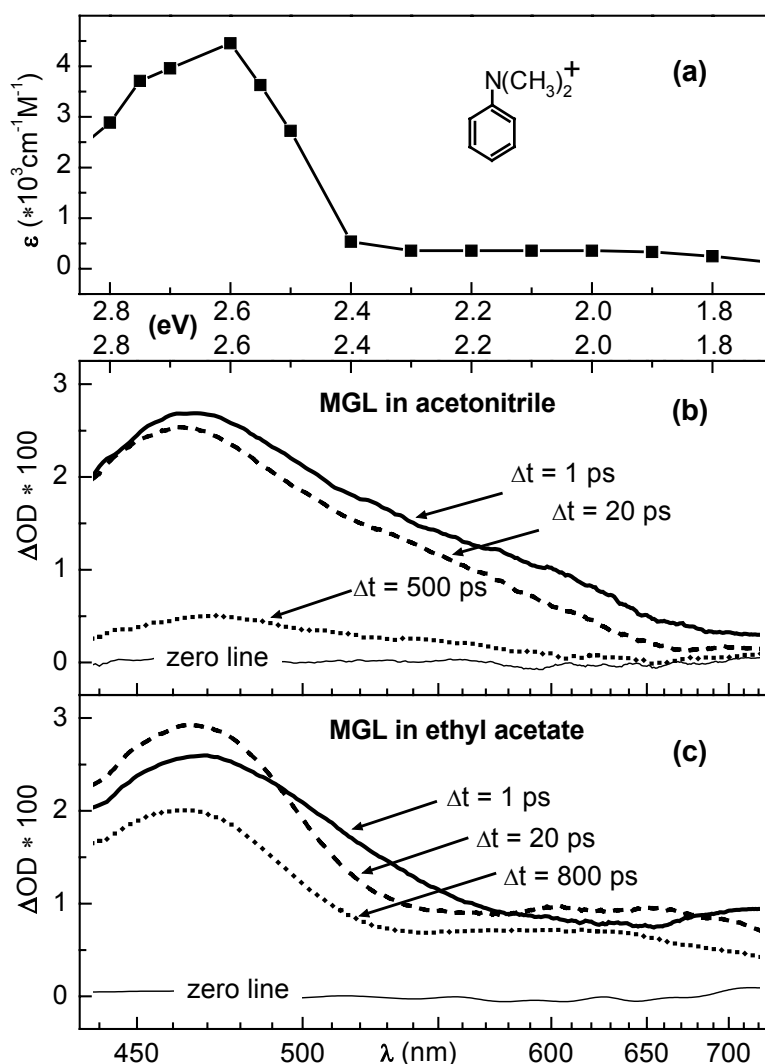
Figure 4.7(a) Absorption spectrum of DMA radical cations taken from Ref. [122]. (b) Transient absorption spectra of MGL in acetonitrile and (c) ethyl acetate recorded at 1 ps (solid lines), 20 ps (dashed lines), 500 ps and 800 ps (dotted lines) after excitation. The zero lines (thin solid) show the signal recorded before the excitation.

4.4 Two-color spectroscopy determines ultrafast dynamics of CT

Transient absorption spectra documenting the appearance of CT products and their subsequent decay show unambiguously that the time of charge transfer studied in both triphenylmethane lactones is shorter than 1 ps (see above). To determine the CT rate on the femtosecond time scale the kinetics of charge transfer process are studied by recording the absorption build-up curves in radical cation bands of PP and MGL (λ_{probe} = 475 nm).

4.4.1 Phthalide and phenolphthalein

Figure 4.8 presents the results of time resolved measurements of PP in acetonitrile and ethyl acetate. The data of Pd dissolved in the same solvents are given for comparison. On the left side of the figure the early stages of the absorption build-up are shown together with the fitting curves, which are obtained assuming multi-exponential decays and a Gaussian cross correlation (CC) with FWHM determined experimentally. Details on the fitting procedure are reported in Appendix A.
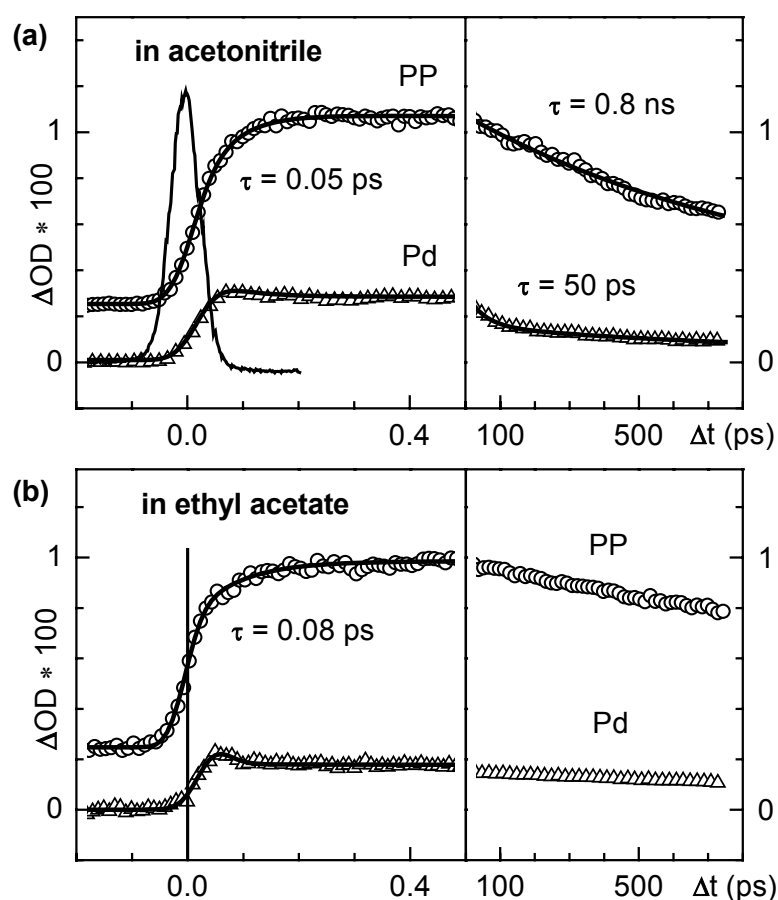
Figure 4.8 Kinetic traces of transient absorption for PP (circles) and Pd (triangles) in (a) acetonitrile and (b) ethyl acetate measured by two-color experiment (λ_{pump} = 270 nm, λ_{probe} = 475 nm). The time constants have been determined from the fits (solid lines) obtained by assuming multi-exponential decays and a Gaussian cross correlation (Appendix A). Left side of this figure shows early stages while the right side presents long time behavior. Absorption traces of PP are shifted along y axis for better visibility.

In order to visualize the difference between observed signal and instantaneous build-up of transient absorption the comparison between measured data and two types of CC curves is presented in Figure 4.9. The left side of the figure shows the integrated CC traces obtained

from the fitting procedure, where a Gaussian cross correlation is assumed and fitted to the measured curves together with a multi-exponential decay. To avoid any uncertainties (due to the assumed Gaussian or other artifacts coming from the fit) on the right side of the Figure 4.9 are presented the CC curves which are obtained from direct integration of the measured CC traces. Both types of CC curves show that the build-up of Pd absorption in acetonitrile and in ethyl acetate essentially corresponds to the integrated cross correlation, which means that excited state absorption of Pd appears immediately after excitation without a measurable time delay. Contrary to Pd, PP shows an absorption rise consisting of an exponential build-up with a time constant of 0.05 ps in acetonitrile and 0.08 ps in ethyl acetate.
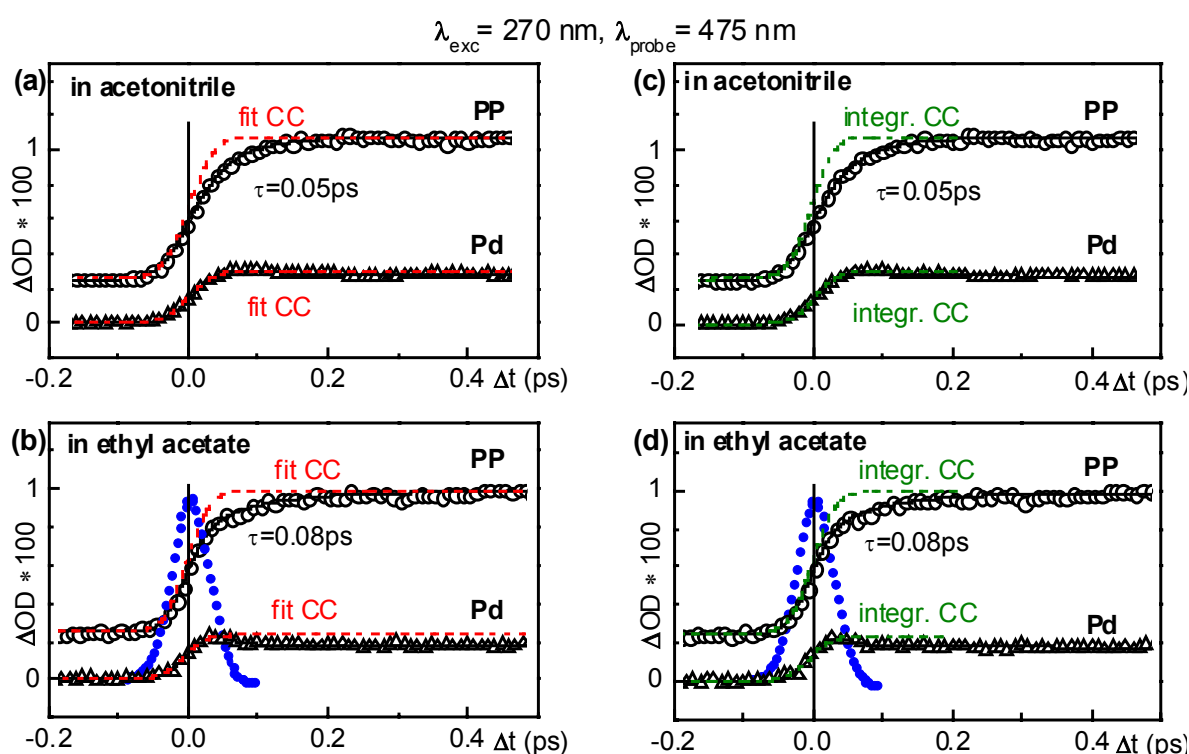
Figure 4.9 Two types of CC-presenting curves obtained from the fitting procedure (red dashed lines in (a) and (b)), and from integrated CC measured experimentally (green dashed lines in (c) and (d)) are compared to the measured data from PP (circles) and Pd (triangles) in acetonitrile ((a), (c)) and in ethyl acetate ((b), (d)). All CC curves are normalized to the maximum of the measured data. Black lines represent the corresponding fits, and blue symbols measured CC traces. The appearance of the Pd absorption corresponds to the CC, while PP shows an absorption rise consisting of an exponential build-up with a time constant of 0.05 ps in acetonitrile and 0.08 ps in ethyl acetate.

Figure 4.10 presents again the kinetic traces of PP in acetonitrile but includes additionally two curves simulating the absorption build-up of PP in acetonitrile, obtained with slightly different build-up time constants than that obtained in the fit ($\tau_1 = 0.05$ ps),

with other fit parameters kept constant as in the fitting. The two simulation curves obtained with τ_1 equal to 0.035 ps or 0.07 ps are distinctly different from the transient absorption trace of phenol radical cation formation and clearly demonstrate the limits of accuracy in the experiment. Based on these simulations the error is estimate to ± 0.01 ps.
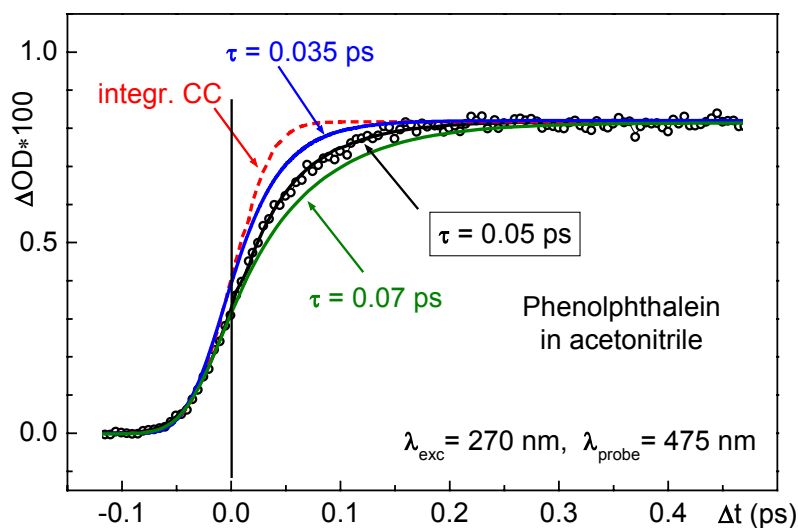
Figure 4.10 Transient absorption curve of PP in acetonitrile (circles) and corresponding fit with a rise time of 0.05 ps (black solid line) are presented together with two simulated transient absorption build-ups obtained with other time constants: 0.035 ps (blue solid line) and 0.07 ps (green solid line). Integrated CC (red dashed line) visualizes the difference between an instantaneous build-up of signal and that with finite time constant observed in the experiment.

PP is excited to the S_1 state, thus the time constants of the transient absorption rise in the phenol radical cation band (τ_1=0.05 ps in acetonitrile and 0.08 ps in ethyl acetate) reflect the rate with which the product of electron transfer appears and therefore is identified with the rate constant of the intramolecular ET process, $\tau_1 = \tau_{ET} = 1/k_{ET}$.

After the fast rise of the transient absorption a week decay component is observed. It is shown in Figure 4.11 that despite its small amplitude this second time constant (τ_2) is necessary to obtain proper fits. Due to its small amplitude there is large uncertainty of the time constant values. In acetonitrile the region from 0.6 ps to 4 ps is recovered from fitting and in ethyl acetate only the order of magnitude of 10 ps can be determined. This time constant indicates close relationship with diffusive solvation times reported for acetonitrile and ethyl acetate (see Table 4.1). As discussed above (see Section 4.3), contribution of τ_2 reflects the effect of temporal evolution of the fluorescence spectrum on the transient spectrum during the solvation process of the emerging intramolecular CT state. Such a low amplitude of the

τ_2 component suggests that the effect of diffusive solvation is almost not significant at wavelengths around 475 nm where the appearance of the radical cation is monitored.
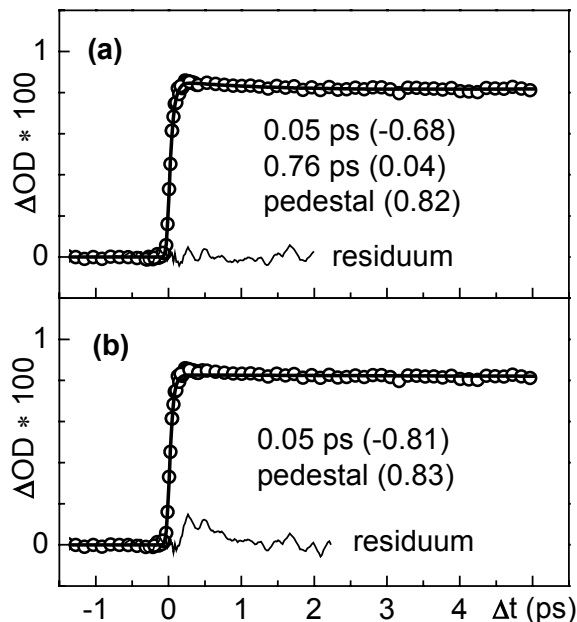
Figure 4.11 Time resolved data of PP in acetonitrile (circles) in the first 5 ps fitted with (a) three and (b) two time constants. The second constant is needed for the fit (solid lines) to suit the measured data properly. The amplitudes of time constants are given in brackets. The residuum line is multiplied by a factor 5.

Long decay times shown on the right side of Figure 4.8 represent the charge recombination process and the recovery of the ground state population. PP in acetonitrile shows a decay of 0.8 ns, while in ethyl acetate the corresponding time constant is slower than our experimental limit ($\tau_3 > 2$ns). There is no data of fluorescence quantum yield available from literature, because PP was generally considered as non luminescent molecule.

4.4.2 Malachite green lactone (MGL)

Figure 4.12 shows the results of kinetic measurements for MGL dissolved in aprotic solvents of different polarity and the corresponding fitting curves (fitting is performed assuming multi-exponential decays and a Gaussian cross correlation as reported in Appendix A). The probing wavelength of 475 nm corresponds to the DMA radical cation band, as discussed above (see Section 4.3.3). Thus the initial time constant shows the appearance of the DMA radical cation as a consequence of charge transfer.
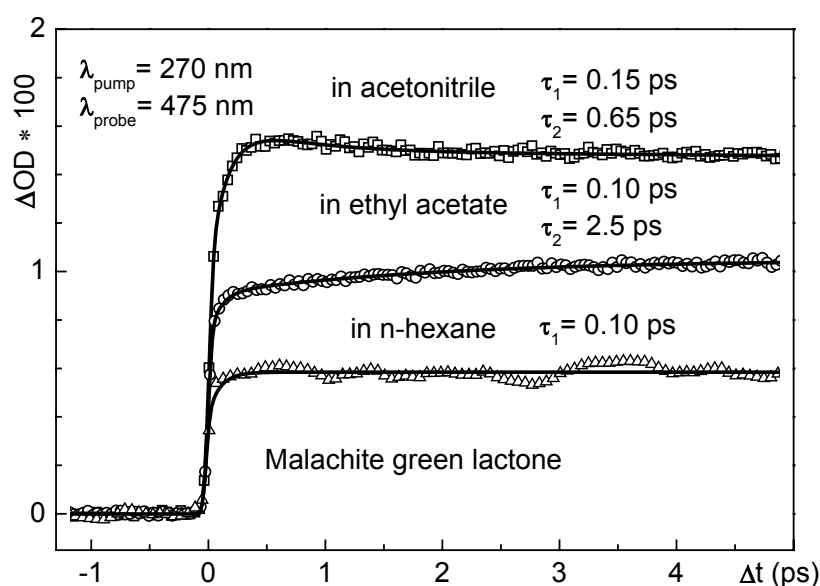
Figure 4.12 Time resolved measurements of MGL in acetonitrile (squares), ethyl acetate (circles) and n-hexane (triangles) during the first 5 picoseconds show two time constants in polar solvents (acetonitrile and ethyl acetate) and one in nonpolar solvent (n-hexane).

Somewhat longer rise times of transient absorption measured for MGL solutions (0.15 ps in acetonitrile and 0.10 ps in ethyl acetate) reflect the fact that MGL is excited to the S_2 state and indicate that the CT process occurs after the electronic relaxation $S_2 \rightarrow S_1$ which should delay the appearance of the DMA radical cations in the system by $0.01 - 0.10$ ps [123]. In such a case, the intrinsic time of CT in MGL would be comparable to that found for PP, i.e. on the order of 0.05 ps. Alternatively, 0.15 ps corresponds to the rate of electron transfer if the CT process proceeds from the S_2 state. Excitation to the S_1 state of MGL is needed to clarify this issue. In cyclohexane MGL shows a very fast transient absorption build-up which is fitted with a time constant of $\tau_1 \leq 0.10$ ps. Only this upper limit can be obtained due to uncertainties in accounting for the solvent coherent artifact in the initial phase of the kinetic trace. The observed rise of the transient absorption at 475 nm indicates that ET process in MGL occurs also in nonpolar environment without any need for assistance from solvation control. This result is consistent with broad and strongly Stokes shifted fluorescence spectrum of MGL in n-hexane which indicates fluorescence from the emerging CT state.

The values of the second time constant of 0.65 ps in acetonitrile and 2.5 ps in ethyl acetate, recovered from fitting shown in Figure 4.12, can be attributed to the reported diffusive solvation times (see Table 4.1). The relaxation process which occurs is a dielectric respond of solvent to the new dipole moment as a consequence of the new charge distribution which appears after emerging CT. The diffusive restructuring of the first solvent shell causes CT state to shift spectrally. At the probing wavelength of 475 nm this shift is observed as a low amplitude decay in acetonitrile and rise in ethyl acetate. The interpretation of the time

constant as a result of orientational solvation process is supported by the absence of this component in nonpolar n-hexane and by a greater contribution detected in the more polar solvent (acetonitrile compared to ethyl acetate).

The long time behavior of MGL dissolved in solvents with different polarity is shown in Figure 4.13. It represents the charge recombination process and the recovery of the ground state population. The dependence of the observed decays on the polarity of the solvent is in agreement with the known values of the fluorescence quantum yield [103], which increase with growing solvent polarity from n-hexane ($\Phi_{fl} = 0.032$) to ethyl acetate ($\Phi_{fl} = 0.069$), but then begins to decrease rapidly towards acetonitrile ($\Phi_{fl} = 0.0018$). Smaller values of the fluorescence quantum yield correspond to a faster decay. The long time decay in acetonitrile is fitted to the value of 0.45 ns while the decays in ethyl acetate and n-hexane are too long to determine the corresponding decay times accurately with the applied experimental setups, which enable time delays up to 1 ns.
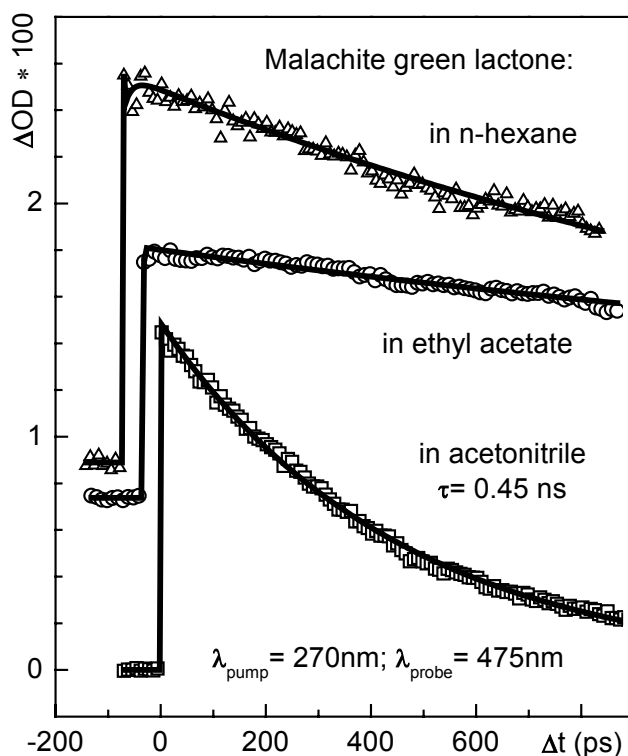
Figure 4.13 Long time behavior of MGL in acetonitrile (squares), ethyl acetate (circles) and n-hexane (triangles) shows slow decay of the transient absorption at 475 nm. Traces recorded in ethyl acetate and n-hexane are shifted along x and y axes for better visibility

4.5 Model of excited state dynamics in aprotic media

A scheme in Figure 4.14 shows a proposed model of ultrafast charge transfer, solvation dynamics and recombination processes in PP and MGL dissolved in aprotic solvents. Upon excitation at 270 nm PP is excited to the S_1 state (see Figure 4.14(a)) and MGL to the S_2 excited state (see Figure 4.14(b)). As a consequence of ultrafast intramolecular charge transfer a highly polar CT state is formed. The structure of this state can be approximated as an intramolecular "radical ion pair" consisting of covalently bound radical cation of the electron donor and radical anion of the electron acceptor. By probing at 475 nm the appearance of phenol radical cation band with an absorption maximum at 440 nm [120] is detected in the PP molecule and DMA radical cation band with an absorption maximum at 465 nm [122] in MGL molecule. For PP the dynamics of CT state formation is given by the time constant with which the transient absorption band of radical ions appears (τ_1 in Figure 4.14). In the case of MGL, where the S_2 state is excited the observed time constant (τ_1) is related to the appearance of DMA radical cation absorption band and includes both the $S_2 \rightarrow S_1$ relaxation and the CT state formation.
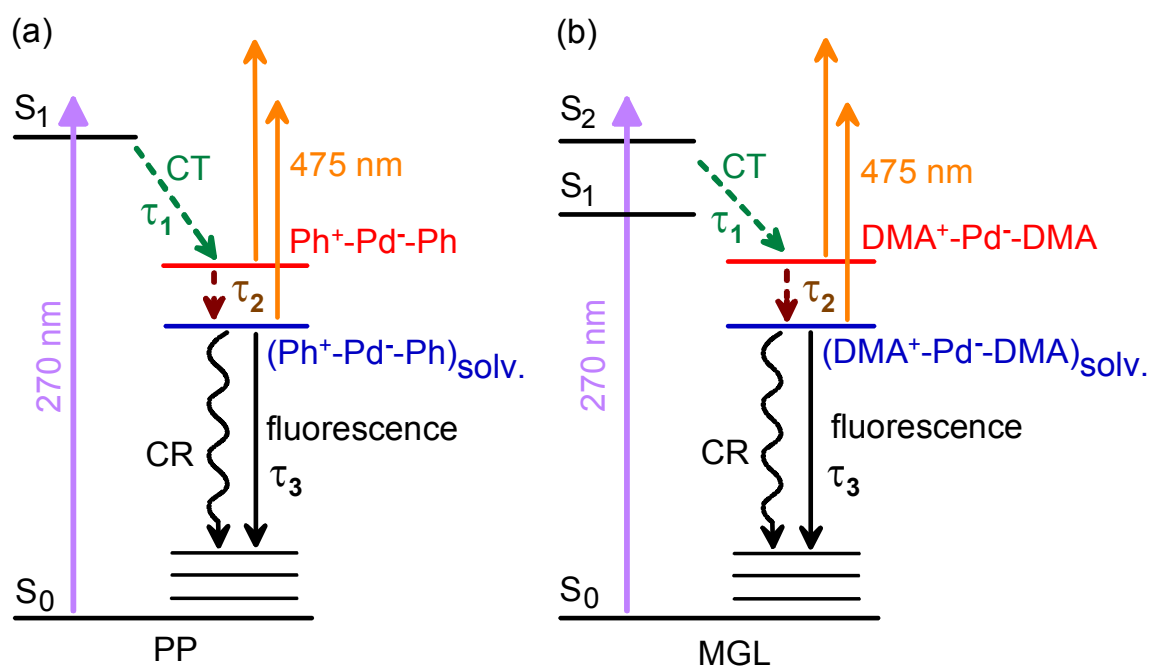
Figure 4.14 Model of excited state dynamics in (a) phenolphthalein and (b) malachite green lactone in polar aprotic solvents. Ultrafast intramolecular CT appearing with a time constant τ_1 is followed by diffusive solvation (τ_2). A long lived CT state recombines with a third time constant (τ_3) via fluorescence and non radiative decay to the ground state.

A low amplitude time constant observed subsequently in acetonitrile and ethyl acetate is described as τ_2 in Figure 4.14. It reflects the effect of the dielectric reorientation of polar solvent molecules due to a new charge distribution of the emerging CT state. The diffusive solvation causes additional spectral shift, which is detected as a rise or decay of the transient absorption spectra at 475 nm.

The intramolecular "radical ion pair" of both investigated molecules finally recombines via fluorescence and non radiative decay, observed as a relaxation process of CT state described with a time constant τ_3 in Figure 4.14.

All observed time constants are given in Table 4.2.

Table 4.2

The time constants obtained from fitting of kinetic curves for MGL in acetonitrile, ethyl acetate and n-hexane as well as for PP in acetonitrile and ethyl acetate

Molecule	solvent	τ_1 / ps	A_1	τ_2 / ps	A_2	τ_3 / ns	A_3
MGL	acetonitrile	0.15	(-0.7)	0.65	(0.2)	0.45	(1.5)
	ethyl acetate	0.10	(-0.2)	2.5	-(0.1)	>2	(1.1)
	n-hexane	≤ 0.10	(-0.1)	no middle decay		>2	(0.7)
PP	acetonitrile	0.05	(-0.6)	2.3	(0.1)	0.8	(0.8)
	ethyl acetate	0.08	(-0.2)	~10	(0.7)	>2	(0.7)

Three time constants are observed and correspond to (i) a rapid transient absorption rise on a 0.05 – 0.15 ps time scale (τ_1), (ii) a slower low amplitude transient absorption rise or decay (depending on solvent) observed during 0.5 – 5 ps (τ_2), and (iii) a long time decay (>0.4 ns) of the relaxed CT state (τ_3). The amplitude of the fitted constants are given in brackets, negative amplitudes indicate rising components in transient absorption traces.

4.6 Opening of the lactone ring in malachite green lactone dissolved in methanol

Steady state spectroscopy and transient absorption experiments are performed on malachite green lactone dissolved in methanol in order to investigate the ultrafast charge transfer process in protic media. The expected lactone ring opening [124] which leads to the appearance of malachite green dye is detected.

4.6.1 Steady state spectroscopy

Absorption spectra of MGL in methanol are generally similar to those in aprotic solvents with the same polarity, as shown in Figure 4.15. The first and the second absorption bands are slightly blue shifted in methanol compared to acetonitrile, slightly red shifted compared to ethyl acetate and more red shifted in the case of n-hexane. Additional bands or other major changes, as indication for the presence of other molecular forms of MGL or ground state complexes with the solvent, have not been observed.
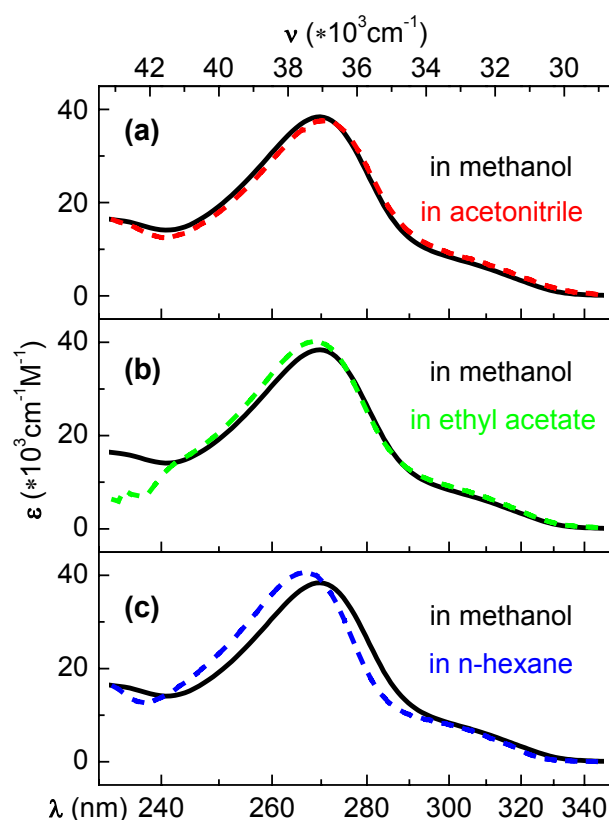

Figure 4.15 Absorption spectrum of MGL in methanol (black solid line) compared to the spectra of MGL in aprotic solvents: (a) acetonitrile (red dashed line), (b) ethyl acetate (green dashed line) and (c) n-hexane (blue dashed line). The spectrum in methanol shows a strong similarity to those in aprotic solvents with the same polarity

In contrast to aprotic solvents, the fluorescence quantum yield of MGL in methanol is very weak (estimated $\Phi_{fl} < 10^{-4}$ [103]). In alcohols, it depends strongly on both the polarity and the length of the aliphatic chain of the solvent molecules [103]. Fluorescence spectra in alcohols consist of one broad band with the maximum at the position corresponding to that in aprotic solvents with equal polarity. Such a decrease of the quantum fluorescence yield indicates additional non radiative relaxation channel of excited MGL. Indications for active participation of protic solvent molecules in the relaxation process was reported for the similar molecular system crystal violet lactone [125]. This can be explained by hydrogen bonding induced lactone ring opening [124] which leads to the transformation from a tetrahedral conformation of lactone form to a planar conformation of the triphenylmethane molecule. The corresponding chemical reaction is presented in Figure 4.16.

MGL (lactone) MG (zwitterion) MG (cation)
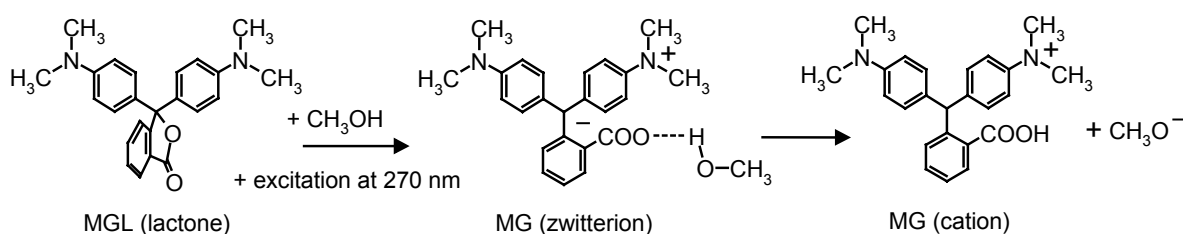
Figure 4.16 Chemical reaction of MGL in methanol after excitation at 270 nm. Ultrafast charge transfer in protic solvents is followed by hydrogen bond formation and a geometrical rearrangement that leads to the appearance of the malachite green cation.

4.6.2 Transient absorption spectra of MGL in methanol

The hypothesis of lactone ring opening in MGL in methanol is positively verified by the transient absorption spectra shown in Figure 4.17(a). In the first picosecond a broad band appears with a maximum at 473 nm and a wing extending far to the red. Although this band is slightly red shifted, it can be surely assigned to the absorption band of the DMA radical cation [122], which has its maximum at 465 nm. Like in aprotic solvents (see Sect. 4.3) the appearance of radical cation band indicates photoinduced charge transfer within less than 1 ps. In a next few picoseconds a new band with a maximum at 615 nm appears corresponding to the appearance of malachite green dye (MG), which dissociates in solvents forming MG cations (shown in Figure 4.17(b) [113]). This band indicates lactone ring opening, which results from a geometrical rearrangement and the transformation of the central carbon atom from a tetrahedral (sp^3) to a planar (sp^2) structure. The band of the DMA radical cations (473 nm) decays faster in methanol compared to aprotic solvents because of the additional relaxation channel, which depletes the population of the CT state. The band of the MG cations (615 nm) decays due to charge recombination and slower than the band of DMA

radical cations. In the region of wavelengths longer than 650 nm transient absorption signal disappears with dynamics similar to the formation of MG cation band. This suggests the transformation of MG radical cations, which have broad absorption band over the whole investigated region (see Figure 4.7) to MG cations (Figure 4.17(b)). This can be also due to primary blue shift of the MG cation absorption spectrum.
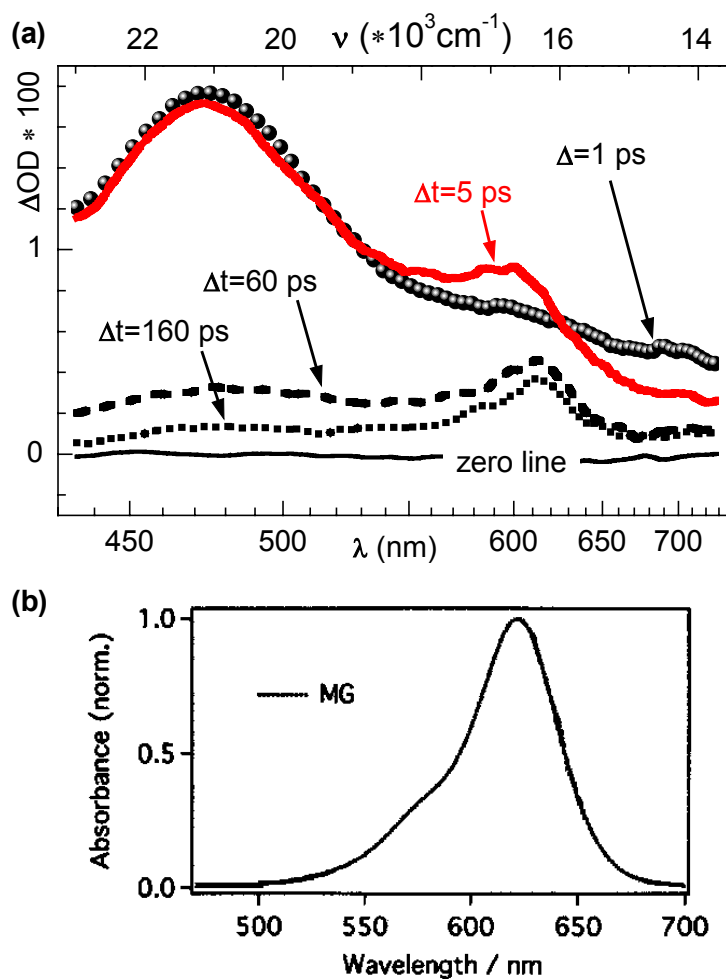
Figure 4.17(a) Transient spectra of MGL in methanol recorded at a delay of 1 ps (circles), 5 ps (red solid line), 60 ps (dashed line) and 160 ps (dotted line) after excitation. They show the initial appearance of DMA radical cations (470 nm) and subsequently the formation of MG cations (615 nm). The zero line (thin solid line) indicates the signal recorded before the excitation. (b) Absorption spectrum of MG cation taken from Ref. [113]

4.6.3 Time resolved measurements of MGL in methanol

Figure 4.18 shows the initial dynamics of MGL in methanol probed at different wavelengths together with the fitting curves. The Table 4.3 presents the results for the fitting parameters obtained by assuming multi-exponential decays and a Gaussian cross correlation (for details see Appendix A).

Figure 4.18 Time resolved data (circles) of MGL in methanol and corresponding fits (black lines) probed at 460 nm (blue), 560 nm (green), 610 nm (red) and 700 nm (pink). Traces at 460, 560 and 610 nm are shifted along x and y axes for better visibility.

Table 4.3

Fitted time constants with corresponding amplitudes in brackets

λ_{probe}	τ_1	(amplitude)	τ_2	(amplitude)
460 nm	0.15 ps	(-0.58)	--	
560 nm	0.15-0.4 ps	(0.28)	3-4 ps	(-0.55)
610 nm	0.15 ps	(0.09)	2-4 ps	(-0.45)
700 nm	0.4 ps	(-0.25)	2-4 ps	(0.46)

Negative value of the amplitude corresponds to a rise of transient absorption.

In the wavelength region of the DMA radical cation absorption band (460 nm) the contribution (build up) of the ultrafast component of 0.15 ps is the strongest one indicating that the CT process is as fast as in aprotic solvents. In the middle wavelength region (λ_{probe} = 560 nm and 610 nm) there is first a small contribution to the signal as a decrease of absorption with a time constant of ~0.15 ps. This region corresponds to the $S_n \leftarrow S_1$ absorption band of DMA (λ_{FWHM} = 550, 650 nm) [121], which is locally excited chromophore of MGL, as discussed above (see Section 4.2 and 4.3.3). The ESA band of DMA appears instantaneously within our time resolution. Subsequently absorption signal decrease in this region with a time constant of 0.15 ps, with which the absorption signal appears in a region of DMA radical cations. This is an additional evidence for the intramolecular CT process, which eliminates the assumption of direct CT transition. It should be noted that this fast decay corresponds to a time constant of low amplitude. A higher contribution to the transient absorption in this region (λ_{probe} = 560 nm and 610 nm) comes from an absorption increase on a time scale of 2 - 4 ps, which corresponds to the appearance of the MG cation absorption band [113] as discussed above (see Section 4.6.2). This time constant indicates its close relationship with diffusive solvation time of 3.2 – 3.3 ps [27, 35] or a dielectric relaxation time of 3.1 ps [112] reported for methanol (see Table 4.1). This subsequent process of solvation appears as a respond of the polar solvent molecules to a change of a charge distribution which results from initial CT process observed with a time constant of 0.15 ps. The dielectric solvent respond corresponds to the orientation of the hydroxyl group in methanol by rotation around its C-OH bond, which seems to be responsible for the opening of the lactone ring. As discussed above (see Figure 4.16), the chemical reaction of lactone ring opening is followed by the formation of MG cation band, which is detected with a time constant of 2 - 4 ps.

In the long wavelength region (700 nm) a decrease of the absorption signal is observed with the same time constant of 2-4 ps, what can reflect depopulation of the CT state, which corresponds to the broad band of DMA radical cation as discussed above (see Figure 4.7).

The long time behavior, shown in Figure 4.19, shows a double exponential decay at all probed wavelengths. The time constant of τ_3 = 20 ps is stronger in the wavelength region of the DMA radical cations while the slower one τ_4 = (300-500 ps) is stronger in the region of dissolved MG cations (amplitudes of fitted constants are shown in the Table 4.4).

Two different long time decays (~50 ps in the region of CT state and ~400 ps in the region of MG cations) imply that no population transfer between the CT state and MG^+ state is possible after 4 ps, so two independent return path ways to the ground state occur. The transient spectra (see Figure 4.17) shows also a faster decay of the DMA radical cation absorption band and a slower one of the MG cation absorption band.

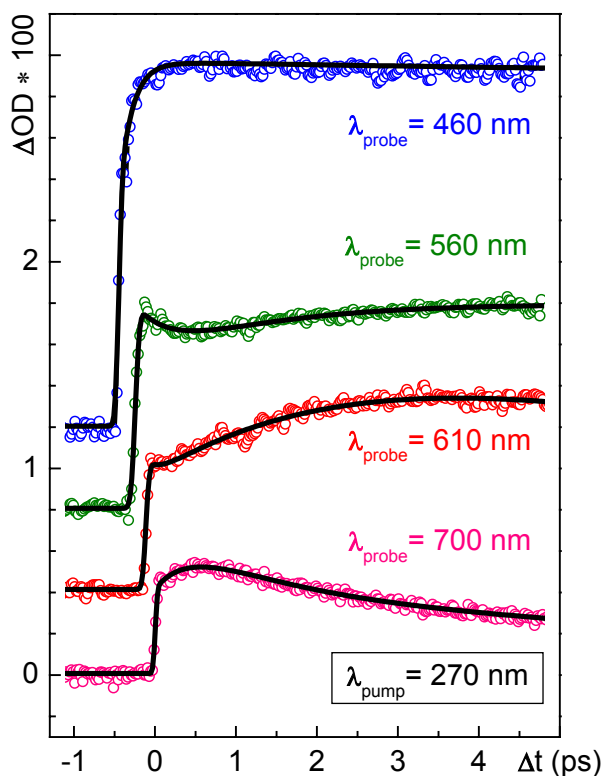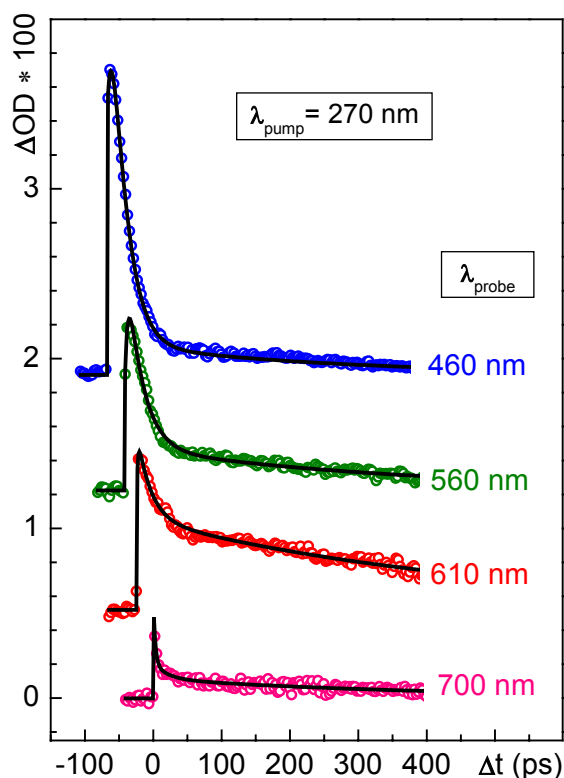**Figure 4.19 Long time behavior of MGL in methanol and corresponding fits (black lines) probed at 460 nm (blue), 560 nm (green), 610 nm (red) and 700 nm (pink).Traces probed at 460, 560 and 610 nm are shifted along x and y axes for better visibilty.**

<u>**Table 4.4**</u>
Fitted time constants with corresponding amplitudes in brackets

λ_{probe}	τ_3	(amplitude)	τ_4	(amplitude)
460 nm	20 ps	(3.03)	317 ps	(0.13)
560 nm	20-40 ps	(1.34)	400 ps	(0.27)
610 nm	20 ps	(0.51)	500 ps	(0.55)
700 nm	15-30 ps	(0.17)	405 ps	(0.11)

The 20 ps time constant is observed over a whole observed spectrum range with different amplitudes reflecting a shape of CT state, which occurs also in MGL dissolved in acetonitrile (see Figure 4.7). This 20 ps decay indicates a new additional relaxation process of the CT state in protic environment, which could be related to another dielectric relaxation time of methanol reported for alcohols [112, 126]. This intermediate time constant in the region from 20-50 ps originates from the rotation of the free monomeric molecule and is also observed as one time constant of multi-exponential fit describing polar solvation dynamics

[27]. It is possible that this kind of molecular reorientation of protic solvents causes faster recombination of the radical ion pair of the CT state.

The longer time constant (τ_4) reflects the recombination of MG cation to the ground state. A small contribution of τ_4-time constant in the wavelength region outside the MG cation absorption band (λ_{probe} = 460 nm and 700 nm) indicates that corresponding absorption band is broader than shown with cw-spectrum (see Figure 4.17(b)).

4.6.4 Model of excited state dynamics of MGL in protic environment

A proposed model of excited state dynamics of MGL in methanol is presented in Figure 4.20. The pump pulses at 270 nm excite the S_2 state of MGL. As discussed above (see Section 4.2) predominantly are the DMA groups of MGL optically excited and the charge is transferred from the excited donor to the ground state acceptor producing an intramolecular radical ion pair of the CT state with a time constant τ_1.
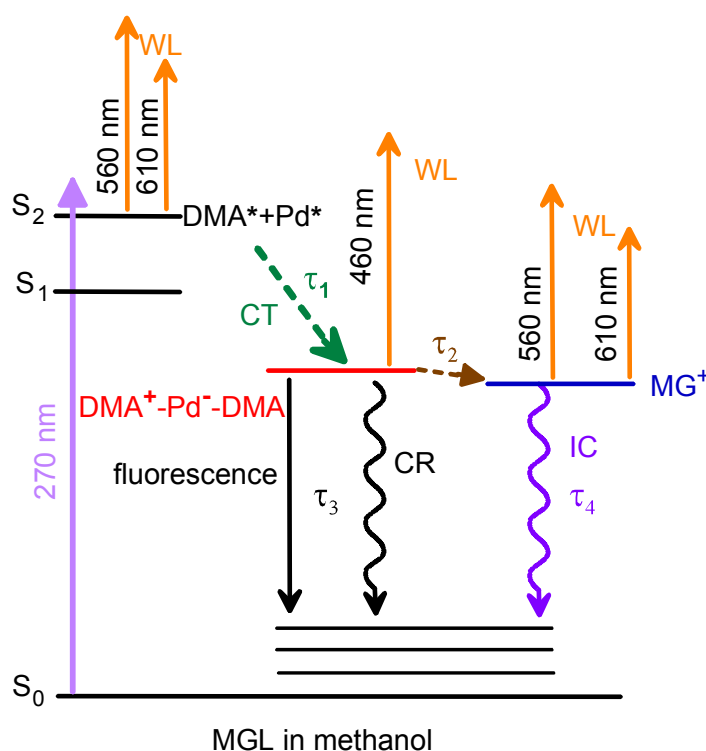
Figure 4.20 A proposed model for excited state dynamics of MGL in protic environment. Ultrafast intramolecular CT appears with a time constant τ_1. Subsequently a diffusive solvation process (τ_2) breaks a lactone ring producing MG cations, which relax on a τ_4-time scale to the ground state. The CT state population influenced with a dielectric solvent relaxation recombines with a time constant τ_3 to the ground state.

Subsequently on a time scale of $\tau_2 = 2 - 4$ ps the absorption band of MG cations appears as a result of lactone ring opening, caused by the diffusive solvation process of methanol molecules. This absorption band relaxes on a τ_4-time scale to the ground state. The CT state population is influenced with a dielectric solvent relaxation, which causes its faster recombination with a τ_3 time constant via fluorescence and non radiative decay.

4.7 Discussion

MGL and PP are molecules with similar, well-defined nearly orthogonal arrangement of electron donating groups in relation to the acceptor moiety. In PP two phenol rings are twisted almost perpendicular (72.9°) with respect to each other and are oriented with dihedral angles of 73.6° and 74.4° with respect to the heterocyclic Pd ring [127]. All C-C bonds of the central carbon atom (two with phenols and one inside the lactone ring) are nearly equally long and their lengths (0.1509 – 0.1525 nm [127]) indicate that the delocalization of electrons from aromatic rings does not extend to the central C atom. Similar values have been found for MGL [103]. Due to the additivity of the molar extinction coefficients the absorption spectra of MGL and PP in the low energy region are considered as a superposition of the spectra of their structural subunits. These spectral properties in line with the structural features lead to the conclusion that the ground state interactions between the structural subunits in MGL and PP can be neglected and point out that there are no direct optical CT transitions in both LTAMs. This statement is also supported by time resolved measurements of MGL in methanol performed in this work, where an instantaneous rise of absorption is observed in the region of ESA of the locally excited DMA chromophore [121]. Subsequently the decrease of the ESA of DMA is detected with the same time constant as the absorption increase of DMA radical cation band. Such electronic decoupling of structural components in the ground state has been also observed for spiropyrans [128] and various leuco forms of triarylmethanes, including malachite green leuconitrile [104-106].

Upon excitation of their structural subunits, PP and MGL undergo ultrafast intramolecular charge transfer (CT) with formation of a long-lived, highly polar CT state. Its structure can be approximated as an intramolecular "radical ion pair" consisting of a radical cation of the electron donor and a radical anion of the electron acceptor being covalently bound subunits of the molecule. Subsequently diffusive solvation in aprotic solvents leads to a small shift of the transient spectrum detected as a low amplitude absorption decay or rise. In protic media the diffusive reorientation of solvent molecules causes the hydrogen bonding induced lactone ring opening [124], which provides a significant geometrical rearrangement needed for the transformation from a tetrahedral to a planar conformation of the molecule. Finally the recombination occurs via fluorescence and non radiative decay to the ground state with a

time constant which depends on polarity of the solvent (in high polar acetonitrile $\tau_3 = 0.45$ ns and in methanol $\tau_3 = 0.30$ ns, while in low polar ethyl acetate and non polar n-hexane $\tau_3 > 2$ ns is longer than our experimental limit). This indicates a relationship between the polarity of the solvent and the velocity of the recombination process and implies an influence of the long relaxation time reported for some alcohols on recombination process. This relaxation is attributed to the breaking of the H-bond in molecular aggregates followed by ROH rotation and occurs on a time-scale from 100-2200 ps [112, 126, 129].

Spectral signature of DMA radical cation has been found in nanosecond transient absorption spectra of MGL [103] and of structurally similar crystal violet lactone [130], where only products of photoinduced CT process could be observed because of a limited time resolution. The emitting ^{1}CT state in MGL lies energetically below the excited ^{1}S singlet states of the insulated structural subunits (DMA above 30200 cm^{-1} and Pd above 35700 cm^{-1} [103]) and is strongly stabilised by interaction with the polar environment which is reflected in a huge Stokes shift in polar solvents. The CT process in both LTAMs studied in this work is strongly exothermic with a free energy change, (ΔG) evaluated with the Weller equation [54] (for details see Chapter 2). In acetonitrile ΔG equals to -1.19 eV and -0.84 eV for MGL and PP, respectively. ΔG assumed earlier for MGL (-1.30 eV [103]) has been corrected here by using reduction potential for Phthalide from cyclic voltammetry measurements [131] instead of reduction potential reported by Leedy et al. [132].

According to the two dimensional ET model developed by Sumi and Marcus [25], such a ΔG^0 value would result in ET reaction rates near the maximum of the "bell shaped" curve ($\geq 7 \cdot 10^{12}$ s^{-1}) [133], where the ET processes are predicted to occur in very low energy-barrier or barrierless regime. Because of a well defined single donor-acceptor orientation in PP and MGL simple decay kinetics of primarily excited chromophore and rise kinetics of CT products can be expected and are observed in presented experiments. The ET dynamics is determined mainly by intramolecular vibrational motions and not by the orientational (diffusive) solvation process. This conclusion is strongly supported by observation of CT process in MGL in nonpolar environment (n-hexane), inline with lack of fluorescence from locally excited chromophore in these media and by presence of CT luminescence with large Stokes shift.

Very short times of radical cation formation presented above confirm the earlier estimations from steady state spectroscopy [103] and provide clear evidence for intramolecular ET process in LTAMs that occurs from a vibronically non-equilibrated level and that is markedly faster than the diffusive solvation time scale. According to theories modelling dynamic solvent effect in ET reaction occurring under nonequilibrium conditions [24-26, 37, 91, 134], the ET rate and the trajectory along the reaction coordinate are determined by both the solvent relaxation rate (here the inertial dynamics component [31]) and intramolecular

degrees of freedom. The intramolecular vibration motions of the solute act as the ET promoting modes. The time constant of 50 fs related to the ET of PP in acetonitrile, which occurs upon excitation to S_1 state, is the fastest intramolecular ET rate determined so far by direct observation of ET product build-up kinetics. This value is also distinctly shorter (within accuracy limits of this work, see Figure 4.10) than 70 fs inertial component found in ultrafast solvation dynamics of acetonitrile [30] or even longer times proposed in simulations [29, 32]. The inertial solvation in ACN involves mainly small amplitude rotational motions of solvent molecules described in [29] as the rotation of the cyanide group (-CN) around the CH_3-CN bond of the acetonitrile molecule in the first solvation shell. As found in computer simulation of solvation dynamics this rotational motions account for up to 80% of the total relaxation [30, 32, 91]. If the 70 fs time constant is valid for describing the inertial solvation dynamics in acetonitrile, the observed photoinduced ET in PP in acetonitrile occurs faster than the ballistic motions of the surrounding solvent molecules that stabilize the energy of the solute-solvent system. Effective and very fast CT in nonpolar environment suggests that polar solvation is indeed not a precondition to reach the CT state. This indicates a dominant role of high-frequency intramolecular vibrational mode(s) in the CT process and not to be controlled by solvent dynamics.

In LTAMs such a source of vibrational coupling is provided by C-O bond in lactonic ring, as electron capture by or transfer on the phthalide molecule results in excitation of C-O stretching vibrations, leading to C-O bond instability and high probability of its cleavage [131, 135, 136]. The breakage of this bond leading to the lactone ring opening is experimentally verified for MGL in methanol, where the diffusive reorientation of the solvent molecules influences the structure of the solute (see Section 4.6). The excess of electron energy resulting from electron capture by Pd was found to be preferably deposited in the C-O bond via a nuclear-excited Feshbach resonance [135]. The Feshbach resonance indicates the formation of a dipole-bound Pd^- anion with an excess electron weakly bound by a long range electrostatic field generated by the high (4.9 D) dipole moment of the Pd molecule [137] and residing on a very diffuse orbital outside the molecular frame [138]. Such an orbital should have significant overlap with the orbital of the primarily excited donor part of LTAM molecule, resulting in their coupling, which in turn would lead to the very high ET rates observed in these systems. A large spatial overlap of donor and acceptor orbitals has been found to be a prerequisite for an ultrafast ET [139]. Theoretical work is needed to explore the possibility of occurrence and the electronic structure of such dipole-bound resonance states involving the Pd molecule. Occupation of the diffuse orbital would correspond to formation of a very shortly lived resonance state in the initial phase in the charge transfer process in LTAMs and might be of primary importance for understanding the initial dynamics of charge transfer processes in organic D-A systems.

5 Ultrafast photoionization of indole

5.1 Introduction

Indole is a common chromophore of many nitrogen heterocyclic biomolecules such as tryptophan or indole-3-carbinol (see Figure 5.1). Tryptophan is one of the 20 essential human amino acids with the strongest UV absorption. It is a biologically important probe for protein structure and dynamics due to its strong fluorescence which is highly sensitive on the local environment [140-146]. Indole-3-carbinol is a highly effective anticancer agent which blocks carcinogenic substances and eliminates DNA damage in cell nuclei [147, 148]. Indole is a model compound to study the response of these molecules to photoexcitation.

For a long time the photodissociation of organic molecules into radicals, ions and electrons [149] has attracted large interest since it contributes to the damage of biological substances by UV radiation. Most of the molecular building blocks show very short excited state lifetimes, what makes them capable to minimize dangerous photoreactions in living cells [38-40]. The nonradiative processes presumably are ultrafast internal conversion (IC) back to the ground state and photoionization (formation of solvated electrons) in aqueous solution [12]. Reactions of the solvated electron with biological substances is important for radiation biology since the molecules attacked play a vital role in the life of the cell [150].
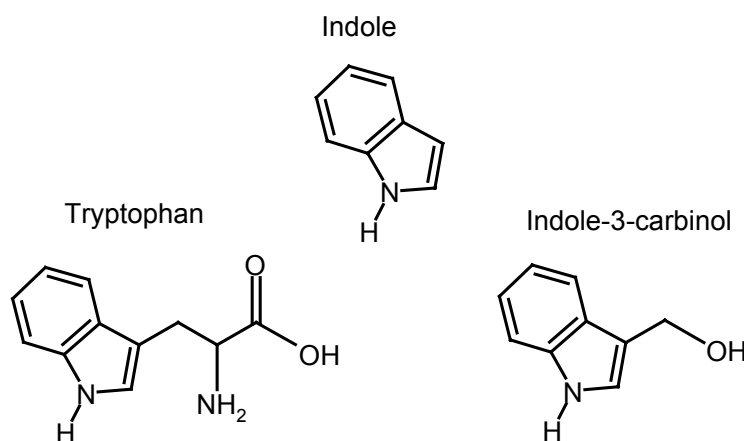
Figure 5.1 Structural formulae of indole and two of its derivatives tryptophan and indole-3-carbinol. Indole is a heterocyclic biomolecule consisting of a benzene and a pyrrole ring.

It is known that tryptophan as well as its chromophore indole exhibits efficient photoionization as additional relaxation channel [13-16, 151-155]. There are many experimental [156-164, reviews: 165, 166] as well as theoretical studies [167-170] describing the

tryptophan fluorescence properties which are basically originating from its chromophore indole. There are only few time resolved experimental studies investigating the photoionization of indole and tryptophan [17-20] but the exact mechanism of the ionization is not yet clarified because of the insufficient time resolution of the experiments (> 200 fs).

Despite the great interest to this topic there are still many open questions. The strongest puzzle of tryptophan and its chromophore indole is the connection between their strong fluorescence with a fluorescence lifetime of a few nanoseconds and a very fast photoionization occurring within 1 ps.

This chapter presents the photodynamics of electronically excited indole in water, which is the most important solvent for biomolecules and compares it with the behavior in other solvents. At applied excitation wavelength (270 nm) there is no photoionization of indole in ethanol and cyclohexane [171]. In such a case the influence of the solvent polarity to the electronic dynamics of indole has been clarified. The chemical structure of the solvents used is given in Figure 5.2. The static dielectric constants and the relaxation times relevant to the solvation processes are given in Table 5.1.
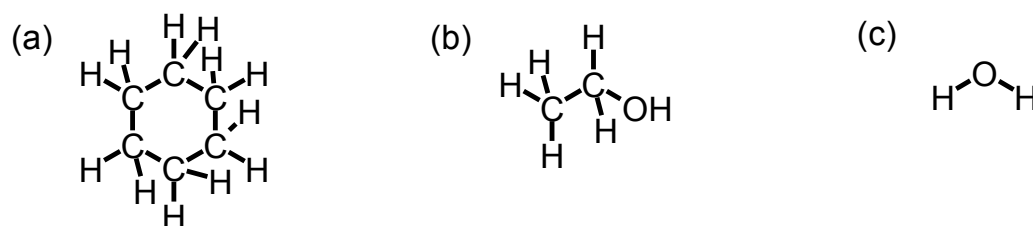
Figure 5.2 Structural formulae of the solvents used in the experiments on indoles: (a) cyclohexane, (b) ethanol and (c) water.

Table 5.1
Static dielectric constants and dielectric relaxation times of the solvents used in the indole experiments

solvent	stat. diel. cons.	diel. relaxation
cyclohexane	2^a	$--^b$
ethanol	25^c	$1.6 \ ps^d$
water	80^e	$\sim 1\text{-}2 \ ps^f$

[a] **At 298 K taken from [109, 111]: 2.02 and at 291 K from [108]: 1.9;** [b] **Time constant is not known;** [c] **Mean value from [111]: 24.3, [109]: 24.55, [108]: 25.1;** [d] **Taken from [17];** [e] **Mean value from [24]: 78.36, [111]: 78.54, [108]: 81.6;** [f] **from [24]: 0.54 ps, [172]: 1.2 ps, [173]: 1.1 ps, [174]: 1.2 ps, [175]: 2.7 ps.**

The femtosecond UV-visible broadband absorption study of indole is considered here for the first time together with the steady state measurements in order to clarify the unusual behavior of a strong fluorescence and simultaneously occurring ultrafast photoionization. Transient spectra of solvated indole are measured in a 120 μm thick, free flowing liquid jet with a crosscorrelation of 80 fs by means of a white light continuum (450 -740 nm) generated in a sapphire disc. The molecules are excited at 270 nm with pump pulses generated by frequency doubling the output of a noncollinearly phase matched optical parametric amplifier (NOPA) (Section 3.1.1). The time resolved traces are probed either with ultrashort pulses at selected wavelength obtained by a second NOPA or with a spectrally resolved white light continuum. Due to the short pump pulses there is a small yet finite probability for two-photon ionization in neat solvents as previously discussed in Section 3.4.2. This allows one to study the spectral properties of the solvated electrons generated in neat solvents compared to the solvated electrons generated in indole solutions. The transient spectra and time resolved traces of the indole solution are corrected for these solvent contributions as shown in Section 3.4.2 and Appendix B.

In order to clarify the origin of solvated electrons the initial solvation dynamics of 1-methylindole in water is investigated. Indole which has a hydrogen atom bound to the nitrogen has a possibility of exhibiting both hydrogen and electron transfer, while 1-methylindole because of its methyl group bound to the nitrogen can only exhibit electron transfer.

5.2 Steady state characterization

5.2.1 Absorption and fluorescence spectra of indole in different solvents

Stationary spectra of indole dissolved in cyclohexane, ethanol and water are shown in Figure 5.3. The absorption spectra present the overlapping bands due to the two lowest electronically excited singlet states: the ^1L_a and ^1L_b state. They are named ^1L_a and ^1L_b because of the phenomenological analogy with similar states of substituted benzenes and naphthalenes [47] following the Platt's classification [176]. The absorption spectrum of the ^1L_b state exhibits a much more pronounced vibronic structure than the one of the ^1L_a state (see Figure 5.3). The fluorescence in nonpolar solvents (cyclohexane) shows structure characteristic for the ^1L_b state, while in polar solvents (ethanol and water) the structureless and more red shifted fluorescence corresponds to a transition from the ^1L_a state. The Stokes shift and width (FWHM) of the fluorescence spectra in different solvents are given in Table 5.2. The values obtained here are in agreement with those reported in literature [18, 165].
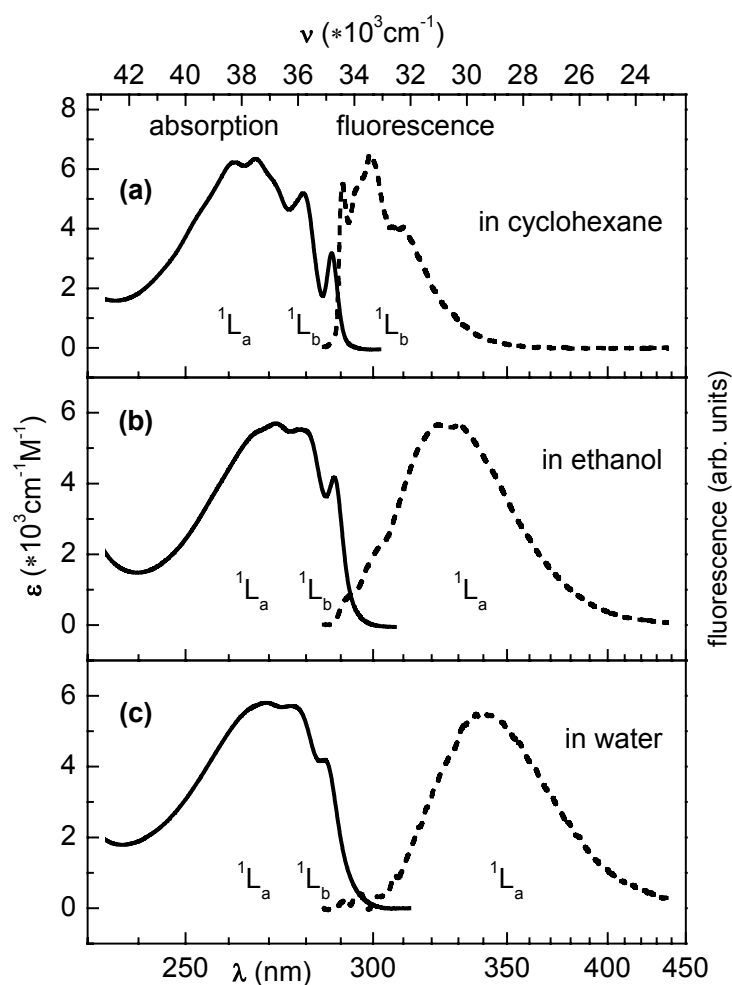
Figure 5.3 Absorption (solid lines) and fluorescence spectra (dashed lines) of indole in (a) cyclohexane, (b) ethanol and (c) water. With the pump pulse at 270 nm the mixture of ^1L_a and ^1L_b state is excited. In nonpolar solvents (cyclohexane) the structured ^1L_b state emits, while in polar solvents (ethanol and water) the structureless ^1L_a state emits.

<u>**Table 5.2**</u>
Fluorescence properties of indole dissolved in different solvents

solvent	$\lambda_{fluorescence}^{max\ a}$ $\pm\ 2$ nm	$\nu_{fluorescence}^{max\ b}$ $\pm\ 250$ cm^{-1}	ν_{abs}-ν_{fluor} ^{c} $\pm\ 250$ cm^{-1}	FWHM ^{d} $\pm\ 300$ cm^{-1}
cyclohexane	299 nm	33450 cm^{-1}	4000 cm^{-1}	3000 cm^{-1}
ethanol	326 nm	30700 cm^{-1}	6500 cm^{-1}	4600 cm^{-1}
methanol	327 nm	30600 cm^{-1}	6500 cm^{-1}	4650 cm^{-1}
water	337 nm	29700 cm^{-1}	7500 cm^{-1}	4780 cm^{-1}

$^{a,\ b}$ **Position of maximum of fluorescence spectrum in nm and cm^{-1} respectively; ^{c} Stokes shift; ^{d} Full Width at Half Maximum of fluorescence spectrum**

With the excitation at 270 nm a mixture of the ^1L_a and ^1L_b state is populated. The unstructured fluorescence spectrum of the ^1L_a state shows a large Stokes shift and a strong solvatochromic effect due to the large change of the dipole moment upon electronic excitation. The changed permanent dipole causes the surrounding solvent molecules, on average, to move in response to the new dipole. This motion is known as solvent-solute relaxation or dielectric relaxation [166]. The dipole moment strength of the ^1L_b state is similar to the ground state value. The directions of the permanent dipole moments in the ground and in the three lowest excited states are shown in Figure 5.4. Their magnitudes collected from literature are listed in Table 5.3. Computational investigations [177, 178] propose that the optically allowed ^1L_a and ^1L_b ($\pi\pi^*$) states intersect with the dark S_3 ($\pi\sigma^*$) state. Due to this crossing the dark state gets populated. The S_3 state exhibits radical changes in the charge distribution as a result of electron density shifting from the rings to the hydrogen atom of the NH group (see Figure 5.4). The strong polarity of the NH bond in this calculated S_3 ($\pi\sigma^*$) state indicates the possibility of electron transfer to the solvent followed with the electron solvation in polar solvents such as water. Recently the existence of an excited $\pi\sigma^*$ state which is dissociative along the indole NH stretch coordinate is verified experimentally by the excited state fluorescence-dip infrared spectra (FDIR) of indole and its derivatives [179].
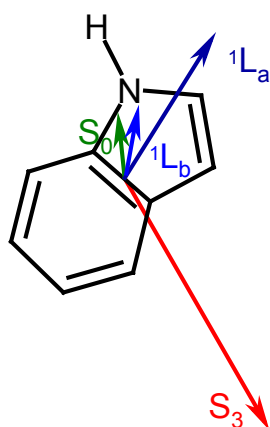
Figure 5.4 The permanent dipole moments of indole computed from ab initio methods for the ground S_0 (green arrow) and the lowest excited singlet states: S_1 (^1L_b) (blue arrow), S_2 (^1L_a) (dark blue arrow), and S_3 state (red arrow) taken from Ref. [166, 177, 180, 181]. The arrow head indicates the positive end of the dipole. The S_3 and S_2 (^1L_a) states differ greatly in magnitude and direction of the dipole moment as compared to the ground or S_1 (^1L_b) state.

Table 5.3

Permanent dipole moments in the ground and the excited states of indole

method	Permanent dipole moment (Debye)				Ref.
	S_0 state	S_1 (^1L_b) state	S_2 (^1L_a)state	S_3 state	
theoretical	2.02 - 2.22 D	2.63 - 2.83 D	5.09 - 5.87 D		[a]
theoretical	1.87 D	1.55 D	6.12 D	11.03 D	[b]
experimental	2.1 D	3.5 D	5.5 D		[c]

[a] **calculated using spectroscopically calibrated semiempirical molecular orbital INDO/S-CI methods: [182],** [b] **calculated using CIS, CASSCF and CASPT2 ab initio methods [177],** [c] **[110], [183]**

In nonpolar solvents like cyclohexane, the ^1L_b state is energetically below the ^1L_a state and the resulting fluorescence exhibits vibronic structure. In polar solvents like ethanol, methanol or water a state reversal occurs after the electronic excitation as a result of the solvent reorientation causing significant lowering of the ^1L_a state, which is responsible for the broad, more red-shifted fluorescence. Due to the larger dipole moment of the water molecules compared to that of ethanol or methanol a somewhat larger Stokes shift of the fluorescence spectrum is observed (see Table 5.2). The loss of structure in the ^1L_a fluorescence band is the consequence of the high degree of inhomogeneous broadening exhibited by the ^1L_a transitions owing to its large dipole change [166].

The state reversal has been already discussed in literature [110, 184, 185]. The explanation for this phenomenon can be the solvent-solute relaxation or dielectric relaxation of solvent molecules around a new charge distribution [166]. It is also suggested that a lowering of the ^1L_a state relative to the ^1L_b state can occur via hydrogen bonding of nearby polar solvent molecules to the π electron cloud of the indole [162, 163]. Although experimentally not yet observed, theoretical calculations indicate that besides the conventional type of H-bonding between the polar solvent and the NH indole bond, a nonstandard H-bonding to the π electron cloud of indole via formation of a so called πH-bond can indeed occur [181, 186].

5.2.2 The fluorescence quantum yield

The fluorescence quantum yield (Φ_F) can be expressed as the ratio between the fluorescence (τ_{fl}) and radiative lifetime (τ_{rad}) (for details see Section 2.1):

$$\Phi_F = \frac{1/\tau_{rad}}{1/\tau_{fl}}. \tag{5-01}$$

To obtain the absolute fluorescence yield of indole the intensity of its fluorescence spectrum was compared to rhodamine 6G and coumarin 47 excited at 488 nm and 404 nm respectively. The same method is applied in the case of o-hydroxybenzaldehyde and discussed in more details below (see Section 6.2). By means of the yields for rhodamine 6G and coumarin 47 reported in literature as 0.88 and 0.64, respectively [187, 188], the fluorescence quantum yield of indole excited at 270 nm is determined to $\Phi_F = 0.1$. The value for indole in cyclohexane is found to be 10 % higher than that in water, ethanol or methanol. This shows a similar tendency as reported previously [160, 161]. The absorption and fluorescence spectra of indole are far in the UV spectral region. It was not possible to find a dye with known fluorescence yield which would absorb and emit in a spectral region more closely related to indole than the ones used here. One has to be aware that the optical elements in the spectrometers cause more losses due to their spectral properties in the UV as in the visible spectral region, what lowers the precision and accuracy of this method. Nevertheless, the value of fluorescence quantum yield estimated here is in qualitative agreement with previously reported values [156-158, 160, 161] indicating a significant population of the fluorescence state. From the values reported for the excitation in the range of 265 nm – 295 nm the mean value of 0.25 is estimated and used below for the calculation of the fluorescence lifetime of indole in water (see Section 5.4).
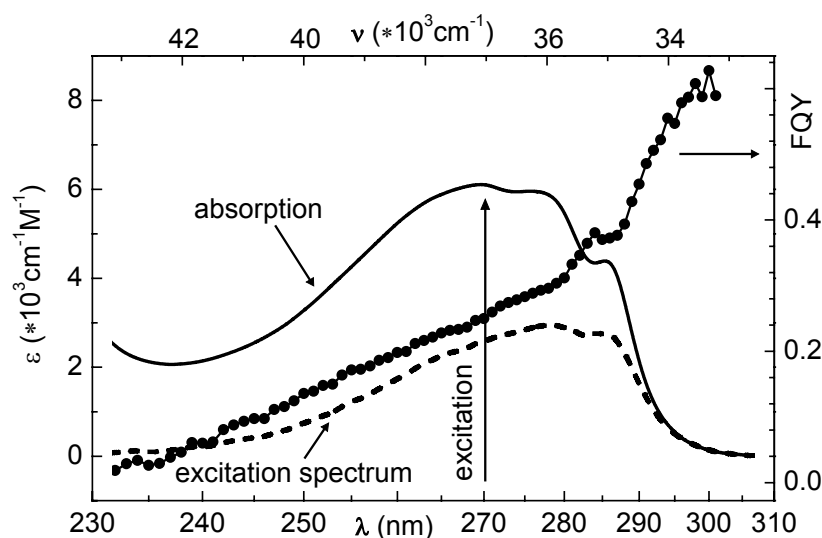
Figure 5.5 Absorption (solid line) and fluorescence excitation spectrum (dashed line) of indole dissolved in water and the corresponding fluorescence quantum yield (circles). The excitation spectrum is recorded on monitoring the fluorescence at $\lambda_{emission}$ = 340 nm.

The excitation spectrum of indole in water measured by monitoring the fluorescence at $\lambda_{emission}$ = 340 nm is shown in Figure 5.5. The behavior of the fluorescence quantum yield in the whole spectral region is calculated by dividing the fluorescence spectrum with the

absorption spectrum. The absolute values are calibrated with respect to the value of 0.25 at 270 nm estimated from literature (see Figure 5.5).

As can be seen from Figure 5.5, the quantum yield of the indole fluorescence increases with increasing the excitation wavelength in the observed spectral region (230-300 nm). This implies the breakdown of Vavilov's law (independence of the fluorescence quantum yield on the excitation wavelength). Steen [189] has reported a similar wavelengths dependence of the fluorescence quantum yield in the short wavelength region 220 - 250 nm but claimed a constant value of fluorescence quantum yield for the excitation wavelengths longer than 250 nm. It is known that in the energy region above the ionization threshold ($\lambda < 287$ nm) the photoionization quantum yield increases with increasing excitation energy [171, 190]. Thus it is expected that the fluorescence quantum yield does not show constant value at least in the region of $\lambda < 287$ nm, but an decrease with increasing excitation energy, as shown in Figure 5.5 and Figure 5.6.

As shown in Figure 5.6, the fluorescence quantum yield of indole dissolved in cyclohexane and ethanol exhibits similar dependence on the excitation wavelength as when dissolved in water. For indole dissolved in water the behavior of the fluorescence quantum yield is shown here at two different temperatures (see Figure 5.6). The observed decrease of the fluorescence yield with increasing temperature can be an evidence for an energy barrier in the radiationless relaxation process, which is competing with the fluorescence. The same temperature dependence is reported by other authors [152, 161, 165].
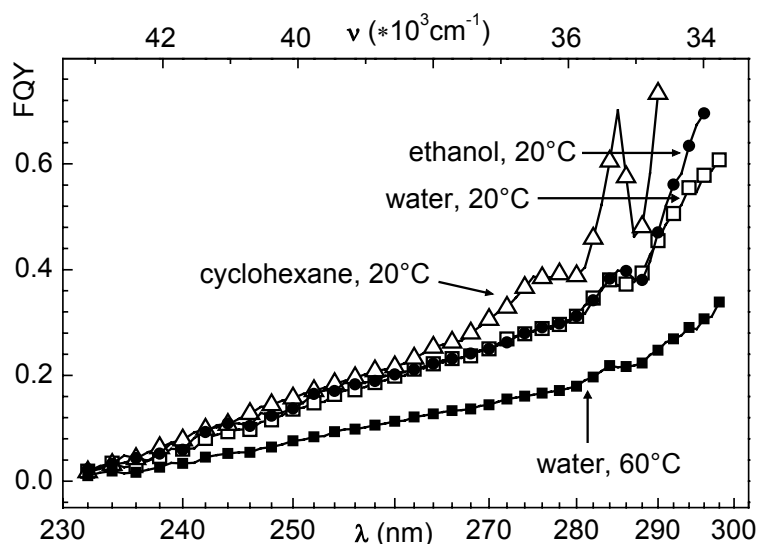

Figure 5.6 Dependence of the fluorescence quantum yield (FQY) on the excitation wavelength for indole dissolved in various solvents: water (open squares), ethanol (full circles) and cyclohexane (open triangles) at 20°C. The fluorescence quantum yield at ~60°C of indole in water is also shown (full squares).

5.2.3 The radiative lifetime

The radiative lifetime of indole dissolved in water (ethanol, cyclohexane) is derived from the $S_0 \rightarrow S_1$ absorption cross-section spectra $\sigma_A(\lambda)$ and the fluorescence quantum distributions $E_F(\lambda)$ by using the Strickler-Berg formula [48, 191], adjusted as presented in equation (5-02) [192].

$$\tau_{rad}^{-1} = \frac{8\pi \cdot c_0 n_F^3}{n_A} \cdot \frac{\int\limits_{S_1-S_0} E_F(\lambda) \cdot d\lambda}{\int\limits_{S_1-S_0} E_F(\lambda) \cdot \lambda^3 \cdot d\lambda} \cdot \int \frac{\sigma_A(\lambda)}{\lambda} d\lambda \qquad (5\text{-}02)$$

where c_0 is the velocity of light in vacuum. The average refractive indices for water and cyclohexane in the $S_1 \rightarrow S_0$ fluorescence (n_F) and in the $S_0 \rightarrow S_1$ absorption (n_A) region, $n_F = 1.349$, $n_A = 1.369$ and $n_F = 1.425$, $n_A = 1.449$, respectively, are determined from the refractive index dispersion of these liquids [193]. The refractive index for ethanol is taken from Ref. [194]. From the absorption and fluorescence spectra shown in Figure 5.3 a value of the radiative lifetime τ_{rad}(indole) = (9 ± 2) ns is calculated. The radiative lifetime indicates the time spent by an excitation state population to decay in the absence of other deactivation channels. From the fluorescence quantum yield and the radiative lifetime the real excited state lifetime can be calculated as presented below (see Section 5.4). The result presented here is in excellent agreement with reported value of 9.1 ns [156] calculated from measured fluorescence lifetime and fluorescence quantum yield.

5.3 Initial dynamics of indole in different solvents

5.3.1 State reversal and population transfer between the electronically excited ^1L_a and ^1L_b states in nonpolar and polar solvents

To characterize the evolution of the electronically excited indole the transient spectra in cyclohexane and ethanol are measured and shown in Figure 5.7. Broad spectra due to excited state absorption appear within our time resolution (0.08 ps) and give rise to a step like increase of the absorption. They extend over the probed region with a broad maximum at 640 nm. The time dependence of the absorption is characterized by a monotonic decrease in nonpolar solvent and an increase in polar solvent as shown in Figure 5.7(a) and (b), respectively.
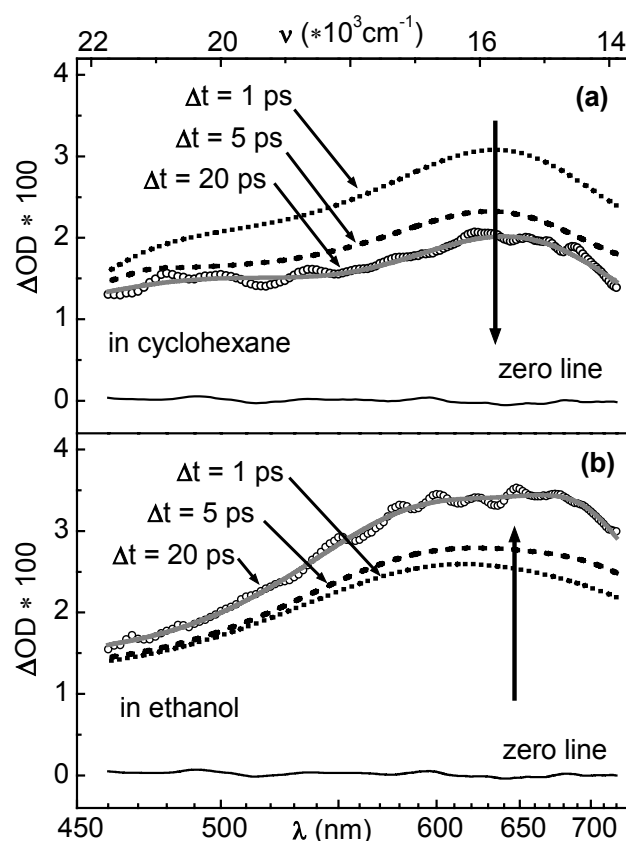
Figure 5.7 Transient spectra of indole dissolved in (a) cyclohexane and (b) ethanol at a delay of 1 ps (dotted line), 5 ps (dashed line) and 20 ps (solid line) after optical excitation. Open circles are the measured data at a delay of 20 ps before averaging. The zero line (thin black line) shows the signal before excitation. Arrows indicate the evolution of the signal.

From the lack of a gradual spectral shift between the transient spectra recorded at various time delays it is concluded that a population transfer between the ^1L_a and ^1L_b state is observed instead of an energetic shift of the ^1L_a or ^1L_b state. The steady state fluorescence spectrum of indole in cyclohexane corresponds to the ^1L_b state and in ethanol to that of the ^1L_a state (see Section 5.2). Thus at the later delay time (20 ps) the indole population in ethanol is located in the ^1L_a state while in cyclohexane in the ^1L_b state. From the comparison of the two traces detected 20 ps after the excitation (Figure 5.7 (a) and (b)) it is clear that the transient absorption in this detection window is stronger for the ^1L_a state than that for the ^1L_b state.
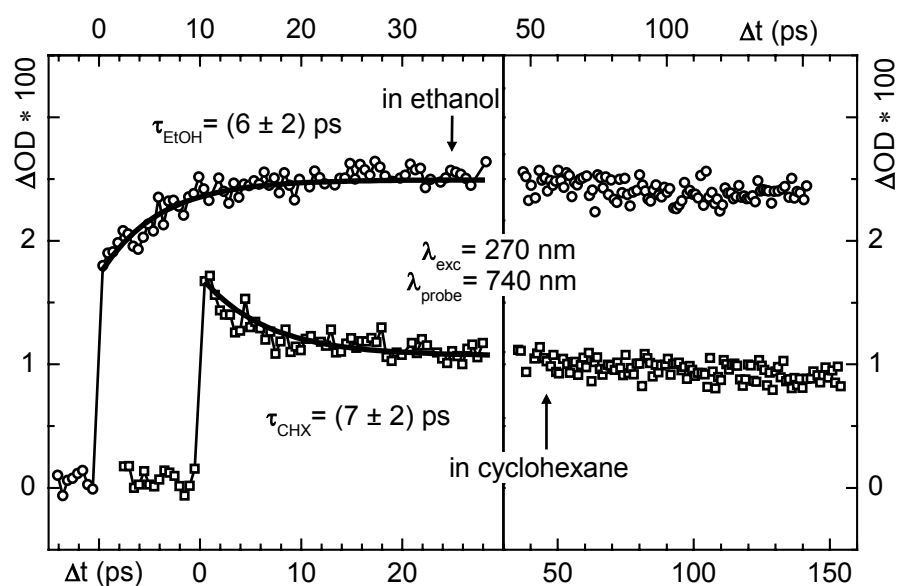
Figure 5.8 Time resolved transmission change of indole dissolved in cyclohexane (squares) and ethanol (circles) is presented as change in optical density (ΔOD). Fitted traces are monoexponential functions. The x-axis of the ethanol solution is translated 10 ps with respect to the x-axis of the cyclohexane solution for better visibility.

Time resolved measurements with a probe wavelength of 740 nm (see Figure 5.8) show the rates of depopulating or populating the ^1L_a and ^1L_b states. The ESA from indole in cyclohexane relaxes with a time constant of 7 ps. This decrease of the ESA signal is due to the population transfer from the ^1L_a state to the lower lying ^1L_b state. The model of the initial dynamics of indole dissolved in nonpolar and polar solvent when no photoionization occurs is proposed in Figure 5.9.
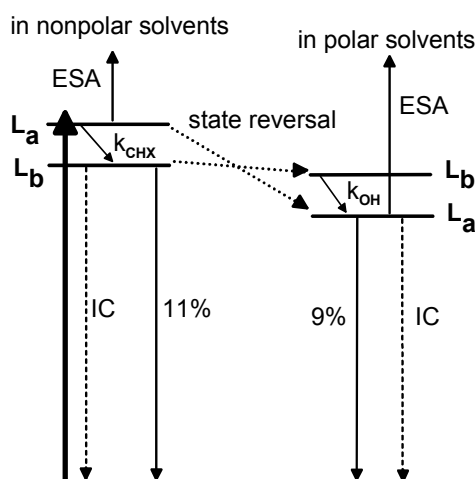

Figure 5.9 Model of the initial dynamics of indole molecule in nonpolar and polar solvent when no photoionization occurs. Contrary to nonpolar solvents, in polar solvents the rearrangement of solvent molecules influences larger shift of ^1L_a state than of ^1L_b state, i.e. state reversal appears.

In ethanol, the polar solvation shell rearranges after the optical excitation of the indole. This leads to a very rapid state reversal and the ^1L_a state slides energetically below the ^1L_b state. The further increase of the transient absorption shows subsequent population transfer from the ^1L_b to the ^1L_a state with a time constant of 6 ps (see Figure 5.8). Solvation dynamics of ethanol is known to occur partly on the 5 ps time scale and might contribute to the population transfer [27].

On the timescale shown in Figure 5.8 the ESA signal of indole in both solvents does not return to zero. After the initial relaxation which corresponds to the population transfer between ^1L_a and ^1L_b states the indole molecules are still in the electronically excited state. They decay via fluorescence and internal conversion on a nanosecond timescale as determined below from the steady state measurements (see Section 5.4).

In cyclohexane no photoionization occurs after excitation at 266 nm [17, 18] and in ethanol the ionization threshold is at 4.85 eV (~256 nm) [171], which is not reached even with the blue wing of the 270 nm excitation pulse which has a width of 3.3 nm. In order to understand the ultrafast photoionization the dynamics of indole dissolved in water has to be investigated and compared to the results presented above.

5.3.2 Ultrafast dynamics of indole in water

Indole in water has an ionization threshold of 4.35 eV (~287 nm) [171, 190] and the photoionization occurs as an additional relaxation process at the excitation wavelength used in this work (λ_{exc} = 270 nm). The reported value for the ionization threshold of indole in gas phase is 7.8 eV [195]. The relation between ionization threshold in gas and liquid phase is discussed in more details in Section 2.5.1. From the reported value of V_0 in water (-1.2 eV) [190], of I_{liq} (4.35 eV) [171, 190] and of I_{gas} (7.8 eV) the value for the effective ionic radius is estimated to be 0.14 nm [18, 171].

The appearance of new species in the water solution is in agreement with the transient absorption spectrum of indole dissolved in water compared to those of indole dissolved in cyclohexane and ethanol, which are presented in Figure 5.10. The initial dynamics is already completed at the delay time of 20 ps after the excitation. The spectrum of species appeared from indole in water shows a broad maximum in the 620 - 700 nm wavelength region. The width of this spectrum is significantly smaller than those from the excited state absorption of indole in ethanol or cyclohexane.
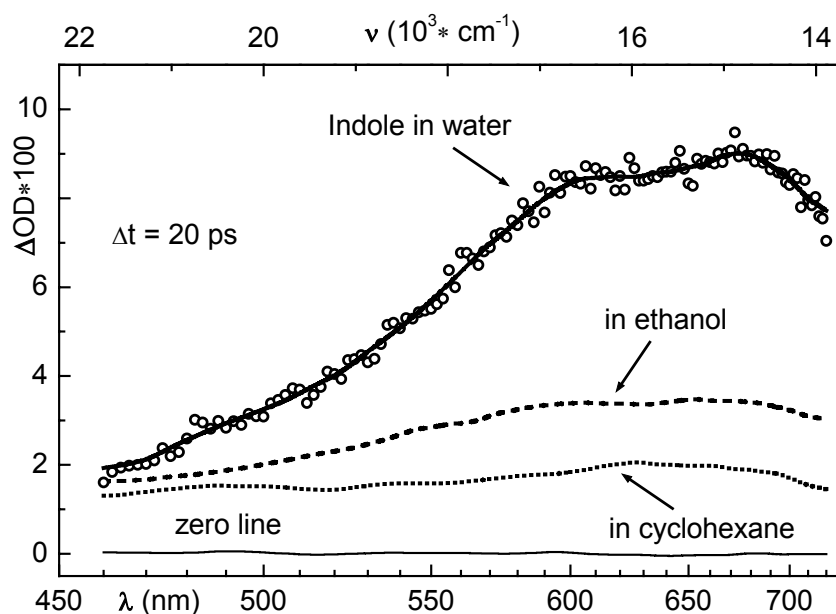
Figure 5.10 Transient spectra of indole dissolved in water (thick solid line), ethanol (dashed line) and cyclohexane (dotted line) at a delay of 20 ps after excitation. Open circles are the measured data of indole in water before averaging of 10 adjacent data points. The zero line (thin solid line) shows the signal before excitation.

The transient spectra of indole dissolved in water at the delay times of 0.5 ps, 1 ps and 20 ps after the excitation are shown in Figure 5.11. Within our time resolution an instantaneous transmission decrease is found at all probe wavelengths due to the appearance of indole radical cations that absorb at shorter wavelengths [151, 196], and presolvated electrons that absorb at longer wavelengths [55, 174, 197-201]. The absorption spectra of the indole radical cation and of the solvated electron overlap over a broad spectral region. The absorption spectrum of the radical cation can be recognized only as a shoulder in the transient spectra, because the relative contribution of the radical cation to the absorbance signals is much smaller than of the solvated electron. Over the whole spectral region there is also excited state absorption as already observed in the case of ethanol or cyclohexane. The exact amount with which each single specie contributes to the observed absorption signal is evaluated in the Section 5.4.

The similarity between the shape of the transient spectra of indole in water and the spectrum of solvated electrons in neat water which is known in literature [75-83] is demonstrated in Figure 5.11. It verifies the formation of solvated electron within the first picosecond in the indole-water solution as a result of the photoionization of the indole molecule.
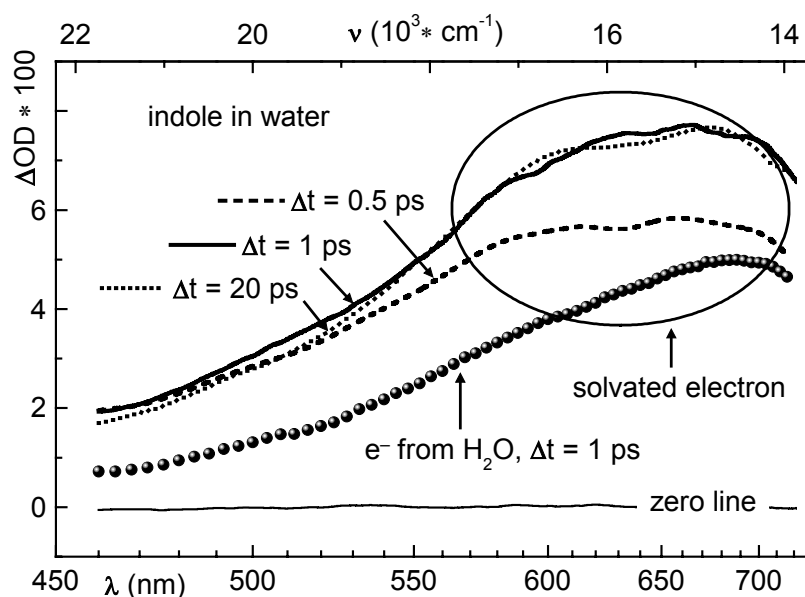
Figure 5.11 Transient spectra of indole in water with a delay time of 0.5 ps (dashed line), 1 ps (solid thick line) and 20 ps (dotted line) after the excitation. The absorption spectrum of the solvated electrons generated in neat water (symbols) is also shown. The spectral region where the solvated electron dominates the absorption signal is indicated with an ellipse. Thin solid line represents the signal before the excitation.

The transient absorption in the red spectral region (630-730 nm) rises to some extend instantaneously and subsequently on the 100-fs time scale to its maximum value. The latter increase is due to further solvation of the presolvated electrons, that are also known as hot or wet or trapped electrons [55, 172, 174, 175, 197-202]. It is reported that a precursor of the solvated electron shows the maximum absorption in infrared spectral region while the solvated electron around 700 nm as shown in Figure 5.11. Detecting the signal in the wavelength region $450 - 740$ nm we are able to observe the formation of the solvated electron absorption band. For observing dynamics of presolvated electron one has to dispose with the detection window in near infrared spectral region.

In the blue spectral region (470-520 nm) where no significant changes are observed after an initial instantaneous absorption rise, the indole radical cation and the excited indole molecules (that do not experience photoionization) dominate the signal. This indicates that the both species (excited indole and indole radical cation) are generated within our time resolution and do not exhibit any significant dynamics on the picosecond timescale. In order to resolve temporally the initial processes of indole in different solvents the time resolved measurements are performed further on (see Section 5.3.3).

5.3.3 Time resolved dynamics of indole

The time resolved measurements of indole dissolved in water, ethanol and cyclohexane presented in Figure 5.12 show that a new relaxation process appears in the water solution. The initial dynamics is probed at the two wavelengths: 525 nm and 660 nm. The difference in the signal behavior is more pronounced at 660 nm which is near to the maximum of the transient absorption.
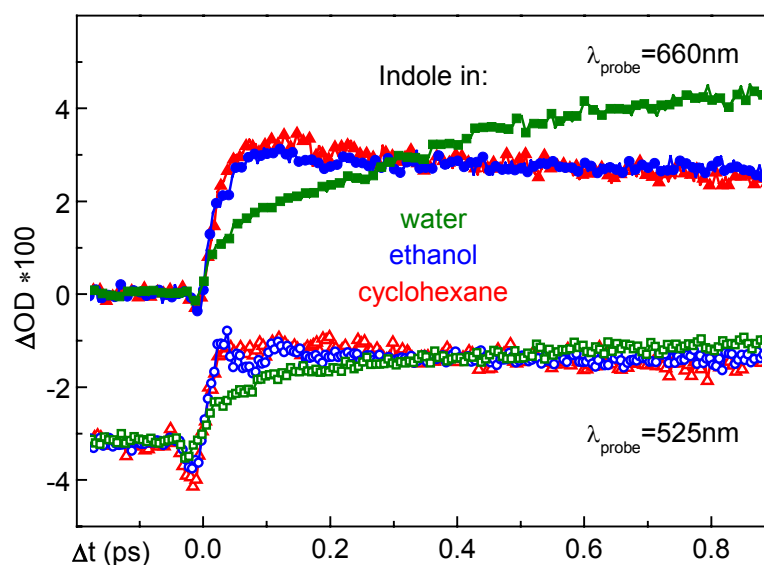

Figure 5.12 Time resolved initial dynamics of indole in water (green squares), in ethanol (blue circles) and in cyclohexane (red triangles) probed at 660 nm (full symbols) and 525 nm (open symbols). Traces probed at 525 nm are vertically shifted along the y-axis for better visibility.

Time resolved absorption changes of indole in water probed with a white light continuum are shown in Figure 5.13. The maximal contribution of the solvated electrons is in the region of longer wavelengths (660 nm and 730 nm in Figure 5.13). The formation of the solvated electrons is fitted by an exponential decay time of about 0.35 ps. The 0.35 ps dynamics is interpreted as a relaxation process associated with the solvation of the presolvated electron generated by the photoionization of the indole molecule.
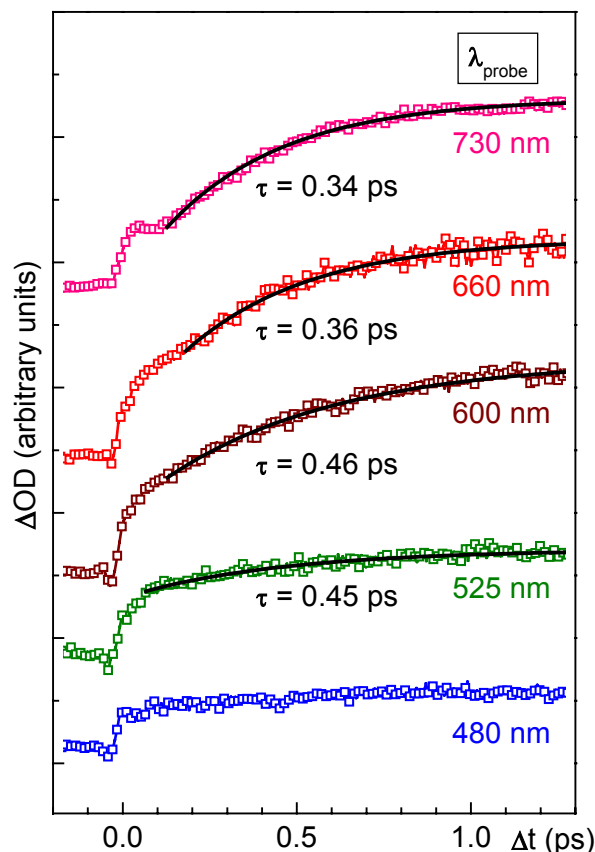
Figure 5.13 Time resolved absorption changes of indole dissolved in water probed at different wavelengths. The solvation dynamics appears as major contribution at 730 nm (pink), 660 nm (red) and 600 nm (wine). At 525 nm (green) and 480 nm (blue) the step-like increase of the transient absorption is the major contribution. It is caused by the instantaneous (within time resolution) appearance of indole radical cations and excited indole molecules.

Time resolved traces probed in the blue spectral region (λ_{probe} = 480nm and 525 nm) show a step like increase of the transient absorption due to the instantaneous appearance of radical cations within the time resolution of the experiments. This fact is verified with the best achieved time resolution of 0.06 ps using a two-color experiment utilizing compressed NOPA-pulses for probing instead of white light continuum. As presented in Figure 5.14 the absorption probed at 475 nm shows again an initial step like increase, which is still within the time resolution and is followed by the solvation dynamics. The solvation process with a time constant of 0.36 ps contributes with a small amplitude to the absorption signal due to a small amount of solvated electron absorption in this spectral region.
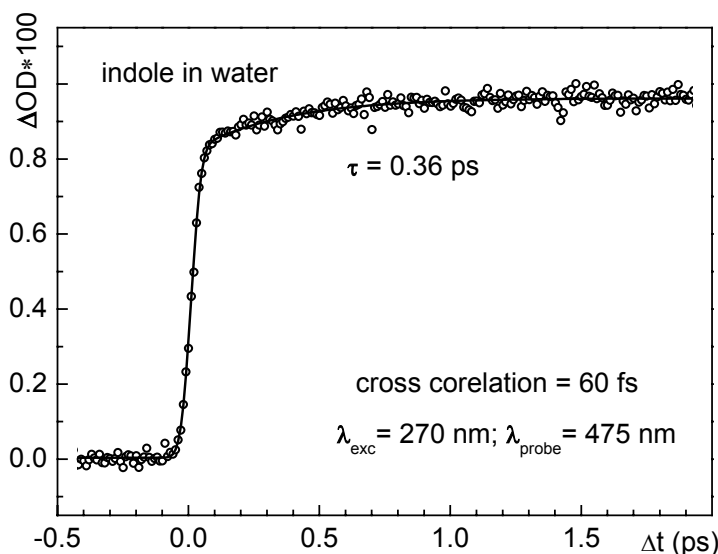
Figure 5.14 Time resolved absorption change of indole in water probed at 475 nm with the best time resolution of 60 fs achieved in these experiments defines the upper limit of the time needed for the appearance of the indole radical cations, presolvated electrons and excited indole molecules.

5.4. Photoionization quantum yield and fluorescence lifetime

In order to determine the amount of molecules which experiences photoionization the photoionization quantum yield (Φ_{ion}) is determined. It expresses the ratio between the concentration of solvated electrons (c_e^-) and the number density of photons that are absorbed by indole molecules ($c_{abs.ph.}$):

$$\Phi_{ion} = \frac{c_{e^-}}{c_{abs.ph.}} . \tag{5-03}$$

The number density of absorbed photons is determined from the initial transmission (T_0) and the excited volume (V_{exc}) of the sample and the total number of photons (N_{ph}) related to the energy of the excitation pulses (E_{exc}):

$$c_{abs.ph.} = (1-T_0)\cdot\frac{N_{ph.}}{N_{Av}\cdot V_{exc}} = (1-T_0)\cdot\frac{\dfrac{E_{exc}\cdot\lambda}{h\cdot c}}{N_{Av}\cdot V_{exc}} , \tag{5-04}$$

where λ is the excitation wavelength, h the Planck constant, c the light velocity in vacuum and N_{Av} the Avogadro number. The excited volume of the sample is calculated from the thickness of the sample and the radius of the excitation pulses in the sample, determined with a pinhole.

If the solvated electrons would contribute alone to the transient absorption in the observed spectral region their concentration could be determined from the detected change of the transmission signal (T/T_0):

$$c_{e^-} = \frac{\Delta OD}{\varepsilon^{solv.elec.} \cdot d} = \frac{-\log \dfrac{T}{T_0}}{\varepsilon^{solv.elec.} \cdot d}, \tag{5-05}$$

where ΔOD is the absorption change, $\varepsilon^{solv.elec.}$ the molar extinction coefficient of the solvated electron in water and d is the thickness of the sample.

However, as already discussed in the previous Section 5.3 at least three species overlap in the investigated spectral region and contribute to the observed transient absorption. Their spectra are shown in Figure 5.15. Although the solvated electrons dominate the signal one can not neglect the contribution of the indole radical cations generated together with electrons through photoionization as well as excited indole molecules which do not experience photoionization. According to some theoretical simulations the neutral indolyl radical can appear instead of a indole radical cation [178, 203]. In order to determine the yield with which particular specie contributes to the total signal it is important to represent their absorption spectra in the units of the molar extinction coefficients which are independent of excitation energy or concentration (see Figure 5.15).
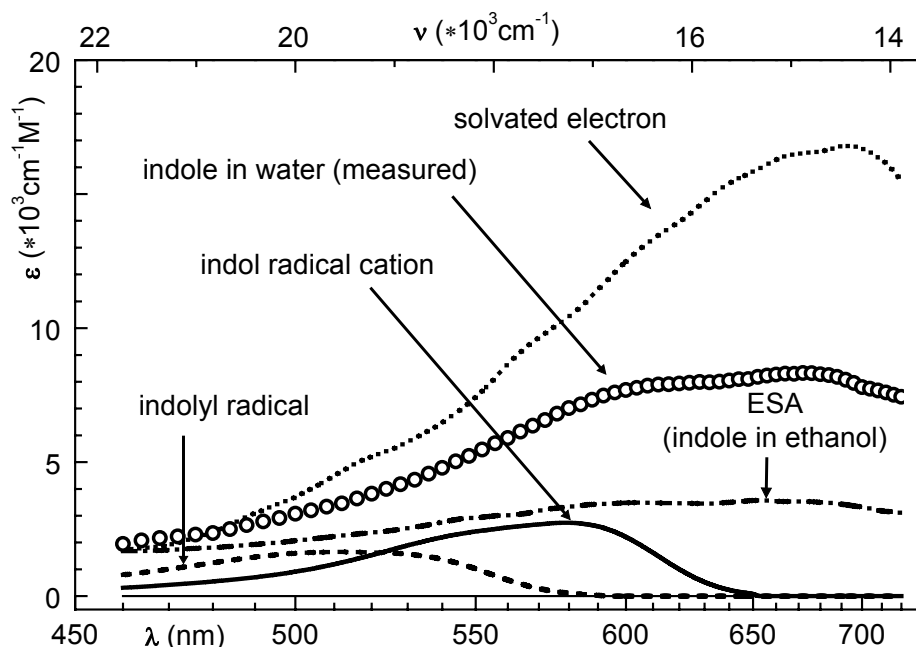

Figure 5.15 The absorption (molar extinction coefficient) of solvated electron (dotted line), indole radical cation (solid line) or indolyl radical (dashed line) and indole in ethanol representing the ^1L_a excited state absorption (dash-dotted line), which all contribute to the absorption of indole in water (circles)

The absorption spectrum of the solvated electron corresponds to the signal observed in neat water. This is scaled to a maximum value of $(16\,800 \pm 1\,500)$ $M^{-1}cm^{-1}$, which is a mean value of 3 reported maximal extinction coefficients [76-78]). The absorption spectra of the indole radical cation and indolyl radical are taken from literature [196]. Indole in ethanol experiences no photoionization at an excitation wavelength of 270 nm, so the observed signal at a delay of 20 ps corresponds only to excited state absorption. The molar extinction coefficient of the excited state absorption is determined from the observed spectrum (T/T_0) scaled with the calculated concentration of the number density of absorbed photons (5-04) and the thickness of the sample, d:

$$\varepsilon^* = \frac{-\log\dfrac{T}{T_0}}{c_{abs.ph.} \cdot d} \qquad (5\text{-}06)$$

The value of 3 600 $M^{-1}cm^{-1}$ is determined for the maximum of the absorption, which is in good agreement with the reported value of 4 000 $M^{-1}cm^{-1}$ [19].

In the same way as for the excited state absorption (5-06) the molar extinction coefficient of the total absorption measured for indole in water is determined. It represents the sum of all contributions. The amount with which solvated electrons contribute to the transient absorption of indole in water should be equal to the amount of indole cations and corresponds to the ionization quantum yield. The rest of the excited indole molecules which are not photoionized exhibits excited state absorption. As presented in (5-07) the observed transient absorption of indole in water ($\varepsilon^{*(IndWater)}$) consists of the contribution due to the photoionization ($\varepsilon^{solv.elec.}$, ε^{IndRad}) and of the excited state absorption contribution ($\varepsilon^{*(ESA)}$).

$$\varepsilon^{*(IndWater)}(\lambda) = \Phi_{ion} \cdot \left[\varepsilon(\lambda)^{solv.elec.} + \varepsilon(\lambda)^{IndRad}\right] + (1 - \Phi_{ion}) \cdot \varepsilon(\lambda)^{*(ESA)} \qquad (5\text{-}07)$$

Equation (5.09) can now be fitted to the measured spectrum by varying only the ionization yield Φ_{ion}. With a value of $\Phi_{ion} = 0.38 \pm 0.10$ results the curve shown in Figure 5.16(a) which is in excellent agreement with the measured spectrum of indole in water.

In order to prove the possibility of generating the indolyl radicals instead of indole radical cations the same procedure is performed. As presented in Figure 5.16(b) it is not possible to obtain a successful fit which would correspond to the measured signal. This leads to the conclusion that the shoulder at 600 nm of the observed spectrum is indeed related to the generated indole radical cations and not to neutral indolyl radicals.
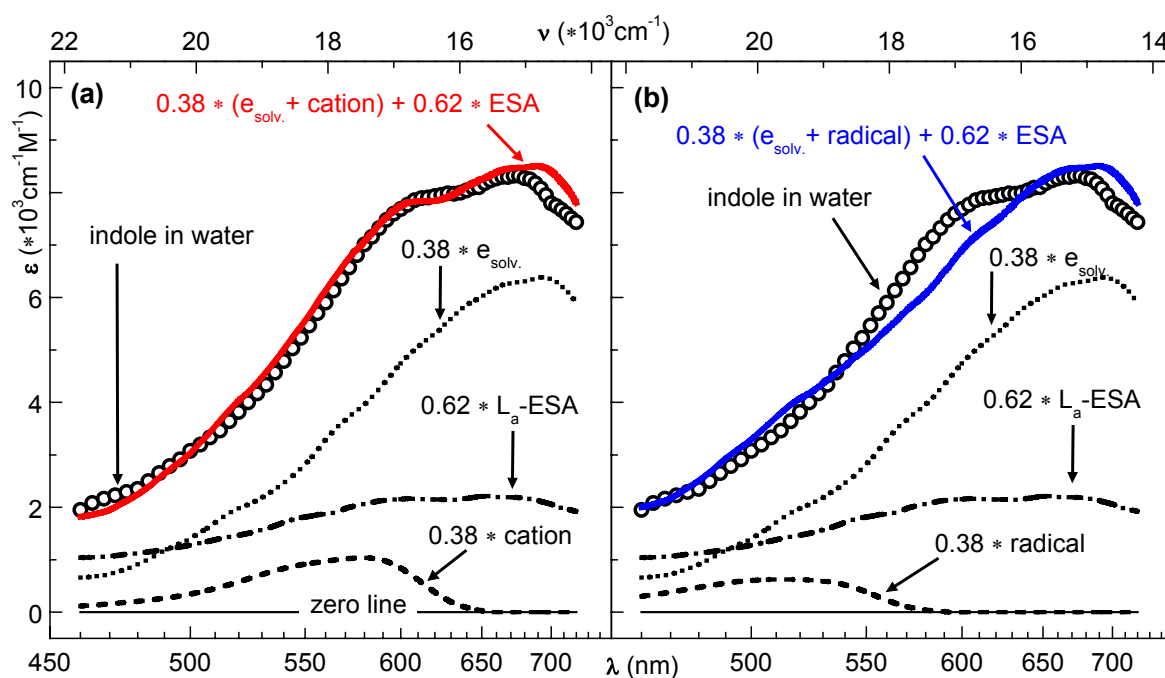
Figure 5.16 Transient absorption spectrum measured 20 ps after excitation of indole in water (circles) is fitted by the sum (thick solid red line) of absorptions spectra from the solvated electron (dotted line), the indole radical cation (dashed line), and the excited state absorption (dash-dotted line). (b) Here the absorption of the radical cation is replaced by the indolyl radical (dashed line) in the sum (thick solid blue line).

Previously reported values for the ionization quantum yield after excitation in the spectral range of 193-270 nm vary between $0.09 - 0.32$ [20, 151-153, 155, 161]. The value of 0.38 reported here lies within the given error in the upper range of the reported values. The good agreement with the experimental data over the complete visible range (see Figure 5.16(a)) gives us confidence in the accuracy of the determined ionization yield.

Considering that a fraction of 62% does not exhibit ionization and is capable of fluorescing, the mean value of the reported fluorescence quantum yields of 0.25 (see Section 5.2.2) is corrected to the new value of 0.4 for those molecules which reached the ^1L_a state. From the corrected fluorescence quantum yield and the radiative lifetime (τ_{rad}) calculated in Section 5.2.3 the lifetime of the ^1L_a state (often named fluorescence lifetime, τ_{fl}) is determined. The calculated value of $\tau_{fl} = \Phi_F * \tau_{rad} = (3.6 \pm 1.0)$ ns is in close agreement with reported values of 4.1 ns [18, 156], 4.3 ns [159], 4.82 ns [160] and 4.9 ns [158] in literature.

5.5 Model of the excited state dynamics

After excitation at 270 nm two independent relaxation processes of indole are observed: fluorescence and photoionization. On one side the ^1L_a state decays on the ns-time scale via fluorescence and internal conversion. On the other side the ultrafast photoionization is found to occur within 100 fs. In order to connect both sides an ultrafast branching between the fluorescing state and the state that experiences photoionization is suggested. Since the radical cation appears in less than 0.06 ps a branching of the excited state population has to occur immediately after photoexcitation.
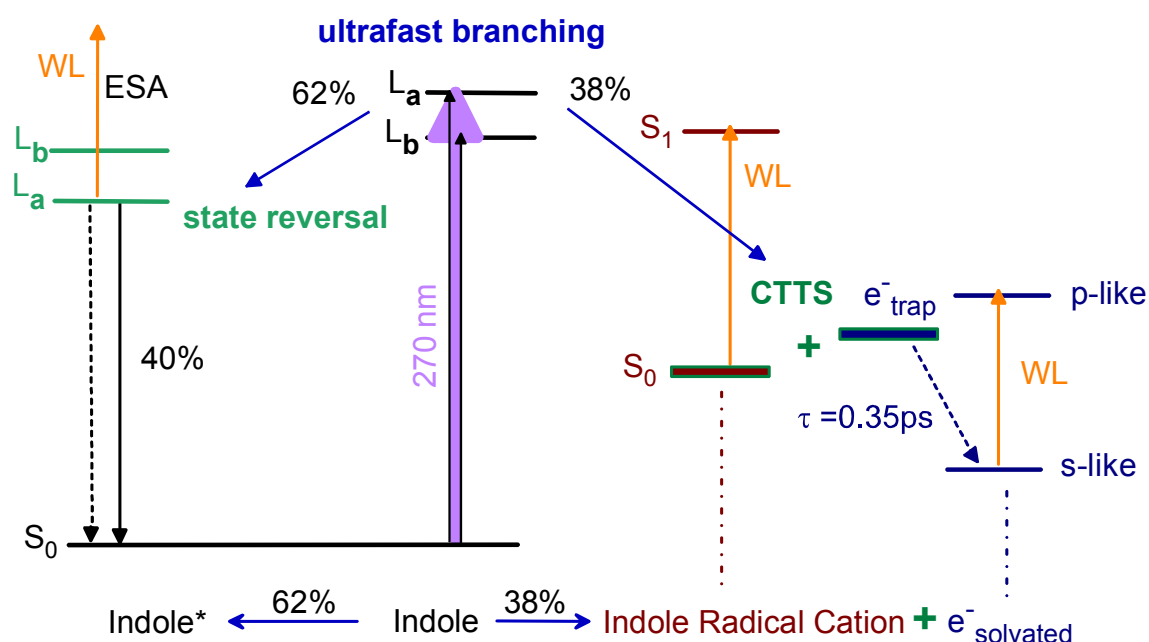

Figure 5.17 Model of the excited state dynamics of indole dissolved in water. Immediately after photoexcitation an ultrafast branching between the fluorescing state and the CTTS occurs. A fraction of 38% experiences photoionization, forming indole radical cations and presolvated electrons (CTTS) within the experimental time resolution and subsequently, shows further solvation and appearance of solvated electrons. The rest of the population relaxes to a fluorescing state, which is the ^1L_a state due to the occurred state reversal. The ^1L_a state relaxes to the ground state via fluorescence and internal conversion. The solvated electrons do not show significant recombination within the first nanosecond. The yellow arrows indicate all contributions to the observed absorption change probed with a white light continuum (WL). Once they are solvated the electrons are excited from their ground (s-like) state to the excited (p-like) state by absorbing in the visible region around 700 nm.

The proposed model of indole in water is shown in Figure 5.17. After the ultrafast branching a fraction of 38% (see Section 5.4) undergoes photoionization creating a charge transfer to solvent state (CTTS). The CTTS state is the resulting state of photoionization in solvents where the excited molecule donates a charge (electron) to the solvent. This highly polar state was already introduced by other authors for the indole-water systems [75, 152, 165], as well as for the sodide-tetrahydrofuran system [233], for aqueous iodide [223-225], and the aqueous hexacianoferrate(II) complex [72, 242].

The presolvated electrons relax further forming fully solvated electrons with the observed time constant of 0.35 ps. Once they are solvated the electrons absorb in the broad wavelength region around 700 nm and exhibit the transition from the ground s-like state to the excited p-like state [238, 239, 240, 247, 249].

The products of the photoionization do not recombine within the first nanosecond as shown in Section 5.6, which is in agreement with the reported lifetime of solvated electron in water (a few hundred nanoseconds [21], or less than a microsecond [55]). It is reported that the indole radical cation has a lifetime of microseconds and decays to give the neutral indole radical [151, 155].

The rest of the population (62%) relaxes to a fluorescing state, which cannot ionize any more. The fluorescence comes from the L_a excited state, that has undergone a state reversal. The population decays with the fluorescence lifetime of ~ 3.6 ns via fluorescence and internal conversion to the ground state.

5.6 Long time behavior

The long time behavior of indole dissolved in ethanol and cyclohexane shows almost no dynamics. After the initial dynamics of 6-7 ps the pedestal shown for the first 50 ps in Figure 5.8 decreases slightly within the next 160 ps. This is in agreement with the results from the steady state data, which show that the fluorescing state (^1L_a in ethanol and ^1L_b in cyclohexane) of indole has a lifetime of several nanoseconds, calculated from the determined fluorescence quantum yield and radiative lifetime (see Section 5.2.2 and 5.2.3). The reported fluorescence lifetime of indole in cyclohexane, determined using frequency-domain fluorometry and fluorescence decay experiments is (7.8 ± 0.1) ns and 4.1 ns in ethanol [160, 251].

In water, where photoionization occurs as additional relaxation channel, no significant relaxation dynamics is observed on a long time scale (1 ns) as shown in Figure 5.18. Indole in water probed in the region of the solvated electron ($\lambda_{probe} = 700$ nm) as well as in the region of the radical cation ($\lambda_{probe} = 470$ nm) shows no significant sign of recombination at the observed time scale. The absence of recombination of the indole radical cation and the sol-

vated electron was also previously reported in the 20 ps - 2 ns [154] and in the 1 - 600 ps time range [20].
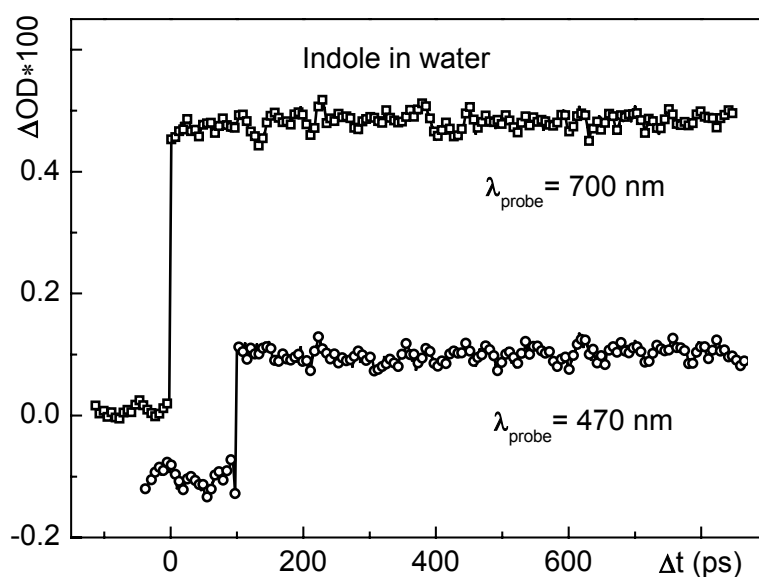

Figure 5.18 Long time behavior of indole in water probed at 470 nm (circles) and at 700 nm (squares) where the solvated electrons mostly contribute to the signal. No significant dynamics on a long time scale is observed. The trace probed at 470 nm are shifted vertically and horizontally along the axes for better visibility.

5.7 Origin of the solvated electron

5.7.1 Theoretical assumptions

In spite of many studies performed on indole in water it is still not known how the solvated electron is generated. Theoretical investigations considering indole surrounded with water (or ammonia) clusters suggest that the primary photochemical process is a hydrogen transfer. After the ejection in water, the hydrogen atom decomposes in the aqueous environment to form a solvated hydronium cation (H_3O^+) and solvated electron [178, 203]. Similar calculations are performed for the water dimer and the hydronium-water cluster [204, 205], where H_3O radicals are formed by a barrierless hydrogen-transfer reaction and then microsolvated to a charge separated complex consisting of a hydronium cation and a localized electron cloud. It is calculated that the hydrated hydronium radical can also be produced by the photodetachment of halide anions in water [206]. Despite the theoretical prediction in the case of the halide anion - water clusters, the REMPI (Resonance Enhanced MultiPhoton Ionization) experiment shows a solvation induced ion-pair formation in the ground state:

$$h\nu + HBr(H_2O)_n \rightarrow H_3O^+(H_2O)_{n-1} + Br + e_{aq}^- \quad [207].$$
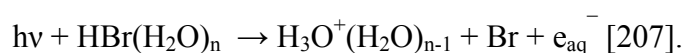
According to other assumptions solvent-anion complexes of the $H_3O\text{-}OH^-$ type may be carriers of the spectroscopic properties of the hydrated electron [75] or the hydrated electron should be viewed as an itinerant H_3O or H_5O_2 radical in water [208, 209].

The experimental difficulty to prove these theories arises from the fact that the absorption spectrum of H_3O is in the same wavelength region as the solvated electron [208]. Neither the OH radical [210] nor OH^- [211] are candidates for the hydrated electron, as they do not absorb in the visible and infrared regions.

5.7.2 Origin of the solvated electron in neat water

Application of the high pump power density ($>10^{15}$ W/m^2) in the region of very short wavelengths (270 nm) enables photoionization of neat solvents due to the two-photon absorption process. In order to have better understanding of the electron solvation in indole it is important to study the photoionization of neat water and compare the solvation in it to the one in indole. It is interesting to investigate if the electrons generated in two different ways show similar dynamics or not. The gas phase ionization threshold for neat water is 12.6 eV [212, 213]. If one corrects it for the electronic polarization energy of liquid water and the minimum energy of the "quasi-free" electron one gets a Born-Oppenheimer ionization threshold of 8.7 eV [214]. It has been suggested that hydrated electrons can be produced below the direct Born-Oppenheimer ionization via dissociation [215-217], which requires an energy of $6.4-6.7$ eV [218]. According to this model, the photodissociation of H_2O generates an OH radical and an H atom, which subsequently due to its excess energy rapidly reacts with a water molecule of the first solvation shell to produce H_3O^+ and the hydrated electron e_{aq}^- [217]:

$$hv + H_2O \rightarrow H_2O^* \rightarrow OH + H_{hot}$$

$$H_{hot} + H_2O \rightarrow H_3O^+ + e_{aq}^-.$$
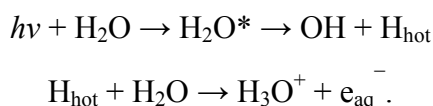
Alternatively, it has been suggested that ionization below the Born-Oppenheimer threshold might involve a proton transfer from the photoexcited water molecule to the solvent yielding H_3O^+ and an electronically excited OH^-, which subsequently can transfer an electron to a solvent trap leading to the net reaction [219]:

$$hv + 2H_2O \rightarrow H_3O^+ + OH + e_{aq}^-.$$
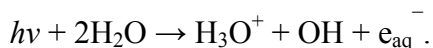
The evidence for two short-lived precursors of the hydrated electron is reported [201]. The following reactions with the formation of $OH{:}e_{aq}^-$ complex and the subsequent electron detachment are suggested:

$$hv + 2H_2O \rightarrow H_3O^+ + OH{:}e_{aq}^- \rightarrow H_3O^+ + OH + e_{aq}^-.$$

These models are supported by the generation of the OH radical, experimentally observed in the indirect photoionization of water [210].

Recently the electron photodetachment was observed from aqueous hydroxide (OH$^-$ strongly bonded to 3-4 water molecules) producing a geminate pair of a hydroxyl radical (OH) and a hydrated electron (e_{aq}^-) [220].

As presented above there are more than one solution modeling the initial dynamics in neat water and the clear picture of the electron solvation is missing. The same question about the origin of the solvated electron arises.

The experiments of charge transfer in HCl in Xe and Kr matrices show also ionization below the Born-Oppenheimer threshold due to the influence of the environment and the interaction between H+ and Xe (Kr): $Xe_{matrice}H^+Cl^- \rightarrow Xe_{matrice}Cl^- +H$ [221]. Thus one can expect that the liquid environment like water enables the photoionization of solute below the Born-Oppenheimer threshold.

For the direct photoionization above the Born-Oppenheimer threshold the nearly immediate reaction of H_2O^+ with a neighboring water molecule and the formation of e_{aq}^-, H_3O^+ and OH is reported [21]:

$$hv + 2H_2O \rightarrow H_2O^+ + H_2O + e_{aq}^- \rightarrow H_3O^+ + OH + e_{aq}^-.$$
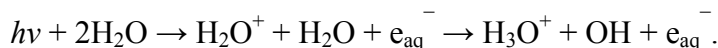
5.7.3 Experimental evidence

Electron solvation dynamics investigated in iodide-(water)$_n$ anion clusters (with n = 4-6) [222] shows an analogy to the dynamics of the CTTS state in iodide dissolved in water [223-225]. This agreement between the experimental studies performed in clusters and liquid phase can be an indication that one can expect a similar behavior between indole dissolved in water and indole-water clusters.

Recent femtosecond photoelectron spectroscopy studies show the expected behavior of hydrogen transfer in indole-ammonia clusters [226-228]. Based on experimental data in indole-water clusters no sign of hydrogen transfer was found [229]. However, it is known that the reaction of H-transfer in water: $H + H_2O \rightarrow H_3O$ is endoenergetic, while the H-transfer in ammonia: $H + NH_3 \rightarrow NH_4O$ is approximately isoenergetic [203]. Ammonia is thus a better hydrogen acceptor than water, what may explain less efficiency or absence of H-transfer in water.

Another femtosecond study reported the appearance of indole radical cations and trapped electrons by photoionization of indole molecules and localization of the electrons as part of the same elementary step. Trapped electrons exhibit subsequent solvation [20].

$$indole* \rightarrow indole^+ + e_{trapped} \rightarrow indole^+ + e_{solvated}.$$

In addition, in the case of neat water the mechanism suggested is as follows:

$$H_2O^+ + H_2O + e_{aq} \rightarrow H_3O^+ + OH + e_{aq}.$$
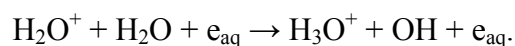
In order to clarify the origin of the solvated electron, 1-methylindole (N-methylindole), a derivative of indole is investigated and compared to indole. As shown in Figure 5.19 the only difference in the structural formulae between the two investigated molecules is a methyl group, which is in the 1-methylindole molecule bonded to the nitrogen atom of the pyrrole ring, instead of a hydrogen atom as in the case of indole.
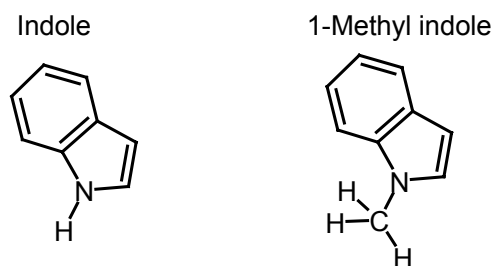

Figure 5.19 Structural formulae of indole and its derivative: 1-methylindole, which has a methyl group bonded to the nitrogen atom of the pyrrole ring.

Owing to its structural properties, 1-methylindole is not able to exhibit hydrogen transfer. If the solvation process observed in indole is really characterized by a H-transfer, it would be expected that 1-methylindole does not show solvation dynamics similar to indole. A similar comparison was performed between pyrrole and 1-methylpyrrole in order to investigate the origin of the observed generation of H atoms in pyrrole [230].

The similar absorption spectra of indole and 1-methylindole shown in Figure 5.20 exhibit no major differences in the spectroscopy of both investigated indole molecules. The absorption of 1-methylindole is more red shifted but shows again the structure of the two strongly overlapping ^1L_a and ^1L_b absorption bands as observed in indole. The reported dipole moments are comparable to those of indole as well as the solvent dependent Stokes shift of the fluorescence [110, 184, 185]. As the reported photoionization potential of 1-methylindole (7.4 eV) is lower than that of indole (7.7 ± 0.2 eV) in gas phase [186, 195], it is expected that 1-methylindole in water also exhibits photoionization at the excitation wavelength of 270 nm.
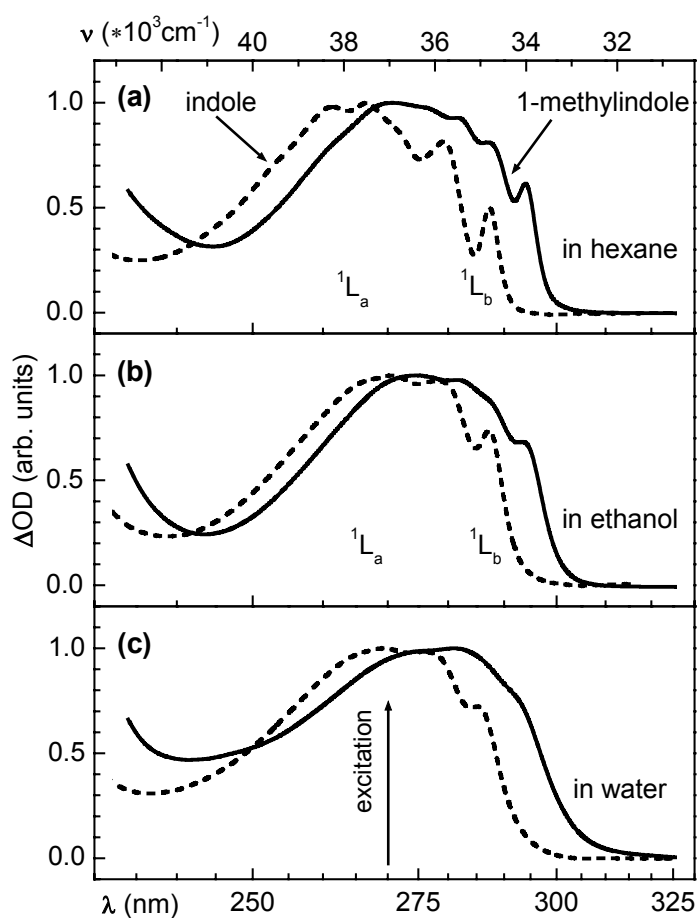
Figure 5.20 The steady state absorption spectra of 1-methylindole dissolved in (a) hexane, (b) ethanol and (c) water are more red shifted compared to the same solutions of indole but show the same structure of two strongly overlapping ^1L_a and ^1L_b absorption bands.

The comparison between experimental data of the initial dynamics of the two different indole molecules is shown in Figure 5.21. Despite the reported theoretical prediction mentioned above the obtained experimental data shows the same initial dynamics for both indole molecules. The solubility of 1-methylindole in water is very low. The signal strength corresponds to the much lower concentration of 1-2 mM (T = 90%) and a bad signal to noise ratio. Still both traces overlap each other due to the same solvation dynamics probed in the region of solvated electron (λ_{probe} = 700 nm). The overlap of both traces is achieved multiplying the absorption signal of 1-methylindole by factor of 11. The same factor is stemming from the ratio between the number of photons absorbed in indole solution compared to those absorbed in 1-methylindole solution.

$$\frac{c_{abs.ph}(indole)}{c_{abs.ph.}(methylindole)} = \frac{1-T_0(indole)}{1-T_0(methylindole)} = 11 \qquad (5\text{-}08)$$

Since the absorption signal of 1-methylindole is smaller only due to its lower concentration the photoionization quantum yield of both species is the same indicating again the same origin of generated solvated electron. The both traces are detected at the same energy of the pump pulses.
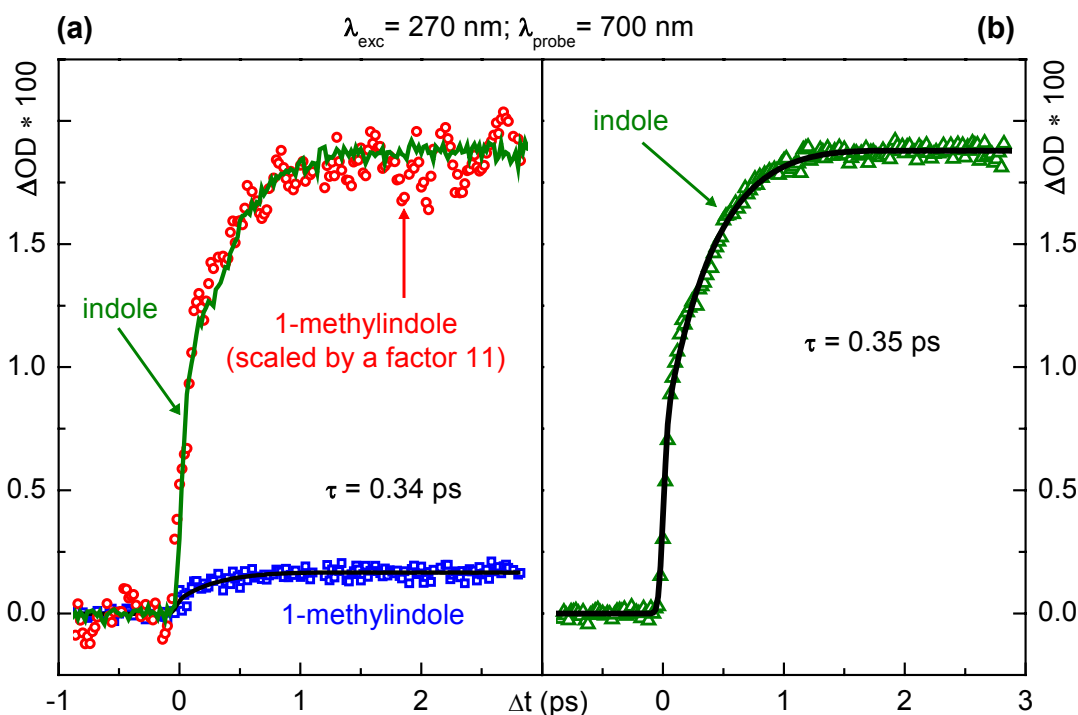

Figure 5.21 Time resolved experimental data of (a) 1-methylindole (blue squares) and (b) indole (green triangles) in water and corresponding fits (solid black lines) obtained assuming multi-exponential decays and a Gaussian cross correlation. Additionally in (a) the measured absorption change of indole (green line) is compared to that of 1-methylindole (red squares) scaled by a factor 11.

The time constants found by fitting an exponential rise convoluted with a Gaussian cross correlation are 0.34 ps and 0.35 ps for 1-methylindole and indole in water, respectively. This time corresponds to the electron solvation (see Section 5.3.2).

In order to exclude any uncertainty the same experiment is repeated with excitation pulses at lower energy, so that no signal is observed due to the two-photon absorption in neat water. The signals are smaller and the signal to noise ratio is worse, but the same monoexponential behavior is found from the fits as shown in Figure 5.22.

From the experimental data presented in this section it becomes clear that the photoionization and solvation of electrons stemming from 1-methylindole are similar to those of indole. It means that the presolvation and solvation processes are not induced by a hydrogen transfer and that the electron alone is the specie which is transferred from the donor molecule to a solvent.
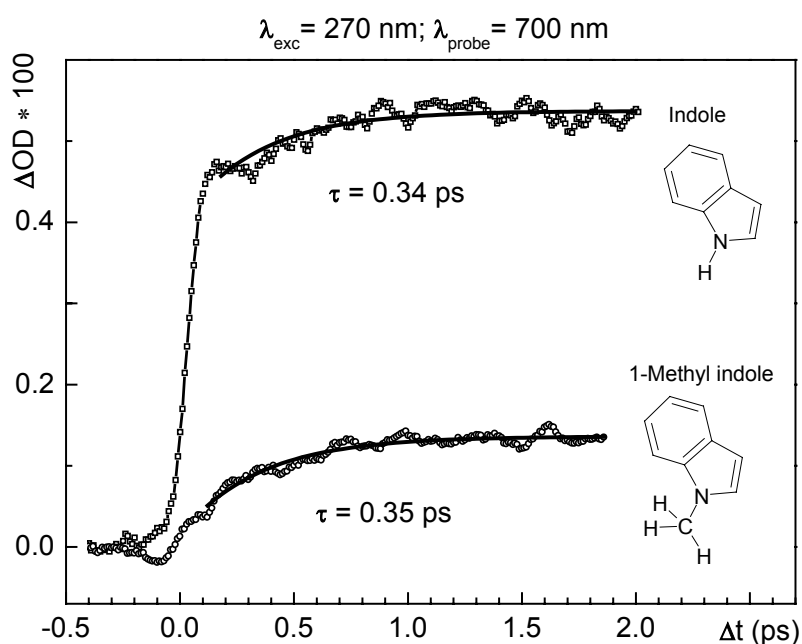
Figure 5.22 Time resolved absorption change of indole (squares) and of 1-methylindole (circles) in water with low excitation energy where two-photon absorption in neat water is avoided. The same monoexponential behavior (solid lines) appears as in the case with higher excitation energy (see Figure 5.21).

The value of 0.14 nm estimated for the effective ion radius of the indole cation (see Section 5.3.2) is much smaller than that of 0.336 nm calculated from the molecular volume and corresponding to the neutral solute molecule [190]. This has been considered to indicate that the positive charge remains localized around the nitrogen atom suggesting that the solvated electron originates from the H atom in indole and analogue from the CH_3 group in 1-methylindole and not from the π electron cloud of the benzene-pyrrole ring.

Furthermore, Köhler et al. proposed that the H-bond between the hydrogen atom on the amino group and the water molecule plays an important role in water induced radiationless processes [231]. This indicates the electron detachment via photoionization of indole in water stemming from the hydrogen bonded to a nitrogen atom.

5.8 Absence of dielectric relaxation for indole and 1-methylindole in water

A comparison of the transient absorption spectra of neat water with the indole and 1-methylindole solutions is shown in Figure 5.23. The initial evolution of absorption signal in neat water is similar to that in indole or 1-methylindole (0.35 ± 0.05) ps, but shows an additional contribution on a timescale of 1 - 2 ps. The formation of electrons stemming from indole is similar to the ionization and solvation process in neat water, except that the time constant corresponding to the dielectric relaxation is missing. This may indicate that the

electron is not completely separated from the indole radical cation and the interaction with the parent molecule disables the dielectric relaxation that occurs in neat water on the time-scale of 1 - 2 ps. This demonstrates that the dynamics of the generated electrons depends on the donor molecule.
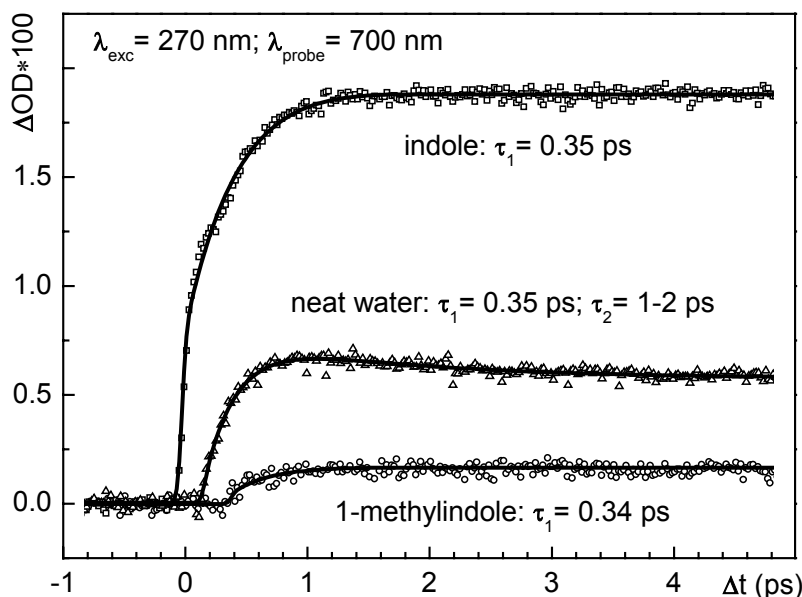

Figure 5.23 Time dependent absorption change of indole (squares) and 1-methylindole (circles) dissolved in water compared to neat water (triangles) probed at 700 nm together with corresponding fits (solid lines). Traces of neat water and 1-methylindole are translated along the x-axis for better visibility.

Another explanation for the observed phenomenon can be the amount of excess energy of the electrons generated by photoionization with an excitation wavelength of 270 nm (4.59 eV). The excess energy equals only 0.24 eV in the case of single photon ionization of indole while it is 2.68 eV in the case of 2-photon ionization of neat water. The reported ionization thresholds of indole and neat water are 4.35 eV [171, 190] and 6.5 eV [21], respectively. The higher excess energy of electrons generated by two-photon ionization of neat water can spread over surrounding solvent molecules resulting in their dielectric relaxation which is observed as the additional time constant of 1-2 ps. During the electron solvation a configurational relaxation of the first solvation shell of water molecules occurs as a response to a generated delocalized electron (quasi-free in conduction band of water) causing its localization, trapping and finally solvation. In the case of more excess energy it is spread further to the second solvation shell so an additional response of the polar environment occurs around the new electric field which is a consequence of the electron solvation. The additional observed time constant of 1-2 ps relates the reported values of the dielectric relaxation in water [173-175, 202].

5.9 Different recombination dynamics in indole, 1-methylindole and pure water

The solvated electrons exhibit no recombination in the time scale up to 160 ps contrary to solvated electrons in neat water as shown in Figure 5.24.
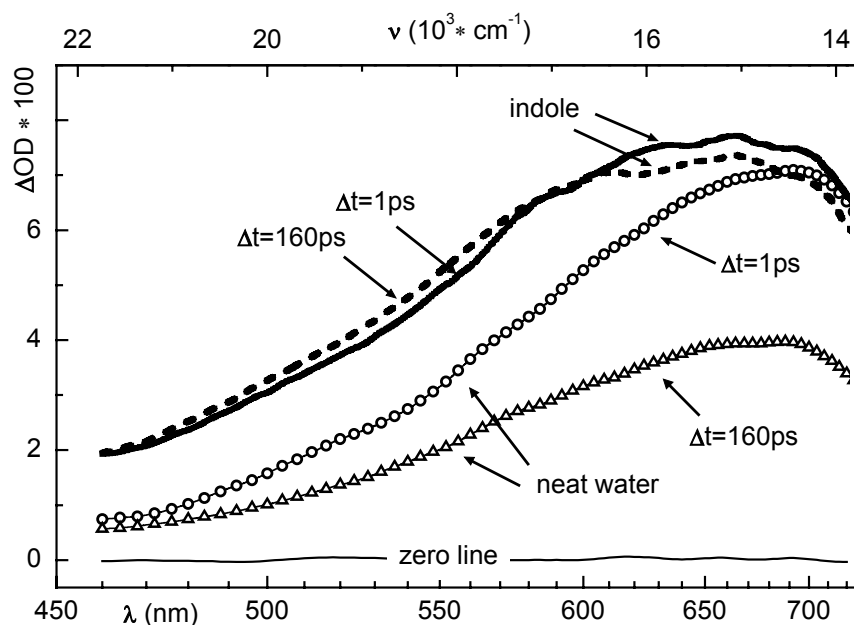

Figure 5.24 Transient absorption spectra of indole in water probed at a delay of 1 ps (solid line) and 160 ps (dashed line) compared to those of neat water at a delay of 1 ps (circles) and 160 ps (triangles) exhibiting different recombination dynamics.

The first 160 ps of the long time behavior of indole in water (discussed above in Figure 5.18) is presented in Figure 5.25 together with that of neat water. As discussed above (see Section 5.6) indole exhibits no significant geminate recombination. The weak decay observed in this time range with a ~40 ps time constant can be related to the relaxation of the excited state absorption in the L_a state which contributes weakly to the signal in the probed wavelength region (λ_{probe} = 730 nm). The long time behavior of the excited state absorption of the L_a state corresponds to the dynamics of indole in ethanol discussed above (see Section 5.6 and Figure 5.8). The 40-ps time decay can also corresponds to a small fraction of ionized molecules which succeeds to recombine.

Contrary to indole, neat water shows a two-exponential decay. The initial time constant of ~ 2 ps is already observed in a short time scale and represents the dielectric relaxation of the solvent. The second time constant of 24 ps corresponds to partial geminate recombination. This behavior agrees with the reported one [23]. The reported time constants corresponding to the dynamics of an iodide anion in solution that forms also a CTTS state are of

0.2 ps, 1.1 ps, 20 ps, and a pedestal on a 400 ps time scale [223]. Such a dynamics is in a perfect agreement with the dynamics being reported here.

If the 40-ps low amplitude time decay observed in indole corresponds to a partial recombination it would be in an agreement with the reported result observed in aqueous iodide which shows that the electrons from two-photon ionization of neat water relax by a factor of 2 faster than the electrons ejected via the anion CTTS pathway in aqueous iodide [225].
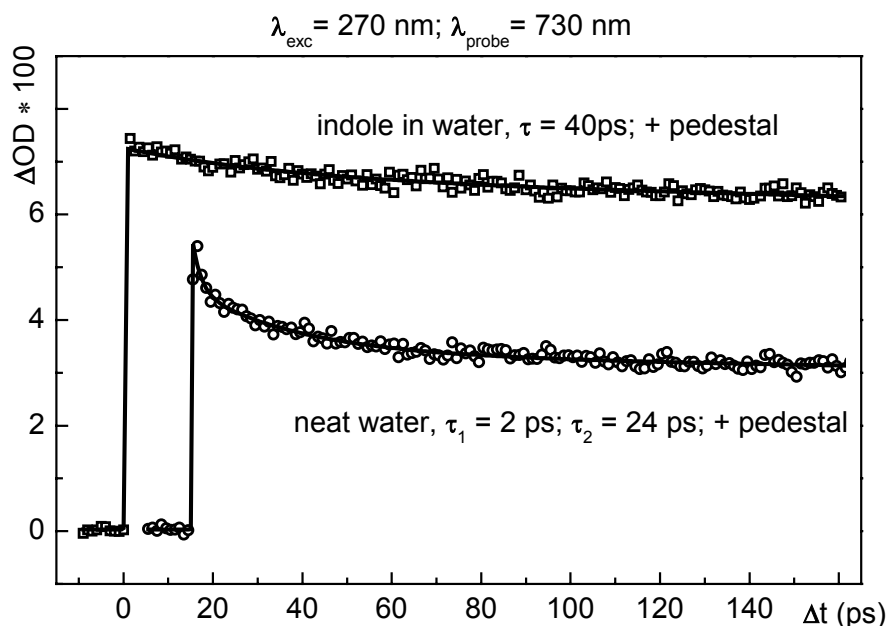

Figure 5.25 Time resolved absorption change of indole in water (squares) shows weak monoexponential decay, while neat water (circles) shows two-exponential decay. Corresponding fits (solid lines) are obtained assuming multi-exponential decays and a Gaussian cross correlation. Note that the amplitude of the 40-ps time decay in indole is much smaller than the one of the 20-ps in neat water. Both curves show pedestal indicating that some fraction of the solvated electrons escapes recombination.

The signal from solvated electrons generated in an indole solution as well as in neat water shows a remaining absorption (pedestal) at times greater than 60 ps due to the electrons that escape geminate recombination. This phenomenon was previously reported in radiolysis experiment [77] as well as in femtosecond studies [23, 175, 202, 210, 223], which show that 50-60% of the solvated electrons escape geminate recombination in neat water as well as in deuterated water [22]. Two recombination pathways of solvated electron in neat water are reported. The relative recombination yields of a solvated electron with OH and H_3O^+ is determined to be 82% and 18%, respectively [210].

Monte Carlo simulations [232] show that within the first picosecond after photoionization the excess electrons relax to an equilibrium ground state and the initial H_2O^+ fragments

to H_3O^+ and OH radical species. The recombination probability of the solvated electron with H_3O^+ per encounter is quite small and the reaction is not diffusion limited.

It is suggested that the fraction of electrons escaping the recombination may have trapping and solvation distances greater than the Onsager radius (the distance at which the potential energy between 2 oppositely charged ions is equal to k_BT, in water 0.7 nm) and escape far from the geminate primary radicals H_3O^+ or OH. Reported thermalization length (the distance between parent ion and departing electron, which is trapped there because of the strong interaction with the solvent molecules [47]) of electrons in liquid water is in the range of 2 - 5 nm [in 202]. Electrons that are not hydrated in the vicinity of H_3O^+ or OH have a low probability of undergoing a fast geminate recombination process because the long range Coulomb type interactions are negligible.

Analogous to neat water, it can be concluded that the thermalization distance in the case of indole-water solution is even longer and the geminate recombination of the indole radical cation with the solvated electron is completely or almost completely inhibited.

Kohler and coworkers reported that the rate of recombination between indole radical cations and solvated electrons is considerably below the diffusion limit, indicating that the geminate pairs are more stable than previously thought and a free energy barrier for adiabatic electron recombination seems to exist [19].

5.9.1 Two independent recombination dynamics observed in Na-THF system

The appearance of two kinds of solvated electrons was reported in the sodide-tetrahydrofuran (Na-THF) system [233, 234]. Low energy excitation produces an excited CTTS state of an immediate solvated electron - sodium atom contact pair in which the solvated electron resides in the same solvent cavity as the sodium atom and recombines in about one picosecond. The high excitation energy produces excited CTTS state wave functions with larger spatial extent, allowing the electron to localize further away from the parent in a long-lived solvent separated contact pair, or to be ejected into the solvent. Recently it was shown how the production and recombination of solvated electrons can be manipulated by low or high energy excitation [235].

The existence of different kinds of solvated electrons can explain the absence of total geminate recombination observed in indole and neat water. Only the electrons which reside in the same solvent cavity as the parent donor molecule are able to recombine on a 10-ps time scale. The electrons which are localized further from the parent are surrounded with the nearby solvent molecules and are not capable of geminate recombination within $\geq$ 1ns.

5.10 Discussion

In order to understand the excited state dynamics of indole the photodynamics in water is compared to the one in ethanol and cyclohexane experimentally verifying the phenomena of the state reversal and the ultrafast branching. The promoting role of the water molecules in electron solvation is discussed and the observed processes are compared to the electron solvation occurring in neat water and several other systems.

5.10.1 State reversal and ultrafast branching

In cyclohexane and ethanol the ionization threshold of indole lies above the applied excitation wavelength and no photoionization occurs. The observed dynamics of 6 ps in ethanol and of 7 ps in cyclohexane corresponds to the population transfer between the ^1L_a and ^1L_b excited states (see Section 5.3.1). The dipole moment of the ^1L_a state differs more in strength and direction from that of the ground state than the ^1L_b state does. Thus the molecules of polar solvent (ethanol) promote the lowering of the ^1L_a state more than of the ^1L_b state, causing the state reversal. This phenomenon of state reversal was already suggested by other authors [110, 184, 185], but it is experimentally verified for the first time here by observing the rates of the population transfer from one excited state to another directly. The observed rate in ethanol is not related to the time of the state reversal itself but to the population transfer as a consequence of the state reversal, since no shift of the transient spectra is observed.

The unusual behavior of indole dissolved in water, that is the long living fluorescence state with a lifetime of a few nanoseconds and ultrafast nonradiative relaxation (photoionization within 1 ps) is explained by an immediate branching of the Franck-Condon excited state to a charge transfer to solvent state (CTTS) and to a fluorescing state. The idea of a branching process is supported by a previously reported experiment [18]. Using the effective singlet quencher Cs^+, which increases the intersystem crossing rate Saito at al. have shown that the fluorescence lifetime of indole decreases with increasing Cs^+ concentration. In contrast to the fluorescence quantum yield the photoionization quantum yield is hardly affected by the quencher ion. This implies that the state corresponding to photoionization has no effect on the fluorescing state and the photoionization process originates from a non-relaxed S_1 state. The same concept of one photon generation of solvated electrons occurring from an unrelaxed excited state of indole and tryptophan was reported [152].

5.10.2 Solvation of the electron in neat water

There are many studies about electron solvation in neat water, which are consistent with the results presented here. Localization and solvation of excess electrons in neat water have been experimentally resolved on the femtosecond time scale [197]. The initial electron,

which is in a presolvated state absorbing in the infrared spectral region, thermalizes in 110 fs within the conduction band and relaxes in 240 fs towards the fully solvated state subsequently. The two-state model of solvated electron is verified by demonstrating the existence of an isosbestic point at 820 nm [198, 200]. At this wavelength the spectra of the presolvated and fully solvated electron intersect and both species have the same absorption coefficient.

The Smoluchowski-Vlasov theory of charge dynamics is in agreement with this statement [236], which predicts at least two stages in the solvation of an electron in water. The first stage is localization: after photoionization the quasi-free electron goes from a delocalized state spreading over a large distance to a localized state in some shallow potential trap. This is followed by the relaxation of the surrounding solvent, which deepens the trap. Once the electron gets trapped it evolves toward the solvated state via a configurational relaxation of the medium (solvent) in the electronic field of the charge (trapped electron). This discussion can be used to interpret the observed time constant of 0.35 ps in neat water as the electron solvation corresponding to the second stage of the solvation process, which is promoted by the reaction of the polar liquid to the charge. It is assumed that the localization of the quasi-free electron corresponding to the first stage of the solvation can not be resolved with the obtained experimental time resolution (60 fs). This is consistent with a recent report of an initial time constant of 50 fs in neat water. It was suggested that the OH-vibrational modes in the first solvation shell as accepting modes for energy relaxation in approximately 300 fs [237].

The existence of two types of electron excited state is observed by direct 1-photon excitation of the solvated electron in water [238, 239]. The transition from the ground s-like state to the p-like excited state is obtained with 800 nm light, while the transitions to the conduction band with 400 nm light. Thus the theoretical model of solvated electron proposing the s-like ground state and p-like excited state [240], as well as the generation of electron in conduction band is experimentally verified. It is demonstrated that the solvation dynamics of the solvated electron depends on the initial degree of the electron delocalization [241]. The conduction band electron, produced by detrapping of the hydrated electron, has the slowest time scale for electron solvation with an average solvation time constant of 400 fs. In contrast, the solvation dynamics are significantly faster for electrons that are produced in presolvated environments as the excited p-state of the hydrated electron and the precursor states involved in UV fs multiphoton ionization of water.

5.10.3 The electron solvation dynamics in neat water and in other CTTS systems

Several groups reported time constants describing the electron solvation in neat water.

The group of Barbara [199] reported to observe in neat water the radiationless transition from the excited state to the ground state of the solvated electron with an average time

constant of (550 ± 170) fs consisting of two time constants. The first time constant is related to the internal conversion from the excited state in the time region of 0.3-0.4 ps, which is followed by ground-state solvation in 1-2 ps [173]. This is in excellent agreement with data presented here.

The similar time constants observed in neat water are 180 ± 50 fs [175, 198] and 300 ± 40 fs [200] for electron localization and 540 ± 80 fs for further solvation [175, 198, 200]. The slightly longer initial time constants reported can be explained by lack of consideration of the coherent artifact (see Section 3.4.2), which could obscure the early time dynamics and a position of a zero point.

Other systems exhibiting electron solvation also show similar dynamics to the one observed in neat water. For example, the observed dynamics after UV excitation of iodide anions in solution, where resonant excitation into the CTTS state occurs, shows time constants of 0.2 ps, 1.1 ps, 20 ps, and a pedestal on a 400 ps time scale [223]. These times constants are very similar to those presented here.

A similar dynamics were observed for aqueous NaCl solution and described with three time constants: <80 fs, 190 fs, 1.2 ps [174].

Photoelectrons detached from aqueous hexacianoferrate(II) complexes ($[Fe(CN)_6]^{4-}$) show dynamics characterized by the instantaneous appearance of the CTTS band (> 60 fs) followed by the solvation of the trapped electron with a time constant of 0.5-0.6 ps [72, 242] indicating again a similar dynamics as observed for indole in water.

Analogously to neat water and to other systems also exhibiting the CTTS state, the observed time constant of 0.35 ps for indole in water can be related to the same electron solvation dynamics. The absence of an additional time constant of 1-2 ps can be explained by considering the excitation with insufficient excess energy as discussed above (see Section 5.8). The process of electron trapping, which occurs within our time resolution (60 fs) is faster than diffusive solvent relaxation indicating that the trapping process is governed by inertial motions of the water molecules, similar to the charge separation process in case of lactones discussed in Chapter 4.

5.10.4 Influence of solvent on the electron solvation

Investigations on electron detachment and solvation in similar systems in literature led to the conclusion that during the solvent relaxation from the Franck-Condon excited state to the fluorescence state solvent reorientation may act favorably for electron ejection of the excited solute and for cation radical generation. Schwartz et al. [233] studied the CTTS-transition in the sodide-tetrahydrofuran system to model the influence of solvent motion to an ET reaction, because the only nuclear degrees of freedom that can move in this system are those

of the solvent. They have found that the Franck-Condon excitation does not produce the halogen atom and the solvated electron directly. Instead the excitation puts the local solvent structure around the anion donor out of equilibrium. The solvent molecules move to reestablish equilibrium and this causes the electron to detach and become solvated in a nearby solvent cavity, which acts as the acceptor. Molecular dynamics simulations [233] indicate that solvent rotational motions dominate the electronic relaxation when only the solute's charge changes, while the slow translational motions of the few closest solvent molecules control the solvation dynamics when realistic reactant size changes. Bradforth and coworkers performed an extensive investigation of the electron detachment and recombination processes of aqueous iodide [223-225]. They found that solvent motions that promote electron detachment occur within 200 fs, while the back ET reaction takes place on a very different time scale of tens of picosecond.

It is proposed that the solvent configurational relaxation causing solvation appears with the longitudinal dielectric relaxation time (τ_L), which is discussed in Section 2.5.2 [236]. The reported values for water are $\tau_L \sim 0.2$ps [236] and $\tau_L = 0.5$ps [24]. Theoretical analyses confirm that the water system should relax with a characteristic time of the order of $\tau_L \sim 0.2$ps [243]. The solvation time constant of 0.35 ps presented in this work confirms these reported prediction.

Long et al. [198] proposed that the hydrogen bond dynamics is responsible for the solvation process. The mean lifetime of the hydrogen bond in neat water can be deduced from the width of Rayleigh scattering in Raman spectra [244, 245]. This scattering is caused by the dipole moments induced by the photoexcitation and hence by the local polarizability in the liquids. The reported lifetime is temperature dependent and at room temperature equals $0.7 - 0.8$ ps [244, 245]. The order of magnitude of this time constant indicates that the hydrogen bond dynamics is more related to the dielectric relaxation of 1-2 ps observed in water rather than to the solvation dynamics of 0.35 ps.

5.10.5 Interaction between electron and surrounding water molecules

The reported transient resonance Raman spectra of neat water after photoionization show a structural change induced by the strong interaction with the electron. The OH bend of water molecules in the vicinity of solvated electrons are downshifted indicating a formation of a new quasi-molecule [246-249]. This experimental results are also proposed in theoretical considerations below. Electronic structure calculations [250] found that the solvated electron forms two strong electron-hydrogen bonds of $e^- \cdots$ HO type with the hydrogen-bonded water cluster and two of the hydrogen bonds in the neutral water cluster are broken to accommodate these new bonds in order to form possible stable structures.

The calculated potential energy surface for the interaction of indole with one water molecule exhibits minima corresponding to three different ways of interaction: via donating the hydrogen atom of the N-H bond to water, via πH-bonding of water to the π cloud of indole, and finally, via σH-bonding of C-H bonds with water. The most stable complex binds water to the N-H of indole [181].

These discussions fit in our model of solvated electron which interprets it as a stable system consisting of electron surrounded by the first solvation shell of water molecules, living long on a μs-time scale [55, 21].

In summary, after the ultrafast branching a presolvated electron and an indole radical cation are generated within our time resolution of 60 fs and form the CTTS state. Subsequently the process of solvation is observed and for the first time the solvation rate of 0.35 ps is determined. The influence of the solvent is discussed and the diffusive solvent relaxation is found responsible for the electron solvation. The origin of the solvated electron is related to a detached electron from the hydrogen atom bound to the nitrogen atom of pyrrole ring in indole, since the same ultrafast dynamics is observed in 1-methylindole where the electron detachment occurs from the methyl group bound to the nitrogen atom (see Section 5.7).

6 Statistical behavior of internal conversion in o-hydroxybenzaldehyde

6.1 Introduction

The dynamics of hydrogen atoms is a fundamental issue in chemistry and molecular biology [252]. Excited state intramolecular proton transfer (ESIPT) allows to study proton transfer reactions under well-defined conditions [253]. The hydrogen atom of a hydroxyl group in an H-chelate ring is transferred to an acceptor atom on the other side of the ring forming the keto- from the enol-form of molecule as presented in Figure 6.1 [254].
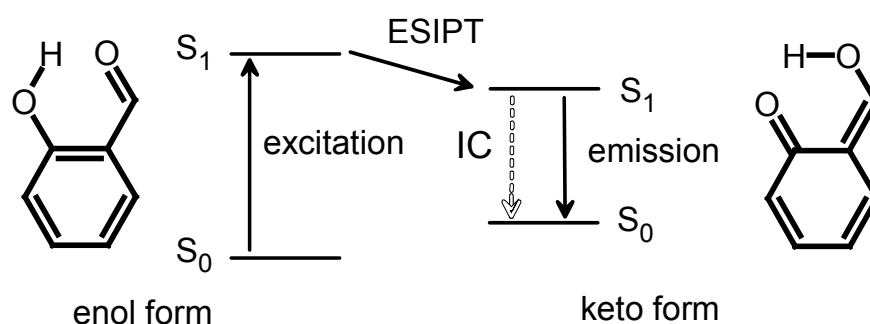

Figure 6.1 Energy level scheme of the ESIPT and the enol and the keto form of o-hydroxybenzaldehyde (OHBA)

The dominant relaxation process after the photoinduced ESIPT is the internal conversion (IC) in these molecules, which brings them back to the electronic ground state. Despite of their similar ESIPT dynamics [3, 253, 255], the lifetime of the first electronically excited state depends strongly on the molecule [256, 257]. It is important to understand the mechanism underlying the different IC dynamics, because this knowledge can be used for protection against UV radiation.

A time scale of less than 100 fs was found for the ESIPT dynamics in several compounds [257-259] and coherent excitation of vibrations has been observed for some examples [260-263]. For 2-(2'-hydroxyphenyl)benzothiazole (HBT) time resolved investigations led to a description of the ESIPT as a ballistic wavepacket motion inducing coherent vibrations in the reactive coordinates [255, 261, 264-266].

Although the ESIPT molecules have a similar electronic structure the time scale of their IC varies with the molecule by three orders of magnitude between 150 fs for TINUVIN P [267, 268] to several hundred picoseconds for HBT [256, 269]. The question is if there is

any coupling between the ESIPT and the IC and what is the reason for this strong variation despite the similar reaction centers?

To answer these questions fluorescence quantum yield measurements on o-hydroxybenzaldehyde (OHBA) solvated in cyclohexane are performed and compared to the transient absorption studies obtained with 30 fs time resolution [270]. The results are compared with recent *ab-initio* calculations [271-275] and data obtained in gas phase by time resolved photo electron spectroscopy [276].

6.2 Steady state spectra and fluorescence quantum yield

The steady state absorption and fluorescence spectra of OHBA are presented in Figure 6.2. The ESIPT leads to a strong and characteristic Stokes shift between the UV absorption of the original enol-form and the fluorescence in the visible which is attributed to the reaction product, the keto-form [254, 256, 277]. The fluorescence excitation spectrum of OHBA solvated in cyclohexane (see Figure 6.2) is similar to the one in gas phase [278, 279].
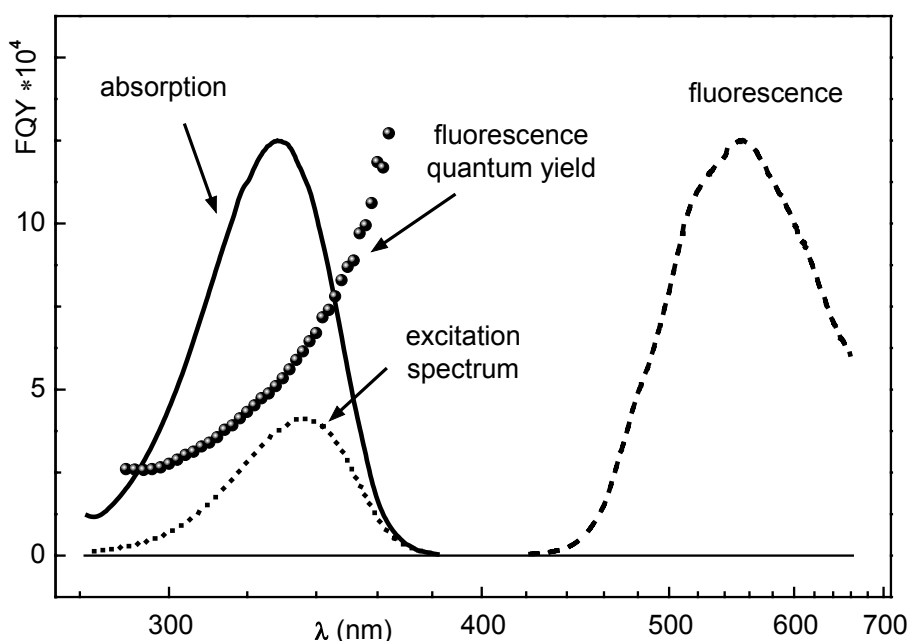

Figure 6.2 Steady state absorption (solid line), fluorescence emission (dashed line) and fluorescence excitation spectrum monitored at $\lambda_{emission}$ = 500 nm (dotted line) of OHBA dissolved in cyclohexane in arbitrary units. The fluorescence quantum yield (symbols) is determined from the absorption and the excitation spectrum. The absolute values (scale on the left, FQY) are calibrated with respect to the calculated value at 340 nm (for details see text).

The fluorescence spectrometer used for measuring the fluorescence spectra of OHBA dissolved in various solvents is not capable to measure the absolute values of fluorescence yields. In order to obtain the absolute values the relative values measured in experiments are compared to the fluorescence yields of some dyes whose fluorescence quantum yields are known from literature [187, 188]. This method is illustrated with equation (6-01).

$$\Phi_F(indole) = \frac{\Phi_F(indole)_{measured}}{\Phi_F(dye)_{measured}} \cdot \Phi_F(dye)_{known} \qquad (6\text{-}01)$$

The substances used in comparative measurements should have similar absorption throughout the excitation bandwidth, closely similar wavelength distributions of the fluorescence spectra, negligible reabsorption of the emission, and identical refractive indices of the two solutions being compared. As presented in Figure 6.3 the fluorescence of OHBA lies between the fluorescence spectra of the two dyes coumarin 47 and rhodamine 6G.
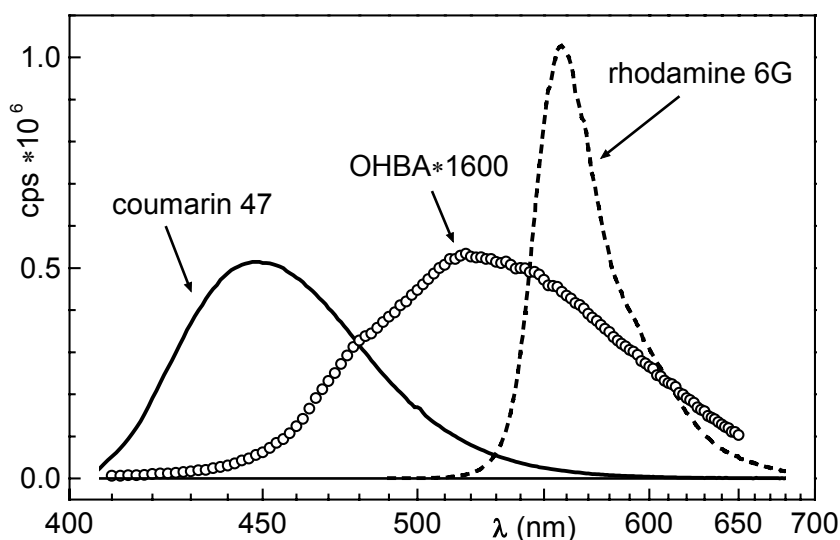

Figure 6.3 The fluorescence spectrum of OHBA (circles) lies in the spectral region between the fluorescence spectra of two dyes: coumarin 47 (solid line) and rhodamine 6G (dashed line), used in comparative measurement.

Both dyes are dissolved in ethanol and after excitation at 404 nm (coumarin 47) and 488 nm (rhodamine 6G) emit with the yields of 0.64 and 0.88, respectively [188]. The concentrations of the used solutions were prepared in the way to adjust the transmission rate of all compared substances at the wavelength of excitation to be approximately equal to 40%.

The ratio of measured values of the fluorescence quantum yields of the two dyes is compared with the reported values [188] and shows a good agreement.

$$\frac{\Phi_F(rhod6G)_{measured}}{\Phi_F(coum47)_{measured}} = 1.38 \qquad \frac{\Phi_F(rhod6G)_{reported}}{\Phi_F(coum47)_{reported}} = \frac{0.88}{0.64} = 1.39$$

The fluorescence quantum yield of OHBA excited at 340 nm is determined to $(6.7 \pm 0.5) \cdot 10^{-4}$. The behavior of the fluorescence quantum yield in the whole spectral region is calculated as a division between excitation and absorption spectrum and scaled to fit the absolute determined value at 340 nm (see Figure 6.2).

From the absorption and fluorescence spectrum the radiative lifetime of the S_1-state was calculated to 52 ns by the formalism described above (see Section 5.2.3). From the fluorescence quantum yield an excited state lifetime of 35 ps results. The biggest uncertainty of this calculation stems from the assumption that the electronic transition dipole moments of the enol and the keto form are the same. However, since the S_1 state is a $\pi\pi^*$ state in both forms [271, 273, 278] no drastic variation is expected. Within this accuracy the result agrees well with the 55 ps decay found in the time resolved measurements discussed below confirming the assignment of this time constant to the S_1 lifetime [270].

6.3 Comparison with the time resolved measurements

The transmission change on the 100-ps time scale is depicted for three probe wavelengths in Figure 6.4 (taken from [270]). The traces were measured with the polarization arranged in magic angle to avoid orientational relaxation effects [85-87]. The solid lines in Figure 6.4 represent the fitted model function which consists of two exponentially decaying components. The corresponding parameters are listed in Table 6.1.

Table 6.1

Fitted time constants and amplitudes of the two-exponential decay on longer time scales

probe wave-length	τ_1 (ps)	$A_1 * 10^3$	τ_2 (ps)	$A_2 * 10^3$
530 nm	9.0	-1.2	61	-0.78
560 nm	8.6	-1.1	48	3.4
630 nm	10.2	0.67	55	0.33

Negative amplitudes indicate rising components in transient transmission traces

The amplitudes of the shorter one at about 10 ps are negative at 530 nm and 560 nm and positive at 630 nm. This corresponds to a blue shift of the fluorescence spectrum which is most probably due to cooling by the solvent since the time scale is typical for molecules solvated in cyclohexane [280]. With the longer time constant around 55 ps the signal decays to zero at all employed probe wavelengths. Therefore the constant is attributed to the lifetime of the S_1 state in agreement with results obtained in 3-methylpentane [277].
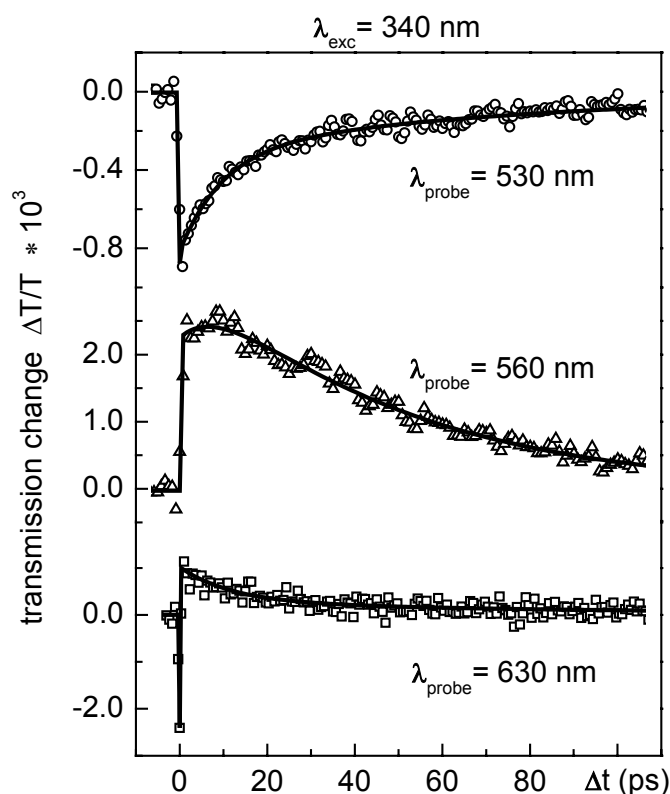
Figure 6.4 Transient transmission of OHBA at the probe wavelengths 530 nm (circles), 560 nm (triangles) and 630 nm (squares) on a 100 ps time scale. The fitted model functions (solid lines) show two-exponential behavior.

6.4 IC mechanism

6.4.1 Energy dependence

The rate of the IC, which is reciprocal to the yield, is shown in Figure 6.5 in dependence on the energy of the excitation photons. IC rates at various excitation wavelengths were previously measured by time resolved photo electron spectroscopy in the gas phase [276]. The absorption spectrum in gas phase [279] is 100 meV blue shifted with respect to the absorption in cyclohexane indicating that the S_1 state is 100 meV higher in energy. Shifting the gas phase data by 100 meV to lower excitation energies and scaling them by a factor of 0.075 results in the data points shown as open squares in Figure 6.5. They match very well the IC rates measured in cyclohexane. This means the IC is slowed down by a factor of 13.3 in liquid phase but the mechanism seems to be the same.
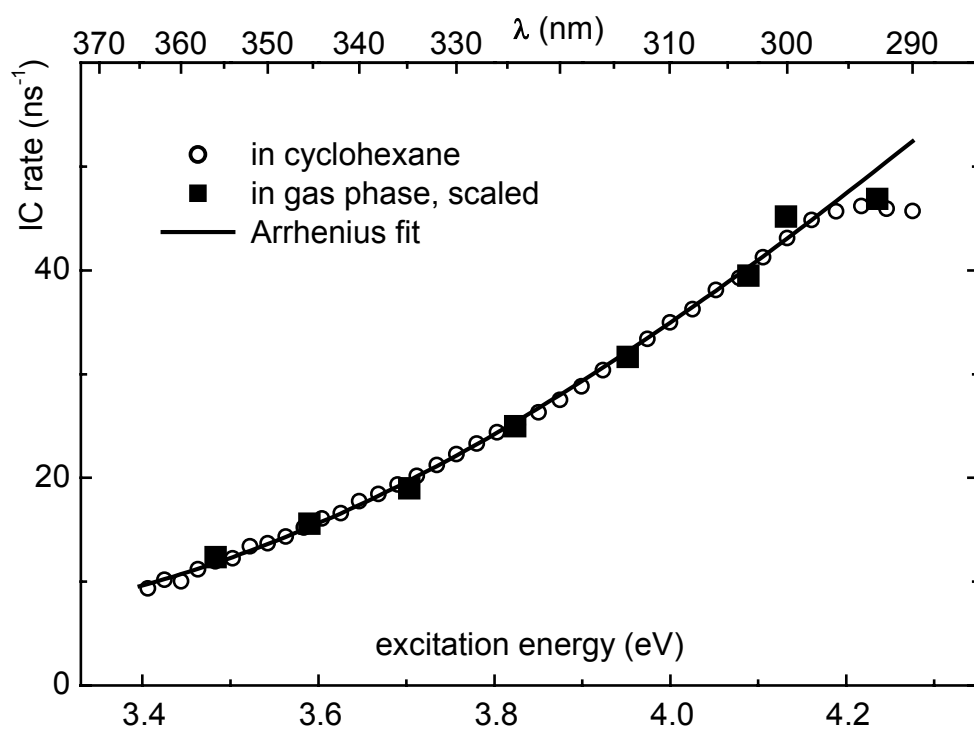
Figure 6.5 Internal conversion rate of OHBA dissolved in cyclohexane (circles) in dependence on the excitation energy. A fitted Arrhenius law is depicted as solid line and gas phase data from ref. [276] scaled by a factor of 0.075 as squares.

On first sight it is surprising that an energy dependence of the IC can be seen in our experiments. The excited state lifetime is in the order of several ten picoseconds whereas the cooling by the solvent occurs on a ten picosecond time scale. Therefore the excess energy should have been transferred to the heat bath of the solvent before the IC occurs. But the cooling seems to be incomplete within this time range and does not lead to a thermal distribution according to room temperature.

We modeled the dependence on the excess energy by applying some vigorous simplifications. Photo electron spectroscopy [276] and *ab-initio* calculations [273] indicate that the keto minimum is about 0.5 eV below the potential energy of the Franck-Condon point which corresponds to the maximum of the absorption spectrum. This allows to calculate the amount of excess energy from the excitation wavelength. To account for the cooling it is assumed that only a portion of the energy stays in the molecule. An internal temperature is calculated by presuming a thermal distribution of the remaining excess energy over the vibrational modes of OHBA. The dependence of the IC rate on the internal temperature is modeled by an Arrhenius law plus a small temperature independent contribution which may result from tunneling or zero point motions. This kind of dependence is quite common for IC processes [46].

The fit of the model function to the IC data is depicted in Figure 6.5 as solid line. Thereby it was assumed that 20 % of the excess energy remain in the molecule. The model describes the observed IC rates very well. The deviations found at high excess energies may be due to contributions of the next higher electronic state. From the fit an energy barrier of 201 meV, a prefactor of 6.4 ps^{-1} and temperature independent contribution of 0.005 ps^{-1} result. A fit to the gas phase data of [276] gives nearly the same values for the barrier and the prefactor, i.e. 173 meV and 6.7 ps^{-1}. This indicates that the slowdown of the IC by a factor of 13.3 in liquid phase is due to the loss of excess energy by cooling.

6.4.2 Three state model

By means of presented results we conclude that the IC proceeds via a thermally activated crossing over an energy barrier in the order of 200 meV (1600 cm^{-1}) as presented in Figure 6.6.
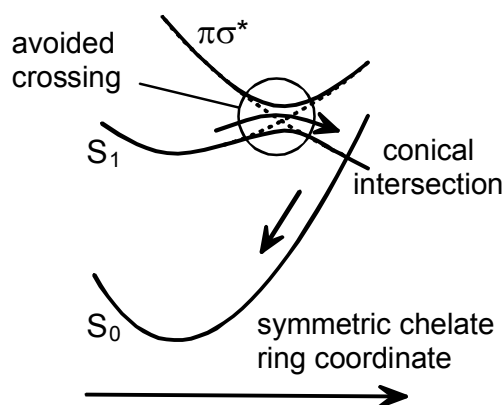

Figure 6.6 Internal conversion mechanism for ESIPT-molecules. The optically excited S$_1$ state is depopulated via an avoided crossing which arises from the coupling of the $\pi\pi^*$ with $\pi\sigma^*$ state. The return to the electronic ground state occurs through a subsequent conical intersection.

According to *ab-initio* calculations on malonaldehyde [281] and on OHBA [271, 273] the IC could be mediated by an $\pi\sigma^*$-state. It shows a strong energy decrease along a coordinate which corresponds to the detachment of the hydrogen atom. It crosses the $\pi\pi^*$-state and forms a conical intersection with the ground state. This route represents a very efficient IC path. The avoided crossing of the $\pi\sigma^*$- and the $\pi\pi^*$-state leads to an energy barrier which is most probably the one that shows up in the experiments. The calculated height is about 0.5 eV in the case of malonaldehyde and in the order of the experimental value reported for OHBA above.

6.4.3 Statistical versus coherent dynamics

After the ESIPT the molecule vibrates in specific modes which initially contain most of the vibrational energy. If they participate in the IC the coherent motion in these modes should periodically modulate the transition rate. No indications for such signal contributions have been found. Anyway, in this case the IC should be quite fast at the beginning and slow down later since internal vibrational redistribution leads to a loss of energy in these modes. A significant decrease of the S_1 population in the first few picoseconds would result in contradiction to the experiment. Obviously, the IC rate is sensitive to the total amount of vibrational energy but not to the energy content of the modes directly excited by the ESIPT. Thus, the significant coordinates for both processes are orthogonal to each other and the energy flow in modes relevant for the IC is associated with vibrational redistribution. This is reflected by the statistical behavior of the IC whereas coherent wavepacket dynamics is observed for the ESIPT [255, 261, 264-266].

7 Summary

Fundamental photoinduced processes like intra- and intermolecular charge transfer and relaxation via internal conversion are investigated in several molecular systems by combining pump-probe femtosecond spectroscopy and steady-state fluorescence studies. After photoexcitation in the deep UV-C spectral region the time resolved dynamics are observed with an unprecedented time resolution of 60 fs for excitation at 270 nm.

Triphenylmethane lactones are investigated as model systems for ultrafast **intramolecular charge transfer** processes. Due to the orthogonal structural configuration in the investigated lactones (phenolphthalein and malachite green lactone) the subunits are decoupled in the electronic ground state and the transient spectral features allow an unambiguous identification of the appearing radical ions. Both lactones undergo ultrafast photoinduced electron transfer (ET) with the formation of a radical ion pair of their structural subunits. This observation confirms earlier predictions deduced from steady-state fluorescence spectra and from the analysis of structurally analogous compounds. The ET process was monitored directly by measuring the kinetics of the radical cation formation after excitation of phenolphthalein to the S_1 state and malachite green lactone to the S_2 state.

In phenolphthalein in acetonitrile the phenol radical cation, a product of the primary charge separation, appears in the transient absorption spectra with a rise of 50 fs. This is the fastest ET time constant directly observed for organic intramolecular donor-acceptor systems. The charge separation occurs on a time scale shorter than what was postulated so far for ultrafast inertial solvation dynamics and is quite likely promoted by vibronic coupling via the C-O bond in the lactone ring.

In malachite green lactone both $S_2 \rightarrow S_1$ electronic relaxation and charge separation are completed within 150 fs in aprotic as well as in protic environment. Subsequently, in protic solvent like methanol opening of the lactone ring is detected directly by observing the appearance of the malachite green cation absorption band. The corresponding time constant of 2 - 4 ps is related to the longitudinal dielectric relaxation of methanol and indicates that diffusive solvation is responsible for the breakage of the C-O bond in the lactone ring of malachite green lactone.

Results of the research work done on triphenylmethane lactones prove that they are ideal model systems for both ultrafast ET and solvation dynamics studies. Triphenylmethane lactones are also excellent candidates for gaining insight into the detailed mechanisms of the very first steps of electron transfer as a fundamental process of photosynthesis in biological donor-acceptor systems.

The response of **indole**, a common chromophore of many nitrogen heterocyclic biomolecules (such as the essential amino acid Tryptophan), to the UV radiation is investigated. The state reversal of the two lowest ($\pi\pi^*$) excited states (the ^1L_a and ^1L_b state) occurring in polar solvents as opposed to nonpolar solvents and gas phase is temporally resolved for the first time by observing the population transfer between the reversed excited states on a 6 - 7 ps time scale.

The controversial behavior of the excited indole in water, which fluoresces on a nanosecond time scale and undergoes photoionization within 100 fs, is explained with an ultrafast branching occurring immediately after excitation. The excited indole population is divided by the ultrafast branching into a fraction which exhibits a state reversal but stays in the optically accessible excited $\pi\pi^*$ states and a fraction that undergoes photoionization via a crossing between the $\pi\pi^*$- and the $\pi\sigma^*$-state resulting in an **intermolecular electron transfer to the solvent**.

The photoionization quantum yield of 0.38 is determined by taking into account the absorption spectra of all contributing species over the complete visible range. The dynamics of solvated electron, which appears from charge transfer to solvent state, is observed. The electron solvation time of 0.35 ps is resolved for the first time allowing us to describe the mechanism of electron solvation stemming from indole in a similar way as reported for neat water.

For a long time the origin of the solvated electron was addressed controversially. The dispute is resolved by observing the initial excited state dynamics of 1-methylindole. Due to its structure 1-methylindole is able to exhibit only electron transfer. Since the same solvation dynamics is observed by both indole molecules it is clear that the photoionization in indole follows the same path and that a direct electron transfer to the solvent and not an H-transfer occurs.

Considering only the population fraction of 62%, which does not exhibit ionization and is capable of fluorescing, the fluorescence quantum yield is corrected to the new value of 0.4 for those molecules which reached the L_a state. From the corrected fluorescence quantum yield and the radiative lifetime calculated from the absorption and fluorescence spectra the lifetime of the L_a state is determined to be (3.6 ± 1.0) ns.

Internal conversion (IC) is a further nonradiative process which occurs in organic compounds upon the UV radiation. The mechanism of internal conversion is investigated in **o-hydroxybenzaldehyde** (OHBA). OHBA belongs to the class of molecules that exhibit excited state intramolecular proton transfer (ESIPT) and show rather fast IC. This makes them good candidates for photostabilizers, which are used to protect other light-sensitive materials from degradation caused by the UV component of the sunlight.

It is found that the IC of OHBA proceeds over an energy barrier of about 200 meV as a thermally activated process. The barrier most likely arises from an avoided crossing between the $\pi\pi^*$- and $\pi\sigma^*$-state. The height of this barrier is sensitive to the energetic location of these two states with respect to each other. Comparatively small changes in a molecular configuration should lead to significant variations of the IC rate. This explains why the IC rate of various ESIPT molecules varies strongly whereas the ESIPT mechanism just involving the $\pi\pi^*$-state is in all cases very similar.

The IC shows pure statistical behavior dependent on total excitation energy although a well-defined wavepacket exists after the ESIPT showing coherent behavior. It indicates that the coordinates drastically changed by the ESIPT are orthogonal to those responsible for the IC and a significant vibrational energy redistribution has to take place before the IC. This is in agreement with the model that the O-H distance is crucial for the ESIPT whereas the IC is due to electronic coupling along coordinates corresponding to a hydrogen detachment.

On the basis of the results presented here we can conclude that in both nonradiative processes, the intermolecular charge transfer to solvent and internal conversion, a dark excited state ($\pi\sigma^*$) promotes the ultrafast nonradiative relaxation via crossing between the light $\pi\pi^*$ and the dark $\pi\sigma^*$ state. Presumably this mechanism can be extended to most ultrafast processes.

Appendix

A Fitting procedure

Fitting curves are obtained assuming multi-exponential decays and a Gaussian form for the cross-correlation. The following model function *S(t)* was used to fit the measured traces:

$$S(t) = S_{CC}(t) \cdot \sum_{i=1}^{n} \left\{ A_i \cdot e^{-\frac{t}{\tau_i}} \right\} \cdot \Theta(t - t_0), \qquad \text{(A-01)}$$

where A_i are the amplitudes of the decays, τ_i the time constants, $\Theta(t)$ is the step function. $S_{CC}(t)$ is Gaussian function representing the cross-correlation signal with the experimentally determined full width of half maximum.
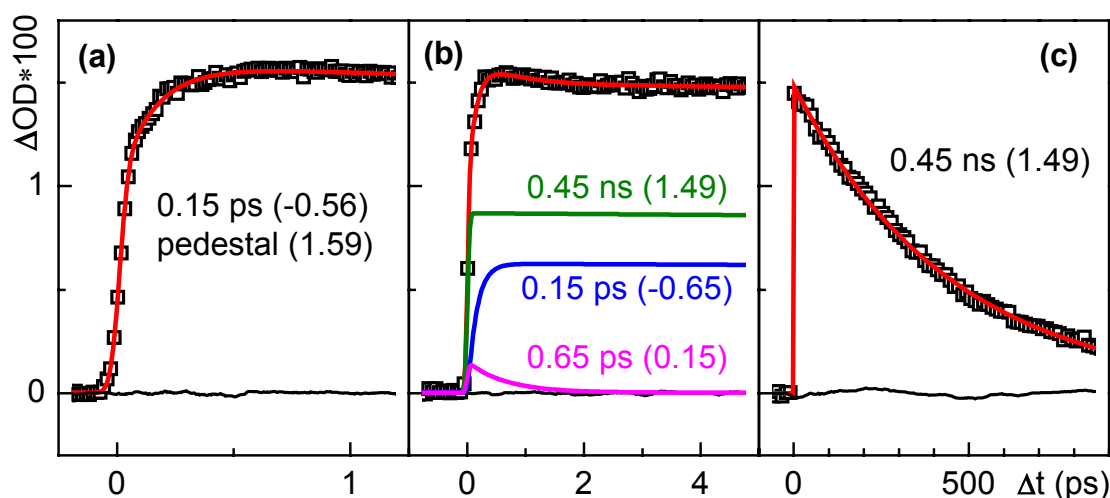

Figure A.1 Fitted traces (red lines) obtained for data of malachite green lactone in acetonitrile (symbols) in various time ranges. Time constant determined from very short and long time regions ((a) and (c)) should also be present in a medium one (b). The partial fits are also presented with corresponding amplitudes in brackets. Negative amplitude indicate an absorption rise.

The multi-exponential relaxation kinetics exhibits time constants on various time scales overlapping each other. The way of relating them all together is illustrated in Figure A.1. With the shortest and longest time region the first and the third constant are defined. In the medium time scale both are combined, in most observed cases giving one middle constant more. In Figure A.2 the actual need for this middle time constant is shown. The fits with only two do not model the data with sufficient accuracy.
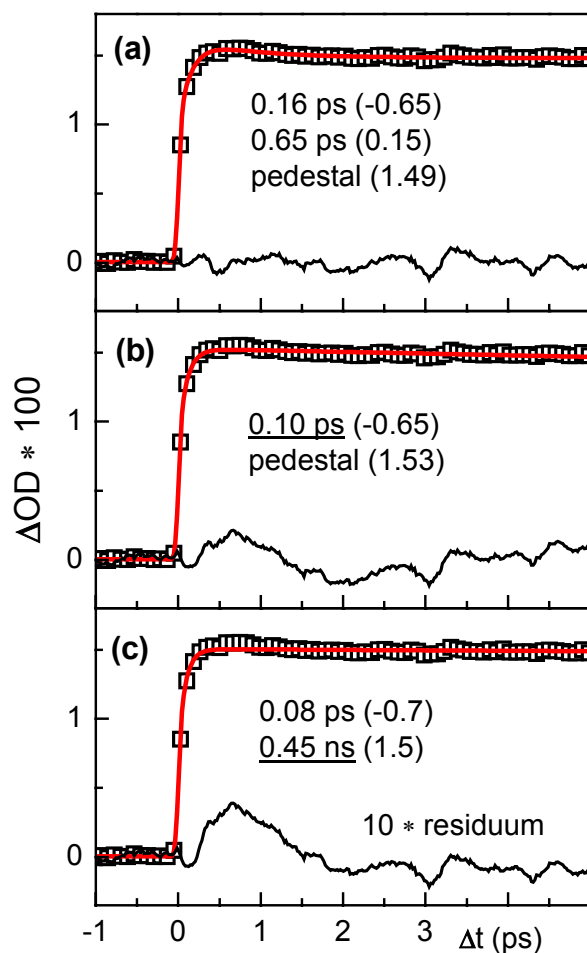
Figure A.2 The measured data of malachite green lactone in acetonitrile (symbols) are fitted with (a) three- and (b), (c) two-time constants (red lines). Underlined time constants are kept constant during the fitting. The thin black lines present the residuum multiplied by a factor of 10 .

If the time constants got from the first fitting-run are not consistent in all time region, one has to perform further fittings till the time constants in all time region correspond to each other (see Figure A.3). The reason for this are low amplitudes of one or more time constants, which weakly influence the total fit leading to a broad region of suitable values.
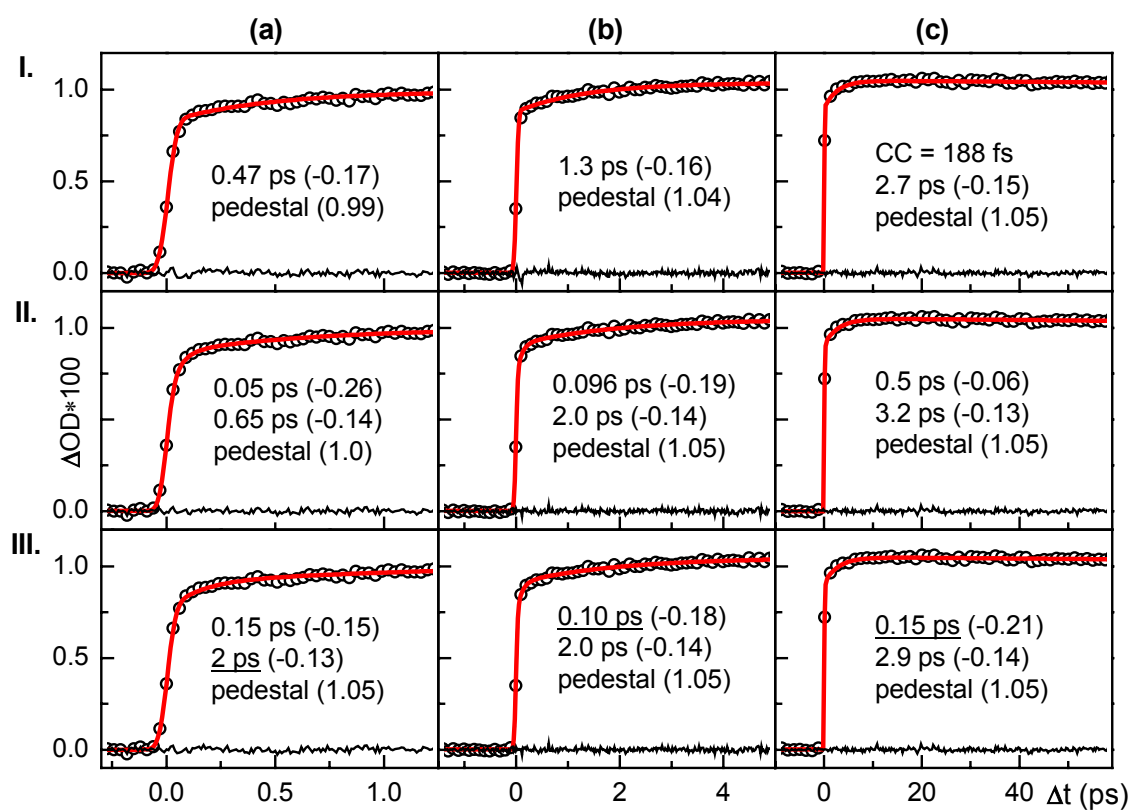
Figure A.3 Fitting procedure obtained for data of malachite green lactone in ethyl ace-tate. A first (I), second (II) and third (III) fitting-run are performed till the time con-stants from the different time region become consistent. Underlined time constants are kept constant in the particular fit.

B Subtraction of solvent contribution

In some experiments solvent effects like two photon ionization contribute to the signal. The solvent contribution is subtracted taking into account that the solvent contribution in the solution is smaller than the contribution measured in neat solvent. A signal coming from the neat solvent due to the 2-photon ionization process can be expressed as:

$$Sig_{solvent} = const. \cdot \int_0^{120\mu m} I^2(z) \cdot dz \qquad (B-01)$$

In the solution the intensity (I) of the excitation pulses decays exponentially along the pulse propagation (z-axis) because it is absorbed from the molecules dissolved in solution:

$$I_{exc}(z) = I_0 \cdot e^{-z/z_0} \qquad (B-02)$$

The constant z_0 of the exponential decay can be determined from the known molar concentration (c) of the sample, that gives a transmission (T) of the excitation energy after passing the sample of thickness d.

$$I_{exc}(d) = I_0 \cdot e^{-\frac{d}{z_0}} = I_0 \cdot T = I_0 \cdot 10^{-c \cdot \varepsilon \cdot d} \qquad (B-03)$$

The molar absorption coefficient (ε) of the investigated molecules is determined from the absorption spectra. In the neat solvents absorption of the excitation pulses can be neglected and the intensity (I_{exc}) stays constant (I_0). This is the reason why only a factor from the measured solvent effect should be subtracted. This factor is the ratio between the signal in solution with dissolved molecule and the signal in neat solvent:

$$\frac{Sig_{solvent}}{Sig_{solution}} = \frac{const. \cdot \int_0^{120\mu m} I_0^2 \cdot dz}{const. \cdot \int_0^{120\mu m} \left(I_0 \cdot e^{-z/z_0}\right)^2 \cdot dz} \qquad (B-04)$$

If a significant solvent effect is found, it is subtracted in this way from the measured signals.

Publications

Results of the work are presented in the following publications:

K. Stock, T, Bizjak, S. Lochbrunner, "Proton transfer and internal conversion of o-hydroxybenzaldehyde: coherent versus statistical exited-state dynamics", Chem. Phys. Lett. 354 (2002) 409.

T. Bizjak, P. B. Bisht, S. Lochbrunner and E. Riedle, „Femtosecond transient spectroscopy of the photoionization of indole in water", Femtochemistry and Femtobiology, VIth International Conference on Femtochemistry, M. M. Martin and J. T. Hynes, eds., Elsevier B. V., Amsterdam (2004) 229.

T. Bizjak, J. Karpiuk, S. Lochbrunner and E. Riedle, "50 fs photoinduced intramolecular charge separation in triphenylmethane lactones", J. Phys. Chem. A108 (2004) 10763.

T. Bizjak, P. B. Bisht, S. Lochbrunner and E. Riedle, "Ultrafast photoionization and electronic dynamics of indole in solution", J. Chem. Phys., in preparation

Bibliography

[1]   R. K. Clayton, Photosynthesis: physical mechanisms and chemical patterns", Cambridge University Press, Cambridge (1980)

[2]   U. Bach, D. Luppo, P. Comte, J. E. Moser, F. Weissörtel, J. Salbeck, H. Spreitzer and M. Grätzel, Nature 395 (1998) 583.

[3]   A. H. Zewail, J. Phys. Chem. A 104 (2000) 5660.

[4]   T. Wilhelm, J. Piel, E. Riedle, Opt. Lett. **22** (1997) 1494.

[5]   E. Riedle, M. Beutter, S. Lochbrunner, J. Piel, S. Schenkl, S. Spörlein, W. Zinth, App. Phys. B 71 (2000) 457.

[6]   J. Jortner and M. Bixon, eds. *Electron Transfer: from isolated molecules to biomolecules*, Adv. Chem. Phys. vol. 106, 107, J. Wiley, New York (1999)

[7]   R. Hubert, J.-E. Moser, M. Grätzel, and J. Wachtveitl, J. Phys. Chem. B 106 (2002) 6494.

[8]   J. Schnadt, P. A. Brühwiler, L. Patthey, J. N. O´Shea, S. Södergren, M. Odelius, R. Ahuja, O. Karis, M. Bässler, P. Persson, H. Siegbahn, S. Lunell and N. Mårtensson, Nature 418 (2002) 620.

[9]   E. Baigar, P. Glich, W. Zinth, M. Stöckl, P. Härter, T. von Feilitzsch and M. E. Michel-Beyerle, Chem. Phys. Lett. 352 (2002) 176.

[10]   D. H. Son, P. Kambhampati, T. W. Kee and P. F. Barbara, J. Phys. Chem. A 106 (2002) 4591.

[011] S. A. Kovalenko, J. L. Perez Lustres, N. P. Ernsting and W. Rettig, J. Phys. Chem. A 107 (2003) 10228.

[12]   A. Reuther, H. Iglev, R. Laenen, A. Laubereau, Chem. Phys. Lett. 325 (2000) 360.

[13]   L. I. Grossweiner and H.-I. Joschek, "Optical Generation of Hydrated Electrons from Aromatic Compounds" in *Solvated Electron*, E. J. Hart (Ed.), Advances in chemistry 50, American Chemical Society, Washington, D.C. (1965) p. 279.

[14]   H.-I. Joschek and L. I. Grossweiner, J. Am. Chem. Soc. 88 (1966) 3261.

[15]   R. Santus and L. I. Grossweiner, Photochem. Photobiol. 15 (1972) 101.

[16]   V. Subramanyan and G. Tollin, Photochem. Photobiol. 15 (1972) 449.

[17]   Y. Hirata, N. Murata, Y. Tanioka, and N. Mataga, J. Phys. Chem. 93 (1989) 4527.

[18]   F. Saito, S. Tobita, H. Shizuka, J. Photochem. Photobiol. A 106 (1997) 119.

[19]   J. Peon, G. C. Hess, J.-M. L. Pecourt, T. Yuzawa, and B. Kohler, J. Phys. Chem. A 103 (1999) 2460.

[20]   J. Peon, J. D. Hoerner, and B. Kohler, to appear in *Liquid Dynamics: Into the New Millenium*, J. T. Fourkas, Ed.; ACS Symposium Series, 2001.

[21]   D. N. Nikogosyan, A. A. Oraevsky and V. I. Rupasov, Chem. Phys. 77 (1983) 131.

[22]   F. H. Long, H. Lu and K. B. Eisenthal, Chem. Phys. Lett. 160 (1989) 464.

[23]   H. Lu, F. H. Long, R. M. Bowman, and K. B. Eisenthal, J. Phys. Chem. 93 (1989) 27.

[24]   M. Maroncelli, J. MacInnis, G. R. Fleming, Science 243 (1989) 1674.

[25]   H. Sumi and R. A. Marcus, J. Chem. Phys. 84 (1986) 4894.

[26]   G. C. Walker, E. Åkesson, A. E. Johnson, N. E. Levinger, and P. F. Barbara, J. Phys. Chem. 96 (1992) 3728.

[27]   M. L. Horng, J. A. Gardecki, A. Papazyan, and M. Maroncelli, J. Phys. Chem. 99 (1995) 17311.

[28]   L. Reynolds, J. A. Gardecki, S. J. V. Frankland, M. L. Horng, and M. Maroncelli, J. Phys. Chem. 100 (1996) 10337.

[29]   R. Biswas and B. Bagchi, J. Phys. Chem. A 103 (1999) 2495.

[30]   S. J. Rosenthal, X. Xie, M. Du and G. R. Fleming, J. Chem. Phys. 95 (1991) 4715.

[31]   M. Maroncelli, J. Mol. Liq. 57 (1993) 1.

[32]   M Maroncelli, J. Chem. Phys. 94 (1991) 2084.

[33]   E. M. Kosower, D. Huppert, Ann. Rev. Phys. Chem. 37 (1986) 127.

[34]   R. F. Loring and S. Mukamel, J. Chem. Phys. 87 (1987) 1272.

[35]   E. W. Castner, Jr. M. Maroncelli, and G. R. Fleming, J. Chem. Phys. 86 (1987) 1090.

[36]   M. A. Kahlow, T. J. Kang, and P. F. Barbara, J. Chem. Phys. 90 (1988) 2372.

[37]   J. Jortner and M. Bixon, J. Chem. Phys. 88 (1988) 167.

[38]   J.-M. L. Pecourt, J. Peon, and B. Kohler, J. Am. Chem. Soc. 123 (2001) 10370.

[39]   J. Peon, A. H. Zewail, Chem. Phys. Lett. 348 (2001) 255.

[40]   P. R. Callis, Ann. Rev. Phys. Chem. 34 (1983) 329.

[41]   T. Werner, J. Phys. Chem. 83 (1979) 320.

[42]   P.-T. Chou, S. L. Studer, and M. L. Martinez, Appl. Spectrosc. 45 (1991) 513.

[43]   J. Keck, H. E. A. Kramer, H. Port, T. Hirsch, P. Fischer, and G. Rytz, J. Phys. Chem. 100 (1996) 14468.

[44]   G. R. Fleming, „Chemical Applications of Ultrafast Spectroscopy", Oxford University Press, New York (1986)

[45]   M. Kasha, Discuss. Farad. Soc. 9 (1995) 14.

[46]   N. J. Turro, Modern Molecular Photochemistry, 2nd ed., University Science Books, Sausalito, California (1991)

[47]   M. Klessinger, J. Michl, Excited states and photochemistry of organic molecules, VCH Publishers, Inc., New York (1995)

[48]   J. S. Strickler, R. A. Berg, J.Chem.Phys. 37 (1962), 814.

[49]   R. A. Marcus, Annu. Rev. Phys. Chem. 15 (1964) 155.

[50]   G. J. Kavarnos and N. J. Turro, Chem. Rev. 86 (1986) 401.

[51]   R. A. Marcus, Angew. Chem. 105 (1993) 1161.

[52]   A. M. Kuznetsov, J. Ulstrup, "Electron transfer in chemistry and biology: an introduction to the theory", John Wiley & Sons Ltd, New York (1999)

[53]   R. A. Marcus, J. Chem. Phys. 24 (1956) 979.

[54]   D. Rehm and A. Weller, Isr. J. Chem. 8 (1970) 259.

[55]   E. J. Hart, J. W. Boag, J. Am. Chem. Soc. 84 (1962) 4090.

[56]   E. J. Hart (Ed.), *Solvated Electron*, Advances in chemistry 50, American Chemical Society, Washington, D.C. (1965)

[57]   R. A. Marcus, "Theoretical Study of Electron Transfer Reactions of Solvated Electrons" in *Solvated Electron*, E. J. Hart (Ed.), Advances in chemistry 50, American Chemical Society, Washington, D.C. (1965) p. 138.

[58]   J. Jortner and S. A. Rice, "Theoretical Studies of Solvated Electrons" in *Solvated Electron*, E. J. Hart (Ed.), Advances in chemistry 50, American Chemical Society, Washington, D.C. (1965) p. 7.

[59]   C. Reichardt, „Solvents and Solvent Effects in Organic Chemistry", VCH Verlagsgesellschaft mbH, Weinheim (1990)

[60]   B. Raz and J. Jortner, Chem. Phys. Lett. 4 (1969) 155.

[61]   I. Messing and J. Jortner, Chem. Phys. 24 (1977) 183.

[62]   M. Born, Z. Phys. 1 (1920) 221.

[63]   L. D. Zusman, Chem. Phys. 49 (1980) 295.

[64]   I. Z. Kozma, P. Baum, U. Schmidhammer, S. Lochbrunner, E. Riedle, Rev. Sci. Instrum. 75 (2004) 2323.

[65]   R. Menzel, Photonics – Linear and Nonlinear Interactions of Laser Light and Matter, Springer-Verlag, Berlin (2001)

[66]   S. A. Akhmanov, V. A. Vysloukh, A. S. Chirkin, Optics of Femtosecond Laser Pulses, American Institute of Physics, New York (1992)

[67]   J.-C. Diels, W. Rudolph, Ultrashort Laser Pulse Phenomena, Academic Press, San Diego (1996)

[68]   R. Huber, H. Satzger, W. Zinth, J. Wachtveitl, Opt. Commun. 194 (2001) 443.

[69]   M. Lorenc, M. Ziolek, R. Naskrecki, J. Karolczak, J. Kubicki, A. Maciejewski, Appl. Phys. B 74 (2002) 19.

[70]   O. Fischer, Justus Liebigs Ann. Chem. 206 (1881) 83.

[71]   W. L. F. Armarego, D. D. Perrin, Purification of Laboratory Chemicals, 4th ed., Butterworth-Heineman, Oxford (1996)

[72]   S. Pommeret, R. Naskrecki, P. van der Meulen, M. Ménard, G. Vigneron, T. Gustavsson, Chem. Phys. Lett. 288 (1998) 833.

[73]   S. Takeuchi, T. Tahara, Chem. Phys. Lett. 347 (2001) 108.

[74]   K. Ekvall, P. van der Meulen, C. Dhollande, L.-E. Berg, S. Pommeret, R. Naskrecki, J.-C. Mialocq, J. Appl. Phys. 87 (2000) 2340.

[75]   T. R. Tuttle, Jr., S. Golden, J. Phys. Chem. 95 (1991) 5725.

[76]   M. S. Matheson, "The Hydrated Electron in Radiation Chemistry" in Solvated Electron, E. J. Hart (Ed.), Advances in chemistry 50, American Chemical Society, Washington, D.C. (1965) p. 45.

[77]   E. M. Fielden and E. J. Hart, Radiat. Res. 32 (1967) 564.

[78]   J. P. Keene, Radiat. Res. 22 (1964) 1.

[79]   W. C. Gottschall and E. J. Hart, J. Phys. Chem. 71 (1967) 2102.

[80]   T. R. Tuttle, Jr., S. Golden, S. Lwenje, and C. M. Stupak, J. Phys. Chem. 88 (1984) 3811.

[81]   T. R. Tuttle Jr and S. Golden, J. Chem. Soc., Faraday Trans. 77 (1981) 873.

[82]   S. Golden and T. R. Tuttle Jr, J. Chem. Soc., Faraday Trans. 77 (1981) 889.

[83]   S. Golden and T. R. Tuttle Jr, J. Chem. Soc., Faraday Trans. 77 (1981) 1421.

[84]   L. M. Dorfman, "The solvated electron in Organic Liquids" in Solvated Electron, E. J. Hart (Ed.), Advances in chemistry 50, American Chemical Society, Washington, D.C. (1965) p. 36.

[85]   H. E. Lessing and A. von Jena, Chem. Phys. Lett. 42 (1976) 213.

[86]   G. R. Fleming, J. M. Morris and G. W. Robinson, Chem. Phys. 17 (1976) 91.

[87]   H. E. Lessing and A. von Jena, Laser Handbook, edited by M. L. Stitch, North-Holland Publishing Company (1979)

[88] B. Bagchi, G. R. Fleming, D. W. Oxtoby, J. Chem. Phys. 78 (1983) 7375.

[89] F. Pöllinger, H. Heitele, M. E. Michel-Beyerle, C. Anders, M. Fuscher, H. A. Staab, Chem. Phys. Lett. 198 (1992) 645.

[90] S. Iwai, S. Murata, M. Tachiya, J. Chem. Phys. 109 (1998) 5963.

[91] R. A. Denny and B. Bagchi, P. F. Barbara, J. Chem. Phys. 115 (2001) 6058.

[92] T. Kobayashi, Y. Takagi, H. Kandori, K. Kemnitz and K. Yoshihara, Chem. Phys. Lett. 180 (1991) 416.

[93] H. Kandori, K. Kemnitz, K. Yoshihara, J. Phys. Chem. 96 (1992) 8042.

[94] M. Seel, S. Engleitner, W. Zinth, Chem. Phys. Lett. 275 (1997) 363.

[95] S. Engleitner, M. Seel, W. Zinth, J. Phys. Chem. A 103 (1999) 3013.

[96] I. V. Rubtsov, H. Shirota, K. Yoshihara, J. Phys. Chem. A 103 (1999) 1801.

[97] A. Morandeira, A. Fürstenberg, J.-C. Gumy, E. Vauthey, J. Phys. Chem. A 107 (2003) 5375.

[98] N. Mataga, H. Chosrowjan, S. Taniguchi, Y. Shibata, N, Yoshida, A. Otsuka, T. Kikuzawa and T. Okada, J. Phys. Chem. A 106 (2002) 12191.

[99] N. Mataga, S. Taniguchi, H. Chosrowjan, A. Osuka, N. Yoshida, Photochem. Photobiol. Sci. 2 (2003) 493.

[100] J. M. Giaimo, A. V. Gusev, M. R. Wasielewski, J. Am. Chem. Soc. 124 (2002) 8530.

[101] V. Balzani (ed.), Electron Transfer in Chemistry, J. Wiley, New York (2001)

[102] J. Karpiuk, Photophysical and photochemical processes in lactone forms of some rhodamines, PhD thesis, Institute of Physical Chemistry, Polish Academy of Sciences, Warsaw (1996)

[103] J. Karpiuk, Phys. Chem. Chem. Phys. 5 (2003) 1078.

[104] M. W. Geiger, N. J. Turro and W. H. Waddell, Photochem. Photobiol. 25 (1977) 15.

[105] A. H. Sporer, Trans. Farad. Soc. 57 (1961) 983.

[106] M. L. Herz, J. Am. Chem. Soc. 97 (1975) 6777.

[107] J. Karpiuk, work in preparation.

[108] H. A. Stuart, G. Klages, Kurzes Lehrbuch der Physik, 11th ed., Springer-Verlag Berlin, Heidelberg (1988)

[109] J. A. Riddick, W. B. Bunger, T. K. Sakano, Organic solvents, Wiley: New York (1986)

[110] H. Lami and N. Glasser, J. Chem. Phys. 84 (1986) 597.

[111] P. W. Atkins, Physical Chemistry, 6th ed., Oxford University Press, Oxford (1998)

[112] G. P. Johari and C. P. Smyth, J. Am. Chem. Soc. 91 (1969) 6215.

[113] Y. Nagasawa, Y. Ando, D. Kataoka, H. Matsuda, H. Miyasaka and T. Okada, J. Phys. Chem. A 106 (2002) 2024.

[114] Z. Tamura, S. Abe, K. Ito, M. Maeda, *Anal. Sci.* 12 (1996) 927.

[115] I. B. Berlmann, *Handbook of fluorescence spectra of aromatic molecules*, New York, Academic Press (1971)

[116] I. L. Belaits and R. N. Nurmukhametov, Zh. Fiz. Khim. 44 (1970) 29.

[117] A. Boguta and D. Wróbel, *J. Fluoresc.* **11** (2001) 129.

[118] J. Gronowska, T. Rakowska and H. Waleryś, Rocz. Chem. **47** (1973) 2101.

[119] R. Hermann, G. R. Mahalaxmi, T. Jochum, S. Naumov, and O. Brede, J. Phys. Chem. A 106 (2002) 2379.

[120] R. Hermann, S. Naumov, G. R. Mahalaxmi, O. Brede, Chem. Phys. Lett. 324 (2000) 265.

[121] W. D. Oosterbaan, M. Koeberg, J. Piris, R. W. A. Havenith, C. A. van Walree, B. R. Wegewijs, L. W. Jenneskens, and J. W. Verhoeven, J. Phys. Chem. A 105 (2001) 5984.

[122] T. Shida, Y. Nosaka, and T. Kato, J. Phys. Chem. 82 (1978) 695.

[123] T. Elsaesser and W. Kaiser, Annu. Rev. Phys. Chem. 42 (1991) 83.

[124] B. A. Kellogg, R. S. Brown, R. S. McDonald, J. Org. Chem. 59 (1994) 4652.

[125]   J. Karpiuk, submitted to J. Phys. Chem.

[126] S. K. Garg, C. P. Smyth, J. Phys. Chem. 69 (1965) 1294.

[127] L. J. Fitzgerald and R. E. Gerkin, Acta Cryst. C54 (1998) 535.

[128] N. W. Tyer, Jr., and R. S. Becker, J. Am. Chem. Soc. 92 (1970) 1289.

[129] M. W. Sagal, J. Chem. Phys. 36 (1962) 2437.

[130] J. Karpiuk, Proceedings: J. Ann. Pol. Chem. Soc. (2001) 271.

[131] M. L. Vincent and D. G. Peters, J. Electroanal. Chem. 327 (1992) 121.

[132] D. W. Leedy and D. L. Muck, J. Am. Chem. Soc. 93 (1971) 4264

[133] Y. Nagasawa, , A. P. Yartsev, K. Tominanga, P. B. Bisht, A. E. Johnson, and K. Yoshihara, J. Phys. Chem. 99 (1995) 653.

[134] P. F. Barbara, T. J. Meyer, M. A. Ratner, J. Phys. Chem. 100 (1996) 13148.

[135] B. G. Zykov, Yu. V. Vasil'ev, V. S. Fal'ko, A. N. Lachinov, V. I. Khvostenko, and N. G. Gileva, JETP Lett. 64 (1996) 439.

[136] Y. V. Vasil'ev, B. G. Zykov, V. S. Fal'ko, A. N. Lachinov, V. I. Khvostenko and N. G. Gileva, Synthetic Met. 84 (1997) 975.

[137] I. Wallmark, M. H. Krackov, S.-H. Chu, and H. G. Mautner, J. Am. Chem. Soc. 92 (1970) 4447.

[138] C. Desfrançois, H. Abdoul-Carime and J.-P. Schermann, Int. J. Mod. Phys. B 10 (1996) 1339.

[139] T. Fiebig, K. Stock, S. Lochbrunner, E. Riedle, Chem. Phys. Lett. 345 (2001) 81.

[140] G. Weber, Biochem J. 75 (1960) 335.

[141] Weber and F. W. J. Teale, Trans. Faraday Soc. 53 (1957) 646.

[142] S. V. Konev, "Fluorescence and Phosphorescence of Proteins and Nucleic Acids" Plenum, New York (1967)

[143] J. W. Longworth, in "Excited States of Proteins and Nucleic Acids" (R. F. Steiner and I. Weinryb, eds.). p. 319. Plenum, New York (1971)

[144] J. M. Beechem and L. Brand. Annu. Rev. Biochem. 54 (1985) 43.

[145] A. P. Demchenko. „Ultraviolet Spectroscopy of Proteins." Springer-Verlag. New York (1986)

[146] Y. Chen and M. D. Barkley, Biochemistry 37 (1998) 9976.

[147] T. A. Broadbent, H. S. Broadbent, The chemistry and pharmacology of indole-3-carbinol (indole-3-methanol) and 3-(methoxymethyl)indole. [Part I]. Curr. Med. Chem. 5 (1998) 337.

[148] T. A. Broadbent, H. S. Broadbent, The chemistry and pharmacology of indole-3-carbinol (indole-3-methanol) and 3-(methoxymethyl)indole. [Part II]. Curr. Med. Chem. 5 (1998) 469.

[149] G. N. Lewis and D. Lipkin, J. Am. Chem. Soc. 64 (1942) 2801.

[150] M. Ebert ans A. J. Swallow, "Reactions of the Hydrated Electron with Substances of Biological Importance" in *Solvated Electron*, E. J. Hart (Ed.), Advances in chemistry 50, American Chemical Society, Washington, D.C. (1965) p. 289.

[151] D. V. Bent and E. Hayon, J. Am. Chem. Soc. 97 (1975) 2612.

[152] H. B. Steen, M. K. Bowman, and L. Kevan, J. Phys. Chem. 80 (1976) 482.

[153] J. Zechner, G. Köhler, N. Getoff, I. Tatischeff and R. Klein, Photochem. Photobiol. 34 (1981) 163.

[154] J. C. Mialocq, E. Amouyal, A. Bernas, and D. Grand, J. Phys. Chem. 86 (1982) 3173.

[155] W. G. McGimpsey and H. Görner, Photochem. Photobiol. 64 (1996) 501.

Bibliography

[156] M. S. Walker, T. W. Bednar and R. Lumry, Molecular Luminescence, (1969) 135.

[157] J. Eisinger, Molecular Luminescence, (1969) 185.

[158] R. W. Ricci, Photochem. Photobiol. 12 (1970) 67.

[159] M. R. Eftink and C. A. Ghiron, J. Phys. Chem. 80 (1976) 486.

[160] A. G. Szabo and D. M. Rayner, J. Am. Chem. Soc. 102 (1980) 554.

[161] R. Klein, I. Tatischeff, M. Bazin, and R. Santus, J. Phys. Chem. 85 (1981) 670.

[162] M. J. Tubergen and D. H. Levy, J. Phys. Chem. 95 (1991) 2175.

[163] S. Arnold and M. Sulkes, J. Phys. Chem. 96 (1992) 4768.

[164] X. Shen and J. R. Knutson, J. Phys. Chem. B 105 (2001) 6260.

[165] D. Creed, Photochem. Photobiol. 39 (1984) 537.

[166] P. R. Callis, Methods in Ezymology 278 (1997) 113.

[167] L. Serrano-Andrés and B. O. Roos, J. Am. Chem. Soc. 118 (1996) 185.

[168] L. Serrano-Andrés, A. C. Borin, Chem. Phys. 262 (2000) 267.

[169] A. C. Borin, L. Serrano-Andrés, Chem Phys. 262 (2000) 253.

[170] D. Toptygin, L. Brand, Chem. Phys. Lett. 322 (2000) 496.

[171] A. Bernas, D. Grand, and E. Amouyal, J. Phys. Chem. 84 (1980) 1259.

[172] Y. Gauduel, S. Pommeret, A. Migus, and A. Antonetti, J. Phys. Chem. 93 (1989) 3880.

[173] P. J. Reid, C. Silva, P. K. Walhout, P. F. Barbara, Chem. Phys. Lett. 228 (1994) 658.

[174] M. Assel, R. Laenen, and A. Laubereau, J. Phys. Chem. A 102 (1998) 2256.

[175] A. Reuther, A. Laubereau, and D. N. Nikogosyan, J. Phys. Chem. 100 (1996) 16794.

[176] P. R. Callis, Int. J. Quant. Chem. 18 (1984) 579.

[177] A. L. Sobolewski, W. Domcke, Chem. Phys. Lett. 315 (1999) 293.

[178] A. L. Sobolewski, W. Domcke, Chem. Phys. Lett. 329 (2000) 130.

[179] B. C. Dian, A. Longarte, and T. S. Zwier, J. Chem. Phys. 118 (2003) 2696.

[180] P. C. Callis and B. K. Burgess, J. Phys. Chem. B 101 (1997) 9429.

[181] K. R. F. Somers, E. S. Kryachko, A. Ceulemans, Chem. Phys. 301 (2004) 61.

[182] P. R. Callis, J. Chem. Phys. 95 (1991) 4230.

[183] A. L. McClellan, Tables of Experimental Dipole Moments, Freeman, London (1963)

[184] M. S. Walker, T. W. Bednar, and R. Lumry, J. Chem. Phys. 45 (1966) 3455.

[185] M. S. Walker, T. W. Bednar, and R. Lumry, J. Chem. Phys. 47 (1967) 1020.

[186] M. Mons, I. Dimicoli, B. Tardivel, F. Piuzzi, V. Brenner, and P. Millié, J. Phys. Chem. A 103 (1999) 9958.

[187] O. G. Peterson, J. P. Webb, and W. C. McColgin, J. Appl. Phys. 42 (1971) 1917.

[188] J. Olmsted, J. Phys. Chem. 83 (1979) 2581.

[189] H. B. Steen, J. Chem. Phys. 61 (1974) 3997.

[190] D. Grand, A. Bernas and E. Amouyal, Chem. Phys. 44 (1979) 73.

[191] J. B. Birks and D. J. Dyson, Proc. Roy. Soc. Lond. Ser. A 275 (1963) 135.

[192] W. Holzer, H. Gratz, T. Schmitt, A. Penzkofer, A. Costela, I. García-Moreno, R. Sastre, F. J. Duarte, Chem.Phys. 256 (2000) 125.

[193] K. Kerl and H. Varchmin, J. Mol. Struct. 349 (1995) 257.

[194] D. R. Lide (Ed.), Handbook of Chemistry and Physics, 76th ed., CRC Press, Boca Raton, New York, London, Tokyo (1995)

[195] J. W. Hager and S. C. Wallace, Anal. Chem. 60 (1988) 5.

[196] S. V. Jovanovic and S. Steenken, J. Phys. Chem. 96 (1992) 6674.

[197] A. Migus, Y. Gauduel, J. L. Martin, and A. Antonetti, Phys. Rev. Lett. 58 (1987) 1559.

[198] F. H. Long, H. Lu, and K. B. Eisenthal, Phys. Rev. Lett. 64 (1990) 1469.

[199] J. C. Alfano, P. K. Walhout, Y. Kimura, and P. F. Barbara, J. Chem. Phys. 98 (1993) 5996.

[200] X. Shi, F. H. Long, H. Lu, and K. B. Eisenthal, J. Phys. Chem. 100 (1996) 11903.

[201] R. Laenen, T. Roth, and A. Laubereau, Phys. Rev. Lett. 85 (2000) 50.

[202] M. Assel, R. Laenen, A. Laubereau, J. Chem. Phys. 111 (1999) 6869.

[203] A. L. Sobolewski, W. Domcke, C. Dedonder-Lardeux and C. Jouvet, Phys. Chem. Chem. Phys. 4 (2002) 1093.

[204] A. L. Sobolewski and W. Domcke, Phys. Chem. Chem. Phys. 4 (2002) 4.

[205] A. L. Sobolewski and W. Domcke, J. Phys. Chem. A 106 (2002) 4158.

[206] A. L. Sobolewski and W. Domcke, J. Phys. Chem. A 107 (2003) 1557.

[207] A. W. Castleman, Jr., results presented on the Kolloquium of Chair for Physical and Theoretical Chemistry at Technical University Munich (June 2004)

[208] F. F. Muguet, H. Gelabert, Y. Gauduel, J. Chim. Phys. 93 (1996) 1808.

[209] F. F. Muguet, G. W. Robinson, in "Ultrafast reaction dynamics and solvent effects", AIP Conference Proceeding 298, Y. Gauduel, P. J. Rossky eds., AIP Press (1994) p. 158.

[210] C. L. Thomsen, D. Madsen, S. R. Keiding. and J. Thøgersen, O. Christiansen, J. Chem. Phys. 110 (1999) 3453.

[211] E. Rabinowitch, Rev. Mod. Phys. 14 (1942) 112.

[212] W. A. Goddard, III and W. J. Hunt, Chem. Phys. Lett. 24 (1974) 464.

[213] O. Dutuit, A. Tabche-Fouhaile and I. Nenner, H. Frohlich and P. M. Guyon, J. Chem. Phys. 83 (1985) 584.

[214] A. Bernas, C. Ferradini, J.-P. Jay-Gerin, Chem. Phys. 222 (1997) 151.

[215] P. Han and D. M. Bartels, J. Phys. Chem. 94 (1990) 5824.

[216] P. Han and D. M. Bartels, J. Phys. Chem. 96 (1992) 4899.

[217] R. A. Crowell and D. M. Bartels, J. Phys. Chem. 100 (1996) 17940.

[218] D. N. Nikogosyan and H. Görner, J. Photochem. Photobiol. B 13 (1992) 219.

[219] A. Bernas and D. Grand, J. Phys. Chem. 98 (1994) 3440.

[220] R. A. Crowell, R. Lian, I. A. Shkrob, and D. M. Bartels, X. Chen and S. E. Bradforth, J. Chem. Phys. 120 (2004) 11712.

[221] V. Berghof, M. S. Gudipati, N. Schwentner, J. Chem. Phys. 120 (2004) 1414.

[222] L. Lehr, M. T. Zanni, C. Frischkorn, R. Weinkauf, D. M. Neumark, Science 284 (1999) 635.

[223] J. A. Kloepfer, V. H. Vilchiz, A. Lenchenkov, S. E. Bradforth, Chem. Phys. Lett. 298 (1998) 120.

[224] J. A. Kloepfer, V. H. Vilchiz, V. A. Lenchenkov, A. C. Germaine, and S. E. Bradforth, J. Chem. Phys. 113 (2000) 6288.

[225] V. H. Vilchiz, J. A. Kloepfer, A. C. Germaine, V. A. Lenchenkov, and S. E. Bradforth, J. Phys. Chem. A 105 (2001) 1711.

[226] V. Stert, L. Hesse, H. Lippert, C. P. Schulz, and W. Radloff, J. Phys. Chem. A 106 (2002) 5051.

[227] H. Lippert, V. Stert, L. Hesse, C. P. Schulz, W. Radloff, and I. V. Hertel, Eur. Phys. J. D 20 (2002) 445.

[228] H. Lippert, V. Stert, L. Hesse, C. P. Schulz, I. V. Hertel, and W. Radloff, J. Phys. Chem. A 107 (2003) 8239.

[229] H. Lippert, V. Stert, L. Hesse, C. P. Schulz, I. V. Hertel, W. Radloff, Chem. Phys. Lett. 376 (2003) 40.

[230] J. Wei, A. Kuczmann, J. Riedel, F. Renth and F. Temps, Phys. Chem. Chem. Phys. 5 (2003) 315.

[231] G. Koehler, Sn. Bakalova, N. Getoff, P. Nikolov and I. Timtcheva, J. Photochem. Photobiol. A 81 (1994) 73.

[232] T. Goulet and J.-P. Jay-Gerin, J. Chem. Phys. 96 (1992) 5076.

[233] E. R. Barthel, I. B. Martini, and B. J. Schwartz, J. Phys. Chem. B 105 (2001) 12230.

[234] I. B. Martini, E. R. Barthel, B. J. Schwartz, Science 293 (2001) 462.

[235] I. B. Martini, E. R. Barthel, and B. J. Schwartz, J. Am. Chem. Soc. 124 (2002) 7622.

[236] D. F. Calef and P. G. Wolynes, J. Chem. Phys. 78 (1983) 4145.

[237] M. S. Pshenichnikov, A. Baltuška, D. A. Wiersma, Chem. Phys. Lett. 389 (2004) 171.

[238] D. H. Son, P. Kambhampati, T. W. Kee, and P. F. Barbara, J. Phys. Chem. A 105 (2001) 8269.

[239] D. H. Son, P. Kambhampati, T. W. Kee, P. F. Barbara, Chem. Phys. Lett. 342 (2001) 571.

[240] J. Schnitker, K. Motakabbir, P. J. Rossky, and R. Friesner, Phys. Rev. Lett. 60 (1988) 456.

[241] P. Kambhampati, D. H. Son, T. W. Kee, and P. F. Barbara, J. Phys. Chem. A 106 (2002) 2374.

[242] V. Lenchenkov, J. Kloepfer, V. Vilchiz, S. E. Bradforth, Chem. Phys. Lett. 342 (2001) 277.

[243] L. D. Zusman and A. B. Helman, Chem. Phys. Lett. 114 (1985) 301.

[244] W. Danninger and G. Zundel, J. Chem. Phys. 74 (1981) 2769.

[245] C. J. Montrose, J. A. Bucaro, J. Marshall-Coakley, and T. A. Litovitz, J. Chem. Phys. 60 (1974) 5025.

[246] M. J. Tauber and R. A. Mathies, J. Phys. Chem. A 105 (2001) 10952.

[247] M. Mizuno and T. Tahara, J. Phys. Chem. A 105 (2001) 8823.

[248] M. J. Tauber, R. A. Mathies, Chem. Phys. Lett. 354 (2002) 518.

[249] M. Mizuno and T. Tahara, J. Phys. Chem. A 107 (2003) 2411.

[250] C.-G. Zhan and D. A. Dixon, J. Phys. Chem. B 107 (2003) 4403.

[251] I. Gryczynski, W. Wiczk, M. L. Johnson and J. R. Lakowicz, Biophys. Chem. 32 (1988) 173.

[252] H. H. Limbach, J. Manz, Phys. Chem. Chem. Phys. 102 (1998) 289.

[253] S. Lochbrunner and E. Riedle, Recent Res. Devel. Chem. Physics 4 (2003) 31.

[254] A. Weller, Z. Elektrochem. 60 (1956) 1144.

[255] A. J. Wurzer, S. Lochbrunner, E. Riedle, Appl. Phys. B 71 (2000) 405.

[256] P. F. Barbara, L.E. Brus, P. M. Rentzepis, J. Am. Chem. Soc. 102 (1980) 5631.

[257] A. Douhal, F. Lahmani, A. H. Zewail, Chem. Phys. 207 (1996) 477.

[258] T. Arthen-Engeland, T. Bultmann, N. P. Ernsting, M. A. Rodriguez, W. Thiel, Chem. Phys. 163 (1992) 43.

[259] J. L. Herek, S. Pedersen, L. Bañares, A. H. Zewail, J. Chem. Phys. 97 (1992) 9046.

[260] C. Chudoba, E. Riedle, M. Pfeiffer, T. Elsaesser, Chem. Phys. Lett. 263 (1996) 622.

[261] S. Lochbrunner, A. J. Wurzer, E. Riedle, J. Chem. Phys. 112 (2000) 10699.

[262] J. Jethwa, D. Ouw, K. Winkler, N. Hartmann, P. Vöhringer, Z. Phys. Chem. 214 (2000) 1367.

[263] N. P. Ernsting, S.A. Kovalenko, T. Senyushkina, J. Saam, V. Farztdinov, J. Phys. Chem. A 105 (2001) 3443.

[264] S. Lochbrunner, A. J. Wurzer, and E. Riedle, J. Phys. Chem. A 107 (2003) 10580.

[265] S. Lochbrunner, K. Stock, E. Riedle, J. Mol. Struct. *in print*

[266] R. de Vivie-Riedle, V. De Waele, L. Kurtz, and E. Riedle, J. Phys. Chem. A 107 (2003) 10591.

[267] C. Chudoba, S. Lutgen, T. Jentzsch, E. Riedle, M. Woerner, T. Elsaesser, Chem. Phys. Lett. 240 (1995) 35.

[268] T. Elsaesser, M. Pfeiffer, K. Lenz, A. Lau, C. Chudoba, S. Lutgen, T. Jentzsch, E. Riedle, and M. Woerner, Ultrafast Processes in Spectroscopy, edited by Svelto et al., Plenum Press, New York (1996)

[269] F. Laermer, T. Elsaesser and W. Kaiser, Chem. Phys. Lett. 148 (1988) 119.

[270] K. Stock, T. Bizjak, S. Lochbrunner, Chem. Phys. Lett. 354 (2002) 409.

[271] A. L. Sobolewski, W. Domcke, Chem. Phys. 184 (1994) 115.

[272] A. L. Sobolewski, W. Domcke, Chem. Phys. Lett. 300 (1999) 533.

[273] A. L. Sobolewski, W. Domcke, Phys. Chem. Chem. Phys. 1 (1999) 3065.

[274] S. Scheiner, J. Phys. Chem. A 104 (2000) 5898.

[275] J. Palomar, J. L. G. De Paz, and J. Catalán, J. Phys. Chem. A 104 (2000) 6453.

[276] S. Lochbrunner, T. Schultz, M. Schmitt, J. P. Shaffer, M. Z. Zgierski, A. Stolow, J. Chem. Phys. 114 (2001) 2519.

[277] S. Nagaoka, N. Hirota, M. Sumitani, K. Yoshihara, J. Am. Chem. Soc. 105 (1983) 4220.

[278] S. Nagaoka, U. Nagashima, Chem. Phys. 136 (1989) 153.

[279] J. Catalán, F. Toribio, A. U. Acuña, J. Phys. Chem. 86 (1982) 303.

[280] N. A. Anderson, S. H. Pullen, L. A. Walker II, J. J. Shiang, R. J. Sension, J. Phys. Chem. A 102 (1998) 10588.

[281] A. L. Sobolewski, W. Domcke, J. Phys. Chem. A 103 (1999) 4494.

Acknowledgments

The presented work was conducted at the **Chair for BioMolecular Optics** of the **Ludwig-Maximilians University Munich**. I would like to thank all those who have helped me to complete this work in every possible way.

First of all, I want to express my gratitude to *Prof. Dr. Eberhard Riedle* for giving me the opportunity of pursuing my Doctoral work in his group and for introducing me to very interesting research topics. I am grateful to him for providing funds for this work and for giving me the chance to present my results at various conferences. I appreciate his ideas, criticism and experience from which I have learned a lot. I am truly honored that I could work in his outstanding group and I am indebted for being able to perform my work in his extremely good equipped laboratories.

I want to express my gratitude to *Prof. Dr. Wolfgang Zinth* for his wise questions and useful comments to my work presented in several internal talks. It was pleasant to work in such a nice and well organized department provided with excellent infrastructure.

I am deeply indebted to my advisor, *Dr. Stefan Lochbrunner*, for his invaluable support, for finding answers to many questions and solutions to problems appearing in line with my work. I thank him for fruitful discussions, insightful explanations, continuous encouragement and extreme kindness. His reviews and suggestions for improving the manuscript of this thesis are gratefully acknowledged.

A special word of thanks goes to *Dr. Ida Z. Kozma* for many useful suggestions, helpful comments and practical solutions she has offered me concerning the English language, optical calculations and most of all for her wisdom and continuous effort to show me how to "♪ always look on the bright side of life ♫".

I thank *Dr. Jerzy Karpiuk* from the Institute of Physical Chemistry of Polish Academy of Science for the very successful collaboration in the project on lactones. He provided us with precious samples and enormous knowledge, which he was always willing to hand on further together with his wide-ranging experience.

I appreciate the nice cooperation with *Dr. Prem B. Bisht* from the Indian Institute of Technology Madras. It was rewarding to learn from him and have a chance to explain him what I know. His competent questions, positive criticism and useful suggestions were a support for the indole project.

I warmly thank all those nice people at our chair who helped me in one way or another. I would like to thank *Peter Baum* and *Dr. Kai Stock* for helping me doing my first steps in

Curriculum Vitae

Personal Data

Name:	Tanja Bizjak
Date of birth:	15.10.1973.
Place of birth:	Zagreb, Croatia
Nationality:	Croatian
Family status:	single
Parents:	Danimir Bizjak, Dipl. Ing of electrical engineering, retired
	Zlata Bizjak, born Levačić, Dipl. Ing. of chemistry, retired

Education

1980 - 1988	Elementary school „Matija Gubec" in Zagreb, Croatia
1988 - 1992	XV. Gymnasium in Zagreb, Croatia
1992 - 2000	Undergraduate study of physics at the University of Zagreb, Croatia
1999 - 2000	Diploma work at the Institute of physics, Zagreb, Croatia
	Thesis title: "High pressure discharge in the sodium-mercury and sodium-cadmium vapor mixtures"
	Supervisor: Dr. D. Veža in the group of Prof. Dr. G. Pichler
since May 2000	PhD work at the Chair for Biomolecular Optics, Ludwig-Maximilians-University Munich, Germany
	Supervisor: Prof. Dr. E. Riedle